Signal Distortion Caused By Tree Foliage in a 2.5 GHz Channel

A Thesis Submitted to the

College of Graduate Studies and Research

in Partial Fulfillment of the Requirements for the Degree of

Master of Science

in the Department of Electrical Engineering

University of Saskatchewan

Saskatoon, Saskatchewan

by

Eric Pélet

PERMISSION TO USE

In presenting this thesis in partial fulfillment of the requirements for a Postgraduate degree from the University of Saskatchewan, I agree that the Libraries of this University may make it freely available for inspection. I further agree that permission for copying of this thesis in any manner, in whole or in part, for scholarly purposes may be granted by the professor or professors who supervised my thesis work or, in their absence, by the Head of the Department or the Dean of the College in which my thesis work was done. It is understood that any copying or publication or use of this thesis or parts thereof for financial gain shall not be allowed without my written permission. It is also understood that due recognition shall be given to me and to the University of Saskatchewan in any scholarly use which may be made of any material in my thesis.

Requests for permission to copy or to make other use of material in this thesis in whole or in part should be addressed to:

Head of the Department of Electrical Engineering
University of Saskatchewan
Saskatoon, Saskatchewan, Canada
S7N 5A9

ABSTRACT

A fixed terrestrial wireless system such as the Microwave Multi-channel Distribution Service (MMDS) can be used as the "last mile" to provide a high speed Internet connection from a base station to a home in a rural or suburban residential area. Such a broadband wireless system works very well under line-of-sight transmission. It works quite well even if the line-of-sight is obstructed with a large number of trees. However, when trees obstruct the line-of-sight, under conditions of wind, the user may experience loss of the RF signal from time to time. This is especially true under gusty conditions.

As part of this research a high precision DSP-based measuring system is devised to accurately measure and characterize the distortions caused by tree foliage on the RF line-of-sight signal. The approach is to digitally generate a signal composed of several tones, up-convert the signal to 2.5 GHz and send it through tree foliage to a receiver where the signal is down-converted and sampled for a duration of five seconds. The samples collected are processed using Matlab to compute the temporal amplitude and phase variations of the tones. The measurement system provides estimates of the amplitude and phase of the receive tones with a time resolution of 3.2 ms. The standard deviation of the amplitude estimates is 0.3% of the actual amplitude of the tones and the standard deviation of the phase estimates is 0.23 degree. This accuracy is obtained when the signal-to-noise ratio of the receive signal is greater than 20 dB.

Measurement in the field with tree foliage in the line-of-sight shows that the swaying of the branches in the wind can cause rapid signal fading. This research determines the type of fade, the depth and duration of the fade, as well as the fading rate.

ACKNOWLEDGEMENTS

First and foremost, I would like to express my heart-felt gratitude to my supervisor, Dr. J. Eric Salt, for his excellent guidance and teaching, and his endless support and encouragement during my pursuit of this Master of Sciences degree. It has been a great privilege and rewarding experience to work under Professor J. Eric Salt.

I would like to extend my deepest gratitude to the management and staff of Canada's communications technology research consortium - TR*Labs* (Saskatoon), particularly Garth Wells and Jack Hanson, for the invaluable technical support and the modern facilities. My thanks also go to the department of Electrical Engineering of the University of Saskatchewan for providing me with generous fellowships.

I would like to express special thanks to my lovely wife, Patricia Pélet, for her generous love and help throughout this journey. Since I met her to this very moment, she has always been there with me whenever I needed her the most, making my life become more focused, meaningful, and pleasant. Thank you also to my little daughters Camille and Emmarie for bringing me even more joy and happiness.

Finally, I would like to thank and dedicate this thesis to my mother and father Rirette and Jean Pélet, who fulfilled very well their role of parents and keep providing me with abundant love, encouragement, and advice.

TABLE OF CONTENTS

LIST OF FIGURES

LIST OF TABLES

LIST OF ABBREVIATIONS

A/D	Analog to Digital
CW	Continuous Wave
D/A	Digital to Analog
D/C	Down-Converter
DAQ	Data Acquisition Board
DFS	Discrete Fourier Series
DFT	Discrete Fourier Transform
DLPF	Digital Lowpass Filter
DMA	Direct Memory Access
DSP	Digital Signal Processing
DTFT	discrete-time Fourier Transform
EEPROM	Electrically Erasable Programming Read Only Memory
FCC	Federal Communications Commission
FFT	Fast Fourier Transform
FPGA	Field Programmable Gate Array
FT	Fourier Transform
I	In-Phase
IIR	Infinite Impulse Response (Filter)
I/O	Input/Output
IF	Intermediate Frequency
IDTFT	inverse discrete-time Fourier Transform
IEEE	Institute of Electrical and Electronic Engineer
ISI	Intersymbol Interference
LMDS	Local Multipoint Distribution Service

LO	Local Oscillator
LOS	Line of Sight
LP	Loop Filter
LPE	Lowpass Equivalent
LTI	Linear Time Invariant (System)
MMDS	Microwave Multi-channel Distribution Service
MS	Measuring System
NCO	Numerically Controlled Oscillator
NLOS	Near Line of Sight
PAPR	Peak to Average Power Ratio
PD	Phase Detector
PLL	Phase Lock Loops
PN	Pseudonoise
p-p	peak-to-peak
PSD	Power Spectral Density
Q	Quadrature
RBW	(Filter) Resolution Bandwidth (Spectrum Analyzer)
RAM	Random Access Memory
RF	Radio Frequency
RMS	Root Mean Square
ROC	Region Of Convergence
RV	Random Variable
SAW	Surface Acoustic Wave (Filter)
SOHO	Small Office Home Office
SNR	Signal to Noise Ratio
U/C	Up-Converter
VI	Virtual Instrument
xDSL	Digital Subscriber Line
WSS	Wide Sense Stationary

1. INTRODUCTION

1.1 Recent Advances in Communication and the Demand for a Fast Internet

The invention of the telephone by Alexander Graham Bell(1847-1922) in 1876 not only marked the end of the telegraph era but also demonstrated the communication potential in being able to transmit speech sounds through electrical wire. During the next 100 years, communication mainly consisted of the transmission of voice using very narrow bandwidth signals.

With the advancement of technology in optical communication and computer networking, telecommunications rapidly evolved in the last decade from narrow-band voice signals to wide-band signals integrating voice, data, images, and video. At the same time, the development of the Internet and its widespread popularity led to the creation of a tremendous amount of multimedia applications and telecommunication services. The high bandwidth required by these Internet-based services continuously puts pressure on the telecommunication industry to increase the transmission rate over the Internet. Not only does the network core have to become faster but also the end user connection to the network core must increase in speed of data transfer. This connection, also called the "last mile", can be realized with fixed wireless communication, such as Microwave Multi-channel Distribution Service (MMDS).

1.2 The MMDS Radio System as the "Last Mile" for High-Speed Internet Access

The Microwave Multi-channel Distribution Service (MMDS) consists of microwave signal transmission in a piece of the radio frequency spectrum allocated by the government of Canada and US for a fixed terrestrial wireless service that provides connectivity from a service provider's base station to subscribers' stationary stations. The topology of MMDS

is shown in Figure 1.1. MMDS systems were designed to be efficient to broadcast information from the base station to the subscriber.

It is convenient at this point to introduce terminology used in MMDS to indicate the direction of information flow. Downstream denotes the transmissions from the base station to the subscribers' stations. Upstream denotes the transmissions from the subscribers' stations to the base station.

The spectrum occupied by MMDS is from 2.5 GHz to 2.7 GHz. It is exclusively licensed in the United States by the Federal Communications Commission (FCC) in portions 6 MHz wide. In Canada, licensing is done by the department of Spectrum Management and Telecommunications of Industry Canada. The spectrum is similar and is also licensed in 6 MHz chunks.

The band is organized to support transmission rates similar to xDSL(Digital Subscriber Line) in each of the 6 MHz channels; DSL is the standard used by telephone companies to support high-speed Internet access over twisted copper pairs.

The FCC and Industry Canada have placed power limits on the service that limit the reach to 48 km. The reach depends upon the terrain, the base station tower height, and

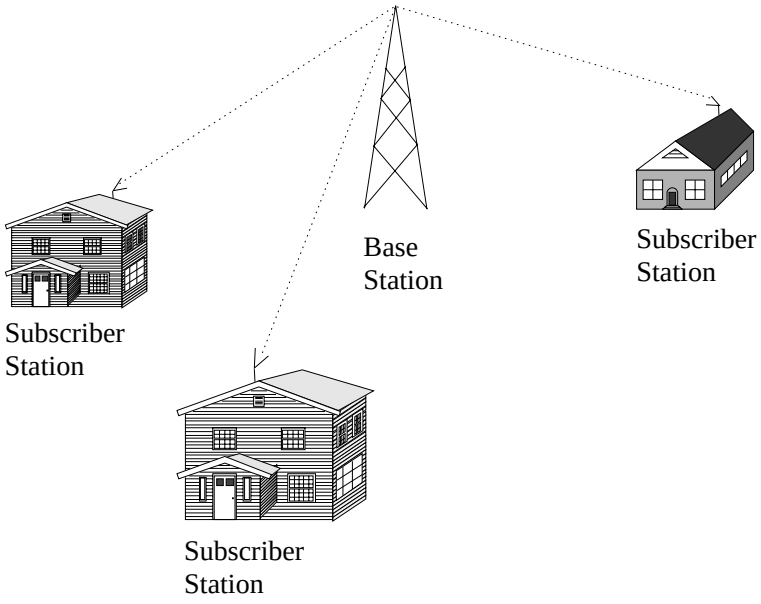

Figure 1.1: Typical MMDS Radio System

the transmitted signal power. It may reach 48 km in rural areas on the prairie where there are no obstructions. High gain antennas are used at the subscribers' stations. These antennas are directional and therefore must be aimed at the base station. The subscriber's station will normally have a Line-Of-Sight (LOS) transmission path (see Figure 1.2 and Section 1.2.1) to the base station.

1.2.1 Near-Line-Of-Sight(NLOS) Transmissions

There are often significant changes in the performance of a system if there are obstructions in the signal path. If there are no direct obstructions in the signal path, the system is said to be a Line-Of-Sight (LOS) system.

A transmission is Line-Of-Sight (LOS) if

1. the antenna at the subscriber's station is aimed at the base station antenna, and
2. there is no obstacle (buildings, tree foliage, etc) in the 1^{st} Fresnel zone. The 1^{st} Fresnel zone is the radius of the signal cone in which the phase of the signal is comprised between 0 and $\frac{\pi}{2}$. This is where the majority of the signal power exists in a Line-Of-Sight transmission.

A tranmission is Near Line-Of-Sight (NLOS) if

1. the antenna at the subscriber's station is aimed at the base station antenna,
2. there are one or more obstructions in the 1^{st} Fresnel zone, and
3. the obstructions in the line-of-sight path are not totally opaque, meaning that there is sufficient signal power at the receiver for the system to work.

The performance of MMDS radio systems with LOS transmission does change slowly with time. However, MMDS systems with NLOS transmission may experience performance degradation from time to time, due to a moving obstruction.

It is pointed out that NLOS can have a different meaning. In recent publications, NLOS refers to a system where the subscriber's antenna is not aimed at the base station

but rather aimed at an object such as a building to receive a reflection of the signal transmitted by the base station. MMDS is not designed for this type of transmission; however, research for this type of transmission is being done but is still at an early stage. In this thesis, the scope of the term Near Line-Of-Sight (NLOS) is limited to a line-of-sight path with translucent obstructions.

1.2.2 Deployment of MMDS Radio Systems

MMDS was initially intended as a one-way link to high schools located in rural areas. The purpose was to provide video programs to aid in teaching. Communication from student to instructor was not accommodated by MMDS. This upstream communication was accomplished by audio conferencing over the telephone network. In 1998, the Federal Communications Commission (FCC) opened the MMDS channel for two-way use and at the same time made the channel available to Internet service providers.

The post 1998 MMDS has two-way communication, long range coverage, relatively low-cost of the infrastructure, and a transmission rate similar to xDSL. The reformed

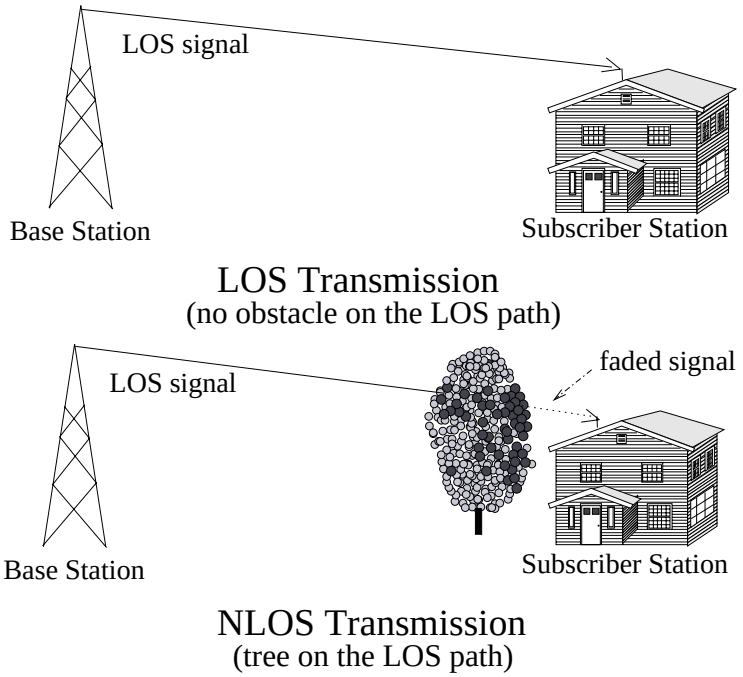

Figure 1.2: LOS Versus NLOS Transmissions

MMDS is a very attractive "last mile" vehicle for high-speed Internet access for residential and "Small Office / Home Office" (SOHO) use. Unfortunately, it is not possible to place a base station so that all subscribers' stations have LOS transmission. One of the most common obstructions is trees in the vicinity of the subscriber's antenna.

It has been suggested that LOS transmission can be achieved only for 40% to 60% of potential subscribers [1]. The exact percentage largely depends on the topography. It will be quite small if the MMDS radio system is deployed in a mountainous region and quite large if the system is deployed in a prairie or flat region.

Typical areas that would be covered with a MMDS radio system are suburban or rural residential areas. As residential areas mainly consist of 1 to 2-storey family homes, the primary obstacle that prevents potential subscribers from having LOS transmission with the base station is tree foliage. MMDS base Internet service has been provided for a few years. Subscribers with LOS paths get reliable service. However, subscribers with a NLOS path, where the obstruction is tree foliage, experience momentary loss of service at times. On dry days with little wind such NLOS systems work very well. However under conditions of rain and wind, momentary losses of the signal can occur due to the motion of wet leaves in the wind, causing a reduction of the throughput rate.

1.3 Objectives of This Research

Models are available to predict the wideband RF signal attenuation caused by tree foliage [2][3][4], and models are available to estimate the channel delay spread [2][5], which is an indication of the multipath structure of the channel. There have been detailed studies of the polarization of backscatter signals from vegetation such as cereal crops [6]. This work shows that scattering from foliage can cause changes in the polarization state of the signal.

Frequency selective attenuations occur if the amplitudes of different frequencies in the bandwidth of interest are attenuated differently. The phase response of the channel is also important. If the phase response is nonlinear, the receiver will not work properly and the bit error rate will increase. Unfortunately, changes in the phase of the signal cannot be detected by measuring power with a single antenna.

Signal distortion caused by the motion of tree foliage obstructing the line-of-sight path translates into variations in the amplitude and phase response of the channel. Knowledge of the variations in the amplitude and phase response of the channel is critical in order to efficiently design a system that can compensate for these variations. The objectives of this research are to:

1. Devise a high precision Digital Signal Processing (DSP)-based measuring system to accurately measure the variations in the amplitude and phase response of the channel caused by tree foliage obstructions to the RF line-of-sight signal.

2. Construct this DSP-based measuring system.

3. Quantify the effect of noise on the measurements obtained with this system, and further process the measurements to reduce the effect of noise.

4. Perform outdoor measurements with one tree and several trees in the line-of-sight under different weather conditions.

5. Perform an analysis of the measurements in order to identify and quantify the type of distortions caused by tree foliage .

To summarize, the objective of this research is to devise a measuring system to accurately measure and characterize the signal distortions caused by tree foliage obstructions to a RF line-of-sight MMDS channel.

1.4 Thesis Organization

Chapter 2 defines the type of distortions that could possibly be introduced to the LOS RF signal of a MMDS radio channel due to tree foliage in the line-of-sight.

Chapter 3 starts by providing a list of the specifications for the measuring system. This chapter continues with a description of a DSP-based measuring system that meets these specifications.The DSP-based measuring system is composed of an acquisition system and a post-processing system. Chapter 4 describes the acquisition system. The post-processing system is described in Chapter 5.

The effect of Gaussian noise on the measurements is addressed in Chapter 6. Chapter 7 indicates how the measurements obtained with this system can be further processed to reduce the effect of this noise.

Outdoor measurements were performed with a single Poplar tree and a bush of Poplar trees in the line of sight. Chapter 8 reports the conditions in which these measurements were performed, and gives the results of these measurements along with an analysis.

The conclusions for this research are given in Chapter 9.

2. DISTORTION OF THE RF LOS SIGNAL

This chapter gives a description of the wireless channel, briefly explains how tree foliage can affect the RF signal, and shows that the distortion of the RF signal can be the result of multipath combined with trees in the line-of-sight path. The results of a literature search on the effect of tree foliage on RF transmissions are also given at the end of this chapter.

2.1 The Wireless Channel

In wireless transmission, the channel is the physical environment surrounding the transmit and receive antennas. Elements such as hills, buildings, or trees located on the path of the RF signal affect the way the signal propagates. Most of the changes occurring on the signal propagation paths can be explained in terms of reflection, diffraction, and scattering. Reflection occurs when the electromagnetic wave impinges the smooth surface of an object having a size much larger than the wavelength of the RF signal. Diffraction takes place when a very dense object with a sharp edge is located very near the LOS path. Waves bend over the sharp edge of the structure and reach the receiver. If the object is opaque and is in the line-of-sight path, then the only signal reaching the subscriber's antenna is the diffracted signal. This phenomenon is called shadowing since the signal reaches the receiver despite the total obstruction of the LOS signal. Scattering occurs when the electromagnetic wave impinges upon objects of size comparable to or shorter than the wavelength. The resulting signal is composed of electromagnetic waves propagating in all directions. Buildings and hills can reflect or diffract the signal(Figure 2.1) while tree foliage, lampposts, or street signs are more likely to scatter the signal.

For ideal LOS transmissions (e.g. no distortion of the signal due to scattering, reflection, or diffraction), only the free space path loss contributes to the attenuation of the RF signal. The attenuation of the RF signal due to propagation in free space is, when expressed in dB, equal to $20\log(4\pi d/\lambda)$ dB, where d is the distance traveled and λ is the

wavelength of the signal.

The presence of objects in the environment often creates reflection, diffraction, or scattering, which causes signal distortion. The received signal will not only consist of the LOS signal, but also of several secondary signals traveling on different paths(see Figure 2.1). These secondary signals are called multipath signals since they originate from the presence of multi-propagation paths. Since these multipath signals travel longer distances than the LOS signal, they arrive at the receive antenna after the LOS signal. The late arrivals become interference and cause distortion to the LOS signal. This type of distortion is frequency selective.

One way to reduce the effect of multipath on the signal is to use a high gain directional antenna. The multipath signals arrive at the receive antenna with different incident angles than the signal from the LOS path (Figure 2.2). The directional antenna does not collect the multipath signals, at least not with the same gain. The multipath signals that add to

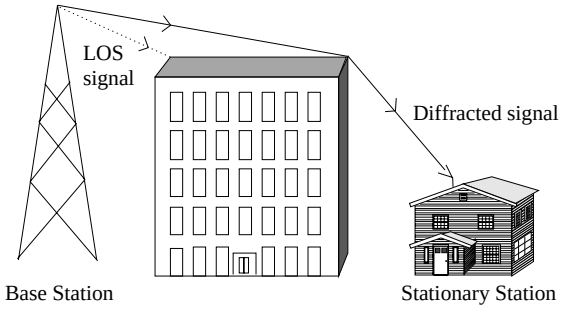

Example of Diffraction

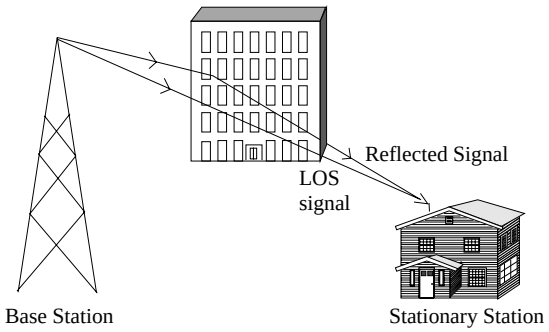

Example of Reflection

Figure 2.1: Examples of Diffraction and Reflection of The RF Signal

the LOS signal are the ones with an incident angle inside the main lobe of the antenna. The main lobe of a high gain antenna is quite narrow, which means only the multipath signals arriving at very small angles are sufficiently amplified to cause distortions to the LOS signal.

The multipath signals arrive later than the LOS path. The multipath signals that are in the main lobe of the antenna arrive a short time after the LOS signal. This is because propagation paths with small incident angles cannot be much longer than the LOS path (Figure 2.2). As the delay spread is very small, intersymbol interference (ISI) is not likely to occur, unless the bit rate is very high. ISI occurs if a symbol of a received sequence of symbols interferes with the next symbol of the sequence.

In addition to reducing the effect of multipath, a high-gain directional antenna is used at the subscriber site of a MMDS radio system because of its high gain. Less power is required at the base station for the transmission of the signal or alternatively the transmission rate can be increased.

2.2 Effect of Tree Foliage on The RF signal

The transmit and receive antenna of the measuring system devised in this research are both vertically polarized. A vertically polarized wave is shown on the top graph of Figure 2.3. The axis along the direction of propagation represents time and the vertical axis represents

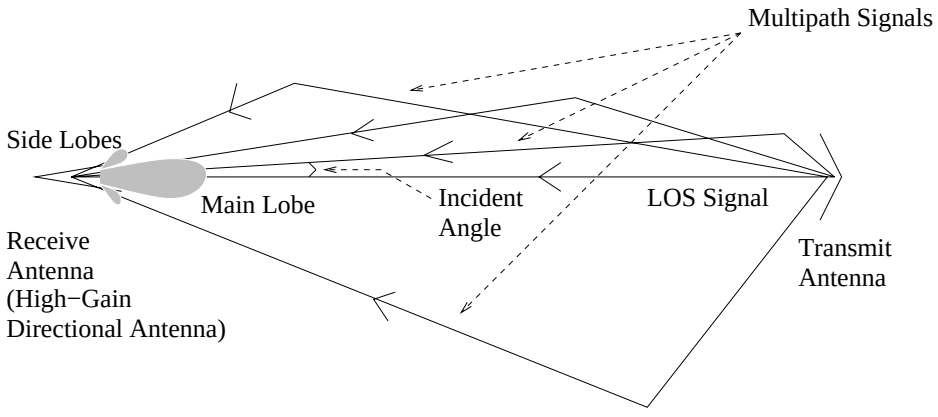

Figure 2.2: Reducing Multipath with a High-Gain Directional Antenna

amplitude.

The problem of interest treats the output of the vertically polarized receive antenna as the signal. The intent is to characterize the time-varying nature of this signal through measurements. The approach taken does not require detailed knowledge of the physics of electromagnetic propagation (e.g. scattering, diffraction, and reflection of the incident wave). However, it is useful to have a general understanding of these phenomena, as they explain the behavior of the signal arriving at the receive antenna.

The polarization state of the transmitted electromagnetic wave can be affected by the vegetation that acts as a scatter [6]. Some of the energy from the transmitted vertical polarization state is transferred to the horizontal polarization state by scattering or reflection of the transmitted electromagnetic wave. The middle graph of Figure 2.3 shows a horizontally polarized wave that could be generated by scattering or reflection of the vertically

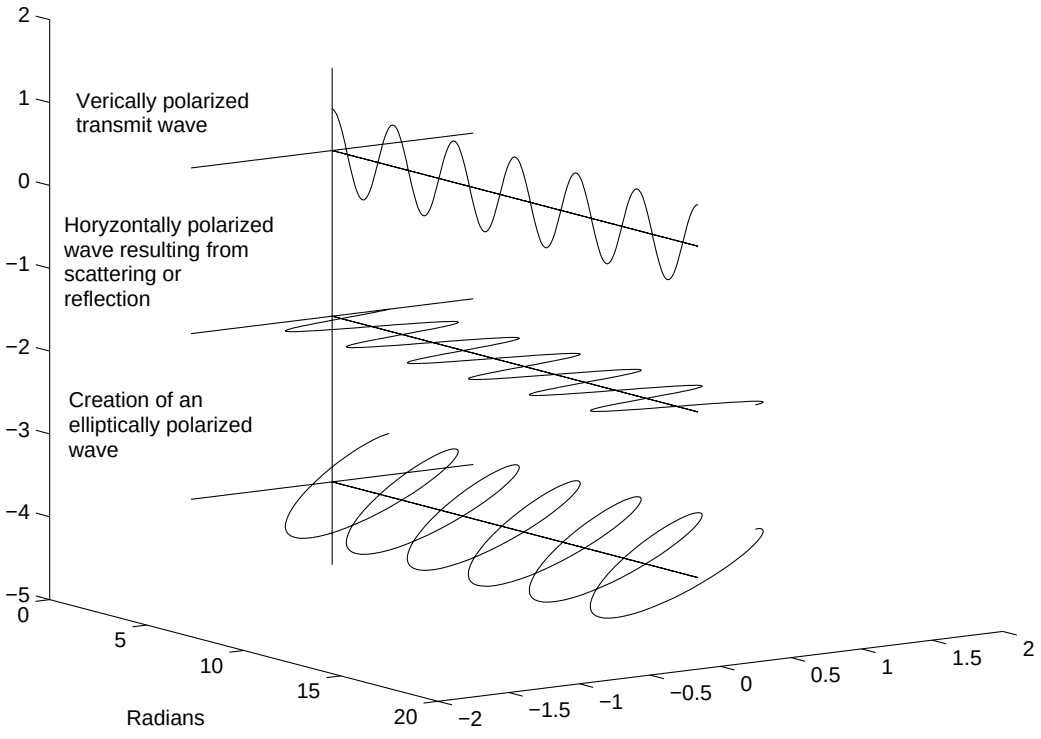

Figure 2.3: Creation Of an Elliptically Polarized Wave ($\Delta\theta = \frac{\pi}{5}$)

polarized incident wave. If the phase difference, $\Delta\theta$, between the vertically polarized and horizontally polarized waves differs from $k\frac{\pi}{2}, k = 0, 1, 2, ...$, then these waves combine into an elliptically polarized wave, as shown by the bottom graph of Figure 2.3, when $\Delta\theta = \frac{\pi}{5}$. The polarization state of the RF signal resulting from the combination of the vertically polarized and horizontally polarized waves is function of the difference of phase, $\Delta\theta$, but also of the amplitudes, E_{0x} and E_{0y}, of these two waves. The polarization state of the receive signal, based on these parameters, is given by [7]

$$(\frac{E_y}{E_{0y}})^2 + (\frac{E_x}{E_{0x}})^2 - 2(\frac{E_x}{E_{0x}})(\frac{E_y}{E_{0y}})\cos(\Delta\theta) = \sin^2(\Delta\theta), \tag{2.1}$$

where E_x is the horizontally polarized component of the receive signal, and E_y is the vertically polarized component of the receive signal. For example if $\Delta\theta = \frac{\pi}{2} + 2k\pi, k = 0, 1, 2, ...$, and $E_{0x} = E_{0y} = E_0$, then (2.1) becomes

$$(E_y)^2 + (E_x)^2 = (E_0)^2. \tag{2.2}$$

Equation (2.2) is the equation of a circle; in other words the polarization is circular. If $\Delta\theta = k\pi, k = 0, 1, 2, ...$, then 2.1 becomes

$$E_y = \pm\frac{E_{0y}}{E_{0x}}E_x, \tag{2.3}$$

and the polarization is linear.

Each branch and each leaf on the RF signal propagation paths will affect E_{0x}, E_{0y}, and $\Delta\theta$ differently. This will result in a receive signal that can be modeled as the sum of an elliptically polarized signal and an unpolarized signal corresponding to noise. Both of these signals vary with time, especially when the wind blows through the trees and changes the structure of the foliage. The system devised in this research measures the temporal variation in the vertically polarized component of the receive signal.

The effect of the leaves may change when the leaves are wet since the RF signal is in the 2.5 GHz frequency range and water is known to absorb radio waves in that frequency range.

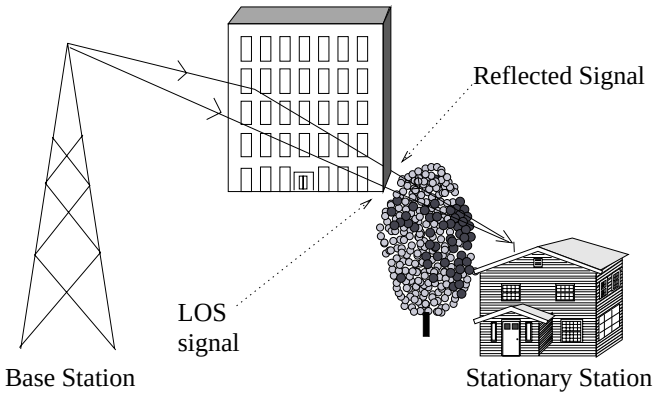

Figure 2.4: Multipath / Tree Foliage LOS Signal Distortions

2.3 Effect of Multipath

Multipath signals are very common on wireless transmission since the presence of one object in the area surrounding the antennas can contribute to the creation of multipath signals. Therefore, it is very difficult to find a site free of multipath, which means that multipath will be present for most subscribers. Multipath due to stationary objects such as buildings or rooftops, causes distortions that do not vary with time. These distortions are usually not harmful for a communication system since they can be corrected with slow equalizers. This ceases to be true when there is tree foliage obstruction to the line-of-sight. For example, Figure 2.4 shows a situation where a signal reflected by a building combines with the LOS signal at the receive antenna. These signals travel through different portions of the tree. If the foliage density is not uniform, these signals are likely to be attenuated differently. If the reflected signal is quite strong, this signal may become stronger than the LOS signal if it is less attenuated than the LOS signal by the tree. The motion of the tree changes the foliage density seen by these two signals. The LOS signal may then become stronger than the reflected signal. This example shows that multipath created by stationary objects can cause selective fading that varies with time due to the swaying of the tree branches present in the line-of-sight.

2.4 Previous Research On Effect of Tree Foliage On RF Transmissions

There have been many publications in the last 5 years on the characterization of wireless channels for MMDS or LMDS (Local Multipoint Distribution Service) radio systems. LMDS and MMDS radio systems are similar; however, the frequency used for the LMDS radio system is approximately 29 GHz. Due to significant attenuation by rain of the 29 GHz electromagnetic waves, LMDS cells are limited to 1 km radius in comparison to 48 km for MMDS.

The results of some of these studies have been compiled in documents [2] published by the IEEE802.16 standard. The IEEE 802.16 Working Group develops standards and recommended practices to support the development and deployment of broadband Wireless Metropolitan Area Networks.

Signal attenuation with or without vegetation, delay spread, Doppler spread, and polarization changes are the main factors found in the literature to characterize the wireless channel. Models for some of these factors are given in [2]. Values for these factors depend on topography, foliage density, type of antennas, and the height of the antennas used.

This section covers some of the published results in situations where one or more trees were present on the LOS path and the terrain was flat.

2.4.1 Signal Attenuation

In an experimental study [3] of RF signal propagation through a plantation of Orchad trees, the propagation loss of a 9.6GHz continuous wave (CW) signal was reported as a function of the number of trees located on the transmission path. The trees were 8-10 meters tall, with a span of branches almost covering the space between trees. Measurements were conducted when trees had no leaves and when trees were fully foliated.

The propagation loss measured for the first 30 meters traveled through the tree canopy was about 1 dB/m with foliage and 0.35 dB/m without foliage. Propagation losses beyond 30 meters were similar when the trees were fully foliated or without leaves. A theoretical explanation of these results for trees in leaf or without leaves was also provided:

With leaves: The LOS signal had a strong attenuation rate in foliage but remained the

main component of the received signal for short distances. Beyond a distance of 30 meters, electromagnetic waves generated by multiple scattering due to the leaves became the main component of the received signal. This signal had a much reduced attenuation rate through foliage than the LOS signal.

Without leaves: Scattering due to branches built up at a slower rate and became the main component of the signal only after 80 meters.

Not only did the results given in [3] apply to an Orchad tree, but they were largely dependent on the propagation path that was selected to perform the measurements. Due to the non-uniformity of the tree foliage, large variations in the received signal power had been reported in [4] when these measurements were performed with various incident angles. However, it was feasible to overlay the curves showing measured signal levels as a function of incident angle with Ricean density functions whose parameters were functions of the foliage structure and the environment in which the experiment was conducted. Therefore, a statistical approach better accounted for the non uniformity of the tree foliage when measuring foliage attenuation.

What made this statistical approach valid was that it was possible to perform enough independent measurements without changing the setup of the experiment. This was accomplished in an anechoic room by placing tree foliage on a table that was rotated by 1 degree between measurements. The antennas remained fixed and only the combined received power for the LOS signal and the scattered signal varied as the foliage was rotated. A 360 degree rotation of the table allowed the measurement of a suitable statistical database. Keeping the antennas fixed while changing the orientation of the foliage by rotating the table produces a homogeneous sample.

To summarize, the received signal after propagation through tree foliage is composed of the attenuated LOS signal and of a signal generated by scattering of the electromagnetic waves by the leaves. These scattered signals may have been generated either by the trees on the LOS path or by the trees located on each side of this path. Models for signal attenuation by tree foliage are based on Ricean distributions whose two parameters are usually defined as the average total power received and the ratio K of the LOS average

signal power and the mean scattered signal power.

2.4.2 Delay Spread

It is very common on a wireless channel for multipath signals to arrive at the receive antenna at different times and with different strengths due to reflection, diffraction or scattering of the electromagnetic waves. The first transmit signal arriving at the receive antenna is the LOS signal. Its propagation path is the direct path between both antennas and therefore is the shortest. Delay spread is an indication of the difference of time of arrival at the receive antenna between the LOS signal and delayed signals caused by reflection, diffraction, or scattering. This parameter is used to predict the amount of inter-symbol interference (ISI) for a given communication scheme.

The RMS delay spread, which is a measure of the delay spread, is reported [5] to be less than 0.25 us based on measurements performed at 1.9 GHz in a suburban area with a fixed terrestrial wireless system which employed a directional antenna at the receive location.

2.4.3 Doppler Spread

For a fixed wireless radio system, the Doppler shift is introduced by foliage moving in the wind. The typical measured Doppler spread at 2.5 GHz is less than 2 Hz [2].

3. A DSP-BASED SYSTEM TO MEASURE THE SIGNAL DISTORTION CAUSED BY TREE FOLIAGE

3.1 Notation

There are many symbols used in this thesis which makes it difficult for the reader to remember what each symbol represents. To help the reader remember and sort out the different symbols, a notation system with some simple rules is used. The name of a function representing a waveform is accompanied by a subscript. An uppercase subscript indicates that it is a continuous-time waveform. A lowercase subscript indicates that it is a discrete-time waveform. The letters used for the subscript also have meaning. For example, the subscript "RF" denotes a continuous-time radio frequency signal and the subscript "l" denotes a lowpass equivalent discrete-time signal. When a superscript is present, it indicates that an action has been performed on the waveform. The superscript "r" indicates that the waveform has been resampled. The superscript "w" indicates that the waveform has been truncated with a window. Using these notations, the continuous-time RF receive signal is denoted by $r_{RF}(t)$. The signal obtained after down-converting $r_{RF}(t)$ to an intermediate frequency (IF) is denoted by $r_{IF}(t)$. The signal obtained after sampling $r_{IF}(t)$ is a discrete-time signal, $r_{if}[n]$. For a sampling period T_r, the sampled signal can be denoted by $r_{IF}(nT_r)$, where n is an integer. The discrete-time signal, $r_{if}[n]$, is equivalent to $r_{IF}(nT_r)$.

A parameter that applies to a continuous-time waveform is written in uppercase letters. Its subscript is also in uppercase. A parameter that applies to a discrete-time waveform is written in lowercase letters. Its subscript is also in lowercase. For example, the carrier frequency of the continuous-time IF receive signal, $r_{IF}(t)$, is denoted by F_{IF}, which is expressed in Hertz. If the intermediate frequency is expressed in radian / second, then it is denoted by Ω_{IF}, where $\Omega_{IF} = 2\pi F_{IF}$.

The sampling rate is defined as the number of samples per second. In case of an analog to digital conversion, the sampling rate indicates how many times the analog signal is sampled per second. In case of a digital to analog conversion the sampling rate indicates how many samples are used per second to generate an analog signal. As the analog-to-digital conversion takes place in the receiver, the sampling rate of the A/D converter is denoted by F_r. As the digital-to-analog conversion takes place in the transmitter, the sampling rate of the D/A converter is denoted by F_t. The sampling frequencies, F_r and F_t, have units of samples/second.

The carrier frequency of the discrete-time IF receive signal, $r_{if}[n]$, is denoted by f_{if}, which is expressed in cycles/sample. This is because the sampling frequency, F_r, has unit of samples / second, and $f_{if} = \frac{F_{IF}}{F_r}$ has units $\frac{\text{cycles / second}}{\text{samples / second}} = \frac{\text{cycles}}{\text{sample}}$. If the intermediate frequency is expressed in radians / sample, then it is denoted by ω_{if}, where $\omega_{IF} = 2\pi f_{if}$.

3.2 A Suitable Measuring System

The objective of this research is to devise a system to accurately measure the distortions introduced to the RF LOS signal of a MMDS radio channel whose line-of-sight is obstructed by tree foliage and vertically polarized antennas are employed at the transmitter and receiver. The NLOS channel of interest has 4 salient features:

1. As the targeted radio channel is a MMDS radio channel, the signal bandwidth is 6 MHz between 2.5 GHz and 2.7 GHz.

2. For NLOS transmissions where tree foliage is the obstruction in the line-of-sight path, the motion of the branches in the direction of the propagation path changes the carrier frequency of the signal as the signal is reflected or scattered by the trees before being collected by the receive antenna. This change in frequency is called the Doppler shift, and it depends on the carrier frequency and the component of the velocity of the branches that is in the direction of the propagation path. For a MMDS radio channel, the maximum Doppler shift due to trees in the line-of-sight path is expected to be less than 2 Hz [2].

3. It is assumed that the rate at which the signal fades is less than 50 dB/s and that

the channel can be considered time-invariant for intervals less than 5 ms. However, the system should be able to measure variation in the channel response for intervals that are much less than 5 ms.

4. It is assumed that the fades last between 100 ms and 1 s and successive fades can occur in an interval whose duration is few seconds. The system should be able to continuously record the receive signal for a duration of at least 5 seconds. Clearly, the signal fading depends on the weather conditions (e.g. rain, wind...). Several acquisitions of the receive signal with the same weather conditions will allow the measurement of a suitable statistical database. Several statistical database are obtained by acquiring the receive signal with different weather conditions, and characterize the signal fading for different weather conditions.

One type of measuring scheme consists of transmitting a band-limited RF pulse. The receive signal is an estimate of the impulse response of the channel. Taking the Fourier transform of this estimate yields an estimate of the channel frequency response. A description of this type of measuring system is given in Appendix A. A train of band-limited RF pulses, where the pulses are separated by ΔT seconds, can be used to estimate the variations in the amplitude and phase response of the channel over intervals of length ΔT seconds. An alternate approach is to send a set of continuous wave (CW) RF tones that are inside the channel bandwidth. The amplitude and phase of the receive RF tones can then be measured at times ΔT seconds apart to estimate the variations in the amplitude and phase response of the channel. This approach has the advantage of eliminating the need for a sharp 6MHz channel filter.

This approach is best described by first considering the case of transmitting a single CW tone, denoted $s1_{RF}(t)$, at a RF frequency F_C. If $s1_{RF}(t)$ has a constant amplitude equal to 1V, and constant phase, Φ, at the output of the transmitter, the transmit signal, $s1_{RF}(t)$, is given by

$$s1_{RF}(t) = \cos(2\pi F_C t + \Phi). \tag{3.1}$$

The transmitted RF tone travels through tree foliage before reaching the receive antenna. This has the effect of changing its amplitude and its phase. The changes in amplitude

and phase also vary with time due to the motion of tree foliage. If $A(t)$ denotes the time-varying amplitude and $\Theta(t)$ the time-varying phase of the single receive tone, then the receive signal, $r1_{RF}(t)$, can be expressed as

$$r1_{RF}(t) = A(t)\cos(2\pi F_C t + \Theta(t)). \tag{3.2}$$

The values of $A(t)$ and $\Theta(t)$ at a particular instant, can be estimated using a finite-time approximation to the Fourier transform. This can be done provided that $A(t)$ and $\Theta(t)$ are essentially constant over the interval that the finite-time Fourier transform is computed. The values computed for $A(t)$ and $\Theta(t)$ over the interval $(t_0, t_0+\Delta T)$ are then estimates of the amplitude and phase of the receive tone at instant of time $\frac{t_0+t_0+\Delta T}{2} = t_0 + \frac{\Delta T}{2}$. Similarly, the computed values for $A(t)$ and $\Theta(t)$ over the interval $(t_0+\Delta T, t_0+2\Delta T)$ are estimates of the amplitude and phase of the receive tone at instant of time $\frac{t_0+\Delta T+t_0+2\Delta T}{2} = t_0 + \frac{3\Delta T}{2}$. The variations in the amplitude and phase response of the channel at frequency F_C can then be estimated over the intervals $(t_0+\frac{\Delta T}{2}, t_0+\frac{3\Delta T}{2})$, $(t_0+\frac{3\Delta T}{2}, t_0+\frac{5\Delta T}{2})$, etc.

These variations in the amplitude and phase response of the channel can be estimated at several other frequencies using several tones. This is achieved by sending N tones in the 6MHz band within 3MHz of F_C. If the N tones sent have respective RF frequencies F_C+F_i $(i=0,\ldots,N-1)$, a constant amplitude of 1V and constant phase, Φ_i, at the output of the transmitter, then the transmit signal, denoted $sN_{RF}(t)$ in this example, is given by

$$sN_{RF}(t) = \sum_{i=0}^{N-1} \cos(2\pi(F_C+F_i)t + \Phi_i). \tag{3.3}$$

The receive signal is then the resultant of the N tones whose amplitude and phase vary as a function of time. The presence of thermal noise and noise impinging on the receive antenna has the effect of corrupting the receive signal. The effect of this noise can be modeled as zero-mean white additive Gaussian noise, denoted $N(t)$. The receive signal, $rN_{RF}(t)$, is then given by

$$rN_{RF}(t) = \sum_{i=0}^{N-1} A_i(t)\cos(2\pi(F_C+F_i)t + \Theta_i(t)) + N(t). \tag{3.4}$$

Sending N CW tones is a suitable system to measure the variations in the amplitude and phase response of the channel over intervals of length ΔT, where ΔT is less than 5ms.

3.3 Estimating the Amplitude and Phase Of The Tones With A FFT

In this thesis, the fast Fourier transform (FFT) is used as the finite-time approximation to the Fourier transform to estimate $A_i(t)$ and $\Theta_i(t)$ at times ΔT seconds apart. To compute estimates for $A_i(t)$ and $\Theta_i(t)$, the signal used for the FFT must be derived from the receive signal, $rN_{RF}(t)$ (3.4). The FFT applies to a discrete-time signal. Therefore, $rN_{RF}(t)$ has to be sampled. This requires using an A/D converter at the receiver. In order to be within the analog bandwidth of the A/D converter, $rN_{RF}(t)$ has to be down-converted to an intermediate frequency (IF), F_{IF}. The down-converted signal is denoted by $rN_{IF}(t)$. If F_r is the sampling rate of the A/D converter then the signal obtained after sampling $rN_{IF}(t)$, is given by

$$\begin{aligned} rN_{if}[n] &= \sum_{i=0}^{N-1} a_i[n]\cos(2\pi\frac{(F_{IF}+F_i)}{F_r}n+\theta_i[n])+\eta[n] \\ rN_{if}[n] &= \sum_{i=0}^{N-1} a_i[n]\cos(2\pi(f_{if}+f_i)n+\theta_i[n])+\eta[n], \end{aligned} \tag{3.5}$$

where $a_i[n] \equiv A_i(nT_r)$ with $T_r = 1/F_r$, $\theta_i[n] \equiv \Theta_i[nT_r]$, and $\eta[n] \equiv N(nT_r)$. As $a_i[n_0]$ and $\theta_i[n_0]$ are respectively equal to $A_i(t_0)$ and $\Theta_i(t_0)$ with $t_0 = n_0T_r$, provided that no aliasing occurs, then estimates of $A_i(t)$ and $\Theta_i(t)$ from $rN_{RF}(t)$ can be obtained by computing estimates of $a_i[n]$ and $\theta_i[n]$ from $rN_{if}[n]$. The FFT is used to compute estimates of $a_i[n]$ and $\theta_i[n]$. At this point, it is convenient to give some brief explanations on how the FFT works in order to help the reader understand how the FFT is applied in this research to obtain good estimates of $a_i[n]$ and $\theta_i[n]$. This will lead us to introduce some new symbols.

The L-point FFT of a sequence $x[n]$ such that $x[n] = 0$ outside the interval $0 \le n \le L-1$ can be defined as

$$X[i] = \begin{cases} \sum_{n=0}^{L-1} x[n]e^{-j2\pi\frac{i}{L}n}, & 0 \le i \le L-1 \\ 0, & \text{otherwise,} \end{cases} \tag{3.6}$$

where L is the number of samples used in computing the FFT (also referred to as the length of the FFT), and L is a power of 2 number. From (3.6), the FFT operation consists of projecting the signal $x[n]$ onto the vectors $e^{j2\pi\frac{0}{L}n}$, $e^{j2\pi\frac{1}{L}n}$, ..., $e^{j2\pi\frac{L-1}{L}n}$. $X[0]$ is the complex factor obtained after projecting $x[n]$ onto $e^{j2\pi\frac{0}{L}n}$, $X[1]$ is the complex factor obtained after projecting $x[n]$ onto $e^{j2\pi\frac{1}{L}n}$, etc. These L vectors or complex exponential

functions, $e^{j2\pi\frac{i}{L}n}$, with $0 \leq i \leq L-1$, are mutually orthogonal over the period L since for 2 complex exponential functions, $e^{j2\pi\frac{j}{L}n}$ and $e^{j2\pi\frac{k}{L}n}$ with $0 \leq j,k \leq L-1$, the inner product $\sum_{n=0}^{L-1} e^{j2\pi\frac{j}{L}n}(e^{j2\pi\frac{k}{L}n})^*$ is equal to [8]

$$\sum_{n=0}^{L-1} e^{j2\pi\frac{j}{L}n}(e^{j2\pi\frac{k}{L}n})^* = \begin{cases} L, & \text{if } j=k \\ 0, & \text{otherwise,} \end{cases} \tag{3.7}$$

where $(e^{j2\pi\frac{k}{L}n})^* = e^{-j2\pi\frac{k}{L}n}$ is the complex conjugate of $e^{j2\pi\frac{k}{L}n}$. Furthermore, as the L complex exponential functions, $e^{j2\pi\frac{i}{L}n}$, form a complete orthogonal set [8] over the period L, then $x[n]$ can be exactly decomposed onto this set and is equal to

$$x[n] = \begin{cases} \frac{1}{L}\sum_{i=0}^{L-1} X[i]e^{j2\pi\frac{i}{L}n}, & 0 \leq n \leq L-1 \\ 0, & \text{otherwise.} \end{cases} \tag{3.8}$$

The orthogonality denoted by (3.7) is a very interesting property that is used when devising the measuring system in order to obtain good estimates of $a_i[n]$ and $\theta_i[n]$. Assume that $x[n]$ is made of the complex exponential functions, $e^{j2\pi f_i n}$, where f_i with $i = 0,\ldots,N-1$ are the digital frequencies defined in (3.5). With this assumption, $x[n]$ can be written as

$$x[n] = \begin{cases} \sum_{i=0}^{N-1} c_i e^{j2\pi f_i n}, & 0 \leq n \leq L-1 \\ 0, & \text{otherwise,} \end{cases} \tag{3.9}$$

where the c_i terms are complex, with magnitude, denoted a_i, and phase, denoted θ_i such that $c_i = a_i e^{j\theta_i}$. If the digital frequencies, f_i, are equal to $\frac{i}{L}$ cycle/sample, then (3.9) can be rewritten as

$$x[n] = \begin{cases} \sum_{i=0}^{N-1} a_i e^{j\theta_i} e^{j2\pi\frac{i}{L}n} = \sum_{i=0}^{N-1} a_i e^{j(2\pi\frac{i}{L}n+\theta_i)}, & 0 \leq n \leq L-1 \\ 0, & \text{otherwise,} \end{cases} \tag{3.10}$$

In this decomposition, $x[n]$ is expressed as a linear combination of the first N of the L complex exponential functions, $e^{j2\pi\frac{i}{L}n}$. To have N distinct frequencies f_i, requires that $L \geq N$. The FFT of $x[n]$ is then equal to

$$X[i] = \begin{cases} La_i e^{j\theta_i}, & 0 \leq i \leq N-1 \\ 0, & i \geq N, \end{cases} \tag{3.11}$$

and the amplitude, a_i, and phase, θ_i, of the complex exponential functions of $x[n]$ can easily be computed. The first N complex exponential functions of the set were used to construct $x[n]$ but any of the L complex exponentials could have been chosen. However, if the digital frequencies, f_i, are not integer multiples of $\frac{1}{L}$, then the complex exponential functions, $e^{j2\pi f_i n}$, of $x[n]$ will not be "aligned" with the complex exponential functions, $e^{j2\pi\frac{i}{L}n}$, and cross-coupling between the components of $x[n]$ will then occur. (3.11) will no longer be valid, and it will then become very difficult to compute a_i and θ_i without introducing a large error. Therefore, two important conditions have to be met when devising the measuring system:

1. The frequencies of the tones in the transmitter must be chosen such that the digital frequencies, f_i, of the sampled receive signal, in the receiver are all integer multiples of $\frac{1}{L}$ cycle/sample.

2. The FFT should be applied on the lowpass equivalent signal of $rN_{if}[n]$ since this signal is equal to [9]

$$rN_l[n] = \sum_{i=0}^{N-1} a_i[n]e^{j(2\pi f_i n+\theta_i[n])} + \eta_l[n], \tag{3.12}$$

   and thus is made of the complex exponential functions, $e^{j2\pi f_i n}$, with amplitude $a_i[n]$ and phase $\theta_i[n]$.

In (3.12), $\eta_l[n]$ is the lowpass equivalent of $\eta[n]$.

If L is sufficiently small such that $a_i[n]$ and $\theta_i[n]$ are essentially constant over the L samples $rN_l[0]$, ..., $rN_l[L-1]$, then the estimates of $a_i[n]$ and $\theta_i[n]$ computed with the L-point FFT of $rN_l[n]$ will be approximately equal to $La_i[\frac{L}{2}]$ and $\theta_i[\frac{L}{2}]$. An error is still introduced in this computation due to the noise term, $\eta_l[n]$, in (3.12). L samples are taken during an interval of LT_r seconds. If $LT_r < \Delta T$, then $a_i[n]$ and $\theta_i[n]$ will be essentially constant over the L samples used in the FFT since $A_i(t)$ and $\Theta_i(t)$ were assumed to be constant over ΔT second.

The L-point FFT of $rN_l[n]$ produces estimates of $a_i[n]$ and $\theta_i[n]$ using the first L samples of $rN_l[n]$. This operation assumes that $rN_l[n]$ is zero outside the interval $0 \leq n \leq L-1$. The next L samples can also be used to estimate $a_i[n]$ and $\theta_i[n]$ with a L-point FFT. This

FFT is equal to $\sum_{n=0}^{L-1} r_l[L+n]e^{-j2\pi\frac{i}{L}}$ with $0 \leq i \leq L-1$. Successive L-point FFTs can then be applied to compute estimates of $a_i[n]$ and $\theta_i[n]$ L samples apart. In order to easily tell which samples of $rN_l[n]$ are used in the L-point FFT, a new symbol is introduced. $rN_l^w[n,k]$ denotes the truncated signal derived from $rN_l[n]$ that is equal to

$$rN_l^w[n,k] = \begin{cases} rN_l[n+kL], & 0 \leq n \leq L-1 \\ 0, & \text{otherwise.} \end{cases} \tag{3.13}$$

The L-point FFT of this signal is equal to $\sum_{n=0}^{L-1} rN_l^w[n,k]e^{-j2\pi\frac{i}{L}n}$ with $0 \leq i \leq L-1$, and is denoted $RN_l^w[i,k]$. The estimates of $a_i[n]$ and $\theta_i[n]$ computed with this FFT are denoted $\hat{a}_i[k]$ and $\hat{\theta}_i[k]$. They are estimates of $A_i((kL+\frac{L}{2})T_r)$ and $\Theta_i((kL+\frac{L}{2})T_r)$.

3.4 A DSP-Based Implementation of The Measuring System

Choosing the frequency of the tones to be transmitted is accurately done in the transmitter by generating the transmit signal with digital signal processing. Digital signal processing is also used in the receiver since the receive signal must be sampled, and the lowpass equivalent signal must be constructed before L-point FFTs can be computed for that signal. Furthermore, imperfections in the transmitter and receiver cause the spectrum of the sampled receive signal to be shifted and compressed/expanded. Reconstruction of the spectrum is achieved with digital signal processing. This reconstruction is required to "re-

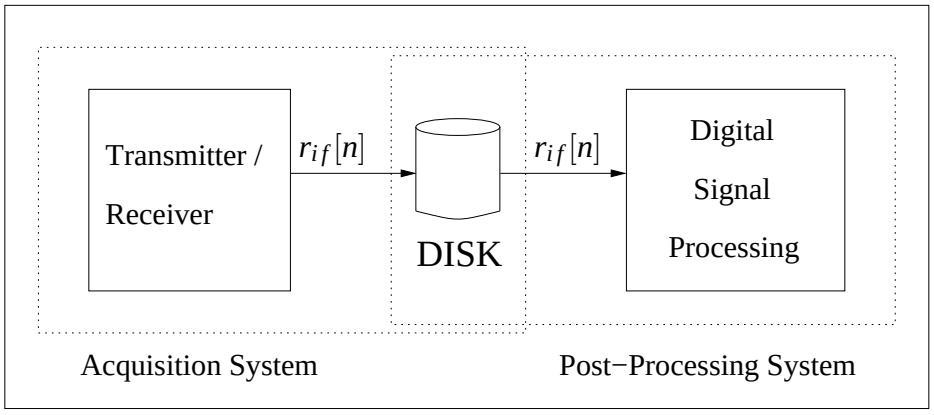

Figure 3.1: Measuring System Block Diagram

align" the complex exponential tones of the lowpass equivalent signal with the complex exponential functions, $e^{j2\pi\frac{i}{L}n}$, used in the L-point FFT. Digital signal processing (DSP) is thus extensively used in this measuring system.

This DSP-based measuring system is composed of 2 sub-systems. This is illustrated in Figure 3.1. The acquisition system is the portion of the system that goes in the field for collecting the data. It includes the transmitter and the receiver. The transmitter generates and transmits a RF signal made of several tones. The signal receive in the receiver is sampled. The sampled receive signal is denoted $r_{if}[n]$ and represents the data collected in the field. The expression for $r_{if}[n]$ is given in Chapter 5 and is based on the expression of $rN_{if}[n]$ given in (3.5). The acquired sampled signal, $r_{if}[n]$, is stored on a disk during the acquisition in the field. No digital signal processing other than sampling the receive signal is performed by the acquisition system. The digital signal processing is done later. Since the digital signal processing is done at a different time than the data collection, it is referred to as post-processing. The post-processing system takes as input the signal, $r_{if}[n]$, recorded in the field by the acquisition system, and computes estimates of the amplitude $A_i(t)$ and phase $\Theta_i(t)$ of the tones.

3.4.1 The Acquisition System

Figure 3.2 shows the data flow diagram of the acquisition system. The IF discrete-time signal generated in the transmitter is denoted $s_{if}[n]$. The expression for $s_{if}[n]$ is given in Chapter 4. $s_{if}[n]$ is converted to analog with a D/A converter and filtered with a reconstruction filter. The reconstructed analog signal, denoted $s_{IF}(t)$, is then up-converted to RF. The up-converted signal, denoted $s_{RF}(t)$, is then transmitted. The RF channel causes the amplitude or phase or both of some or all the tones to vary as a function of time. The MMDS channel is modeled as a filter with a time-varying impulse response. With this model, the RF receive signal, denoted $r_{RF}(t)$, is the output of the channel filter and $s_{RF}(t)$ its input. In the receiver, $r_{RF}(t)$ is down-converted to IF. This means that the center frequency, F_C, of $r_{RF}(t)$ is translated to F_{IF}. The down-converted signal, denoted $r_{IF}(t)$, is then sampled with an A/D converter. The IF sampled signal, $r_{if}[n]$, is then stored on a disk. The detailed operation of the acquisition system is covered in Chapter 4.

3.4.2 The Post-Processing System

The IF discrete-time signal, $r_{if}[n]$, is imported from disk into Simulink. The post-processing consists of computing estimates of the amplitude, $A_i(t)$ and phase, $\Theta_i(t)$, of the tones. This is achieved by correcting the distortions introduced to $r_{if}[n]$ by the acquisition system, generating the lowpass equivalent signal of $r_{if}[n]$, denoted $r_l[n]$, and computing estimates, $\hat{a}_i[k]$ and $\hat{\theta}_i[k]$, of the amplitude and phase of the complex exponential tones of $r_l[n]$, L samples apart. The detailed operation of the post-processing system is covered in Chapter 5.

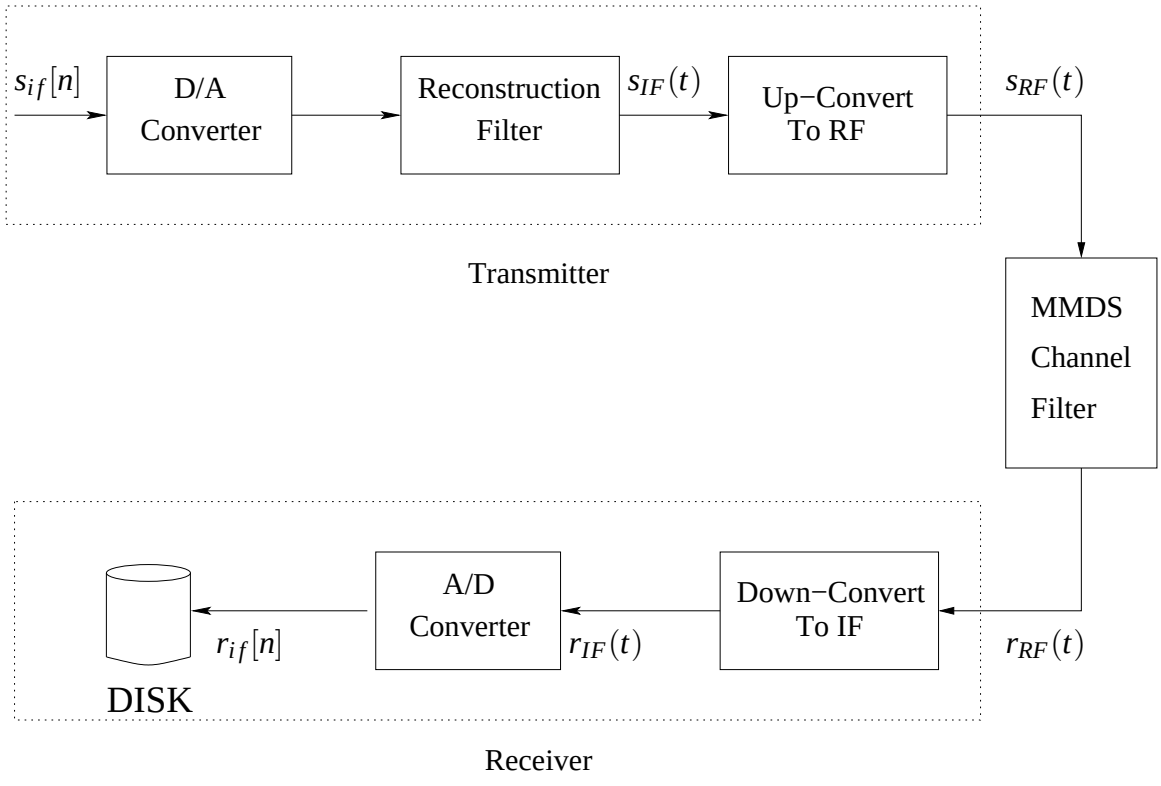

Figure 3.2: Acquisition System Data Flow Diagram

4. THE ACQUISITION SYSTEM

This chapter first gives an overview of the acquisition system along with a description of the hardware. The transmitter and receiver subsystems are described next.

4.1 Acquisition System Overview

The hardware is designed around the TR*Labs* FPGA-based DSP development board [10]. The heart of this board is an Altera APEX FPGA. There are 4 such boards, two of which are used in this project. Two of the boards are populated with a $600,000$ gate APEX part and the other 2 are populated with a $1,000,000$ gate APEX part. All boards include two A/D converters and four D/A converters. Separate development boards are used for the transmitter and receiver. One D/A converter is used in the transmitter, none in the receiver. However, the extra D/A converters are very useful for debugging the Hardware. Figure 4.1 presents the hardware block diagram of the acquisition system. Figure 4.2 shows some views of the acquisition system in the field. Hardware design of the transmitter and receiver is covered next.

4.1.1 Hardware Design of The Transmitter

A TR*Labs* FPGA-based DSP development board is used to generate the digital IF transmit signal, $s_{if}[n]$, and convert this digital signal to an analog signal with a D/A converter running at 100 M samples / second (MSPS). The development board is also used to generate the clock for the D/A converter. The development board has a 10 MHz temperature compensated oscillator that is connected to the clock line of the FPGA. The FPGA has 4 internal PLL units, one of which is used to synthesize a 100 MHz clock for the D/A converter. As the tolerance of the external oscillator is ± 2 ppm (20 Hz), it follows that the tolerance of the 100 MHz clock is also ± 2 ppm (± 200 Hz).

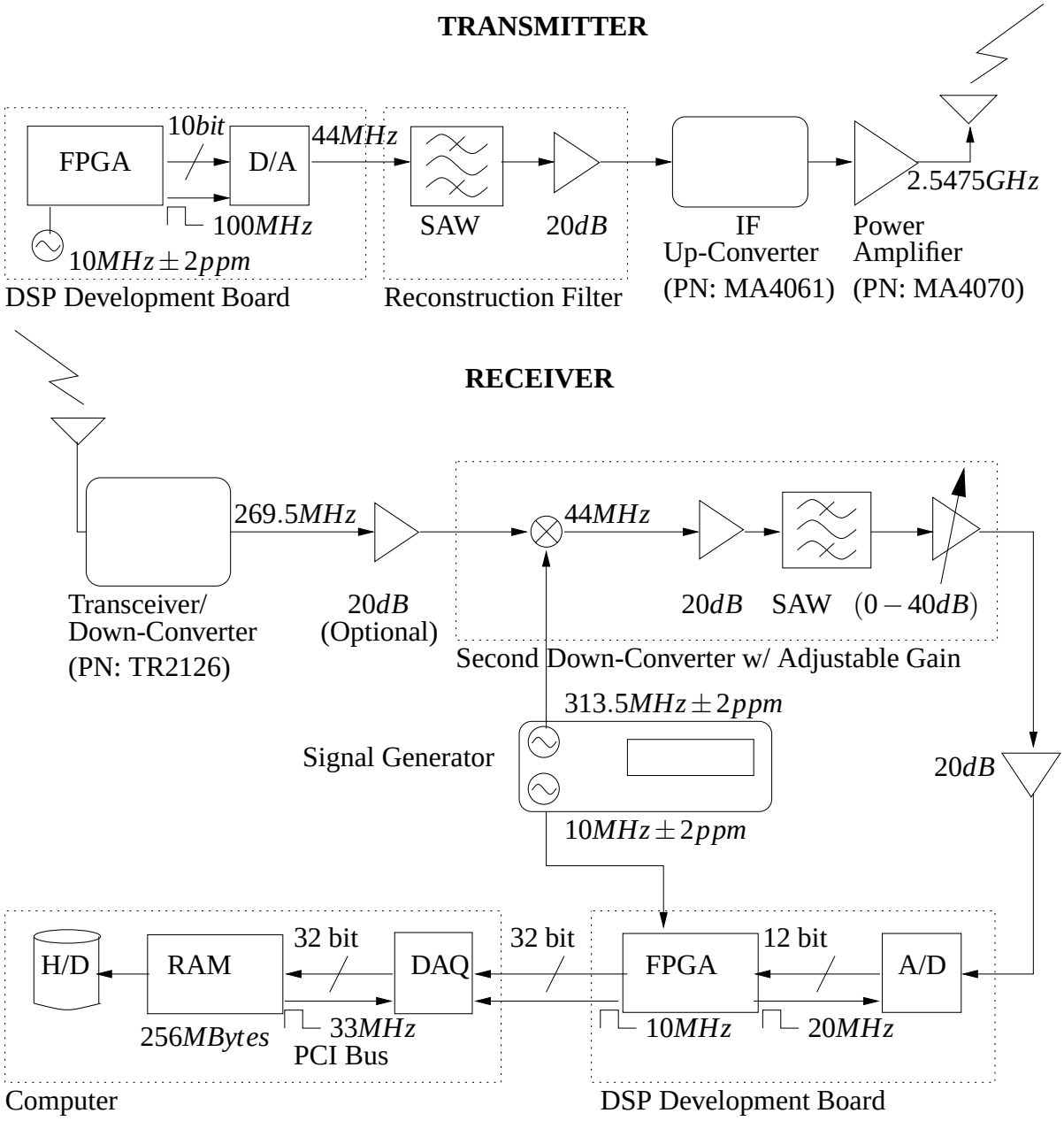

Figure 4.1: Acquisition System Hardware Block Diagram

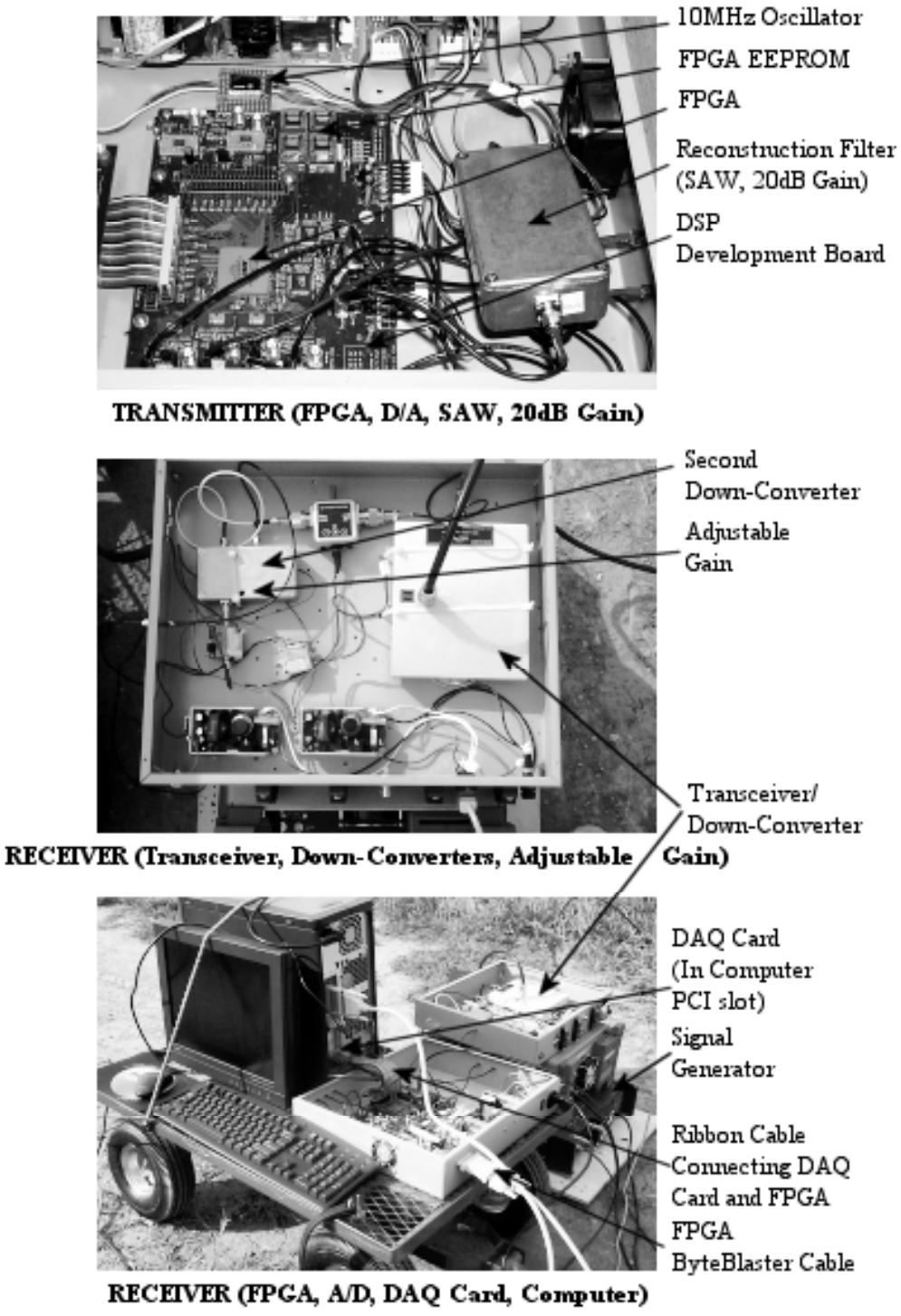

Figure 4.2: Views of The Acquisition System in The Field.

A daughter board was built and connected to the TR*Labs* development board. The daughter board has a band-pass SAW filter and a 20 dB gain amplifier. This board is used as the reconstruction filter for the analog IF output of the D/A. The SAW pass-band filter [11] is centered at 44 MHz and has a bandwidth of 6 MHz. The data sheet indicates that there is a maximum of 1.25 dB p-p ripple in the pass-band and that the p-p phase ripple is at most 4.5 degrees. The maximum insertion loss is 22 dB. The 20 dB gain amplifier of the daughter board is used to compensate for the signal attenuation caused by the SAW filter. The analog signal at the output of the reconstruction filter is up-converted to a RF frequency of 2.5475 GHz, using an off-the-shelf IF up-converter designed for MMDS application [12]. The analog IF signal has a signal level of 25.5 dBmV at the input of the up-converter, which is in the 25 to 35 dBmV recommended range of the up-converter. The level of the output RF signal is set to 0 dBmW or -10 dBmW per tone.

The RF signal is then amplified with an off-the-shelf power amplifier designed for MMDS applications [12]. This amplifier has a fixed gain of 34 dB $\pm$ 2 dB and a gain stability of $\pm$ 0.5 dB (10 to 40^0C) and a gain flatness of $\pm$ 0.3 dB over the 6 MHz band. The power amplifier output is then used to drive the transmit antenna at 30 dBm.

4.1.2 Hardware Design of The Receiver

The RF signal impinging on the receive antenna is down-converted to a frequency of 269.5 MHz. The transceiver / down-converter is an off-the-shelf product designed for MMDS applications. The oscillator of the transceiver / down-converter has a tolerance of $\pm$2 ppm. A second down-converter is used to translate this signal to an intermediate frequency of 44 MHz. An external signal generator is used to synthesize the 313.5 MHz frequency local oscillator signal required to translate the frequency to 44 MHz. A SAW filter identical to the one in the transmitter is used to eliminate the high frequency portion of the spectrum of the down-converted signal, and keep only the portion of the spectrum in the 6 MHz band centered at 44 MHz.

An adjustable gain amplifier allows the user to manually adjust the strength of the IF receive signal before sampling occurs. The quantization performed by the A/D converter in effect adds noise to the digital signal [8]. The quantization noise does not depend on the

signal power. To keep the SNR as high as possible, the receive signal should be amplified to the point of saturating the A/D. The signal level could be adjusted so that the signal p-p is equal to half the range of the A/D so that variation in the amplitude of the signal due to the channel does not saturate the A/D converter.

The A/D converter is a 12 bit resolution device with a 500 MHz analog bandwidth. As F_r is set to 20 MHz and the temperature compensated external oscillator has a tolerance of ± 2 ppm, then the 20 MHz internally generated clock to operate the A/D converter has an accuracy of ± 40 Hz. The A/D voltage range $V_{A/D}$ is 2 V. The format of the digital output is in two's complement.

A data acquisition board (DAQ) mounted inside a computer is used to transfer the receive signal samples from the FPGA into the computer memory in real time. These samples are then written to the computer hard drive (H/D) after the acquisition of the receive signal is complete. The I/O headers of the board where the FPGA is located are used to connect a ribbon cable from the I/O pins of the FPGA to the I/O bus of the DAQ board. The data acquisition card transfers 32-bit words from its input port to the computer RAM through the PCI internal bus of the computer [13]. Tests showed that the system could reliably store 200 M samples, which corresponds to 5 seconds of continuous sampling.

4.1.3 The Antennas

The transmit antenna is a sectoral antenna with a 110 degree azimuthal angle and a 10 degree elevation angle. It is vertically polarized. It has a gain of 13.5 dBi at a frequency of 2.54 GHz. The transmit antenna is shown in Figure 4.3.

The receive antenna is a directional antenna with a beamwidth of 12 degrees. It has a parabolic grid array reflector. As shown in Figure 4.3, it is mounted to collect the vertically polarized component of the incoming RF signal. The feed, as well as the grid, is perpendicular to the ground. It has a maximum gain of 10 dBi at 2.54 GHz.

4.2 The Transmitter of The Acquisition System

Noisy components in the acquisition system and noise impinging on the receive antenna alter the transmit signal and make it more difficult to obtain accurate measurements. The effect of the noise on the transmit signal is minimized by choosing parameters in the transmitter that maximize the Signal-to-Noise Ratio (SNR) at the output of the transmitter. This amounts to maximizing the signal power and minimizing the quantization noise power within the 6MHz bandwidth of the transmit signal.

The signal power should be evenly distributed among the tones after the conversion to an analog signal. For this to happen the tones of the digital signal must be pre-weighted to account for the frequency response of the zero order hold. The zero-order hold inherent to the D/A converter rolls off the higher frequency tones. The amplitude of the i^{th} digital tone is denoted by $(1+\varepsilon_i)$. The $(1+\varepsilon_i)$ terms are calculated as follows. The impulse response of the zero order hold is given by

$$h_{D/A}(t) = \begin{cases} 1, & 0 \leq t < T_t \\ 0, & \text{otherwise,} \end{cases} \tag{4.1}$$

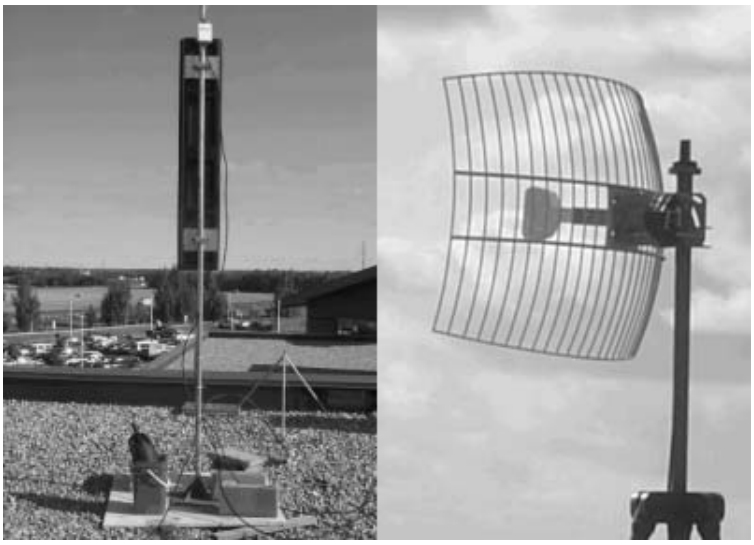

Figure 4.3: Measuring System Antennas: Left - Transmit Antenna, Right - Receive Antenna

where $T_t = 1/F_t$ is the sampling period in the transmitter, expressed in units of seconds/sample. The frequency response is given by the Fourier transform of the impulse response which is expressed as

$$F\{h_{D/A}(t)\} = \int_0^{T_t} e^{-j\Omega t} dt$$
$$H_{D/A}(j\Omega) \equiv F\{h_{D/A}(t)\} = \frac{\sin(\Omega T_t/2)}{\Omega/2} e^{-j\Omega T_t/2}, \tag{4.2}$$

where $H_{D/A}(j\Omega)$ is the frequency response of a zero order hold for T_t second. The normalized frequency response, which is the actual response scaled so that the DC response is unity, is given by

$$H_{D/A,norm}(j\Omega) = F_t H_{D/A}(j\Omega), \tag{4.3}$$

and the digital amplitudes $1+\varepsilon_i$ of the tones with analog frequencies Ω_i are set such that

$$1+\varepsilon_i = \frac{1}{|H_{DA,norm}(j\Omega_i)|}. \tag{4.4}$$

This establishes the relative amplitude of the tones.

FCC and Industry Canada regulations for MMDS channels restrict the peak transmit power. The transmitter is designed such that the peak power of the radiated RF signal satisfies the regulation. In the transmitter, the signal is digitally generated and converted to analog using a D/A converter and a reconstruction filter (see Figure 4.1). The signal at the output of the reconstruction filter is amplified such that the maximum output of the D/A converter corresponds to the maximum allowable instantaneous transmit power. Assuming the board noise level has been minimized, the problem of maximizing the SNR of the transmitted RF signal is equivalent to maximizing the SNR at the output of the D/A converter.

There is no restriction on the phase of the tones so the phases ϕ_i, $i = 0, 1, \ldots, N$, can be chosen to maximize the SNR of the transmit signal. Since quantization noise power is independent of the power level of the signal, the SNR is maximized if the signal power at the output of the D/A converter is maximized. To maximize the signal power at the output of the D/A converter, the phases of the tones should be chosen to minimize the peak to

average power ratio. If all ϕ_i are chosen to be zero, then the peak-to-average-power ratio, assuming that N tones are sent, is

$$R_{P/A} = \frac{(\sum_{i=0}^{N-1}(1+\varepsilon_i))^2}{\sum_{i=0}^{N-1}(1+\varepsilon_i)^2/2}$$
$$R_{P/A} = \frac{2(N+\sum_{i=0}^{N-1}\varepsilon_i)^2}{N+2\sum_{i=0}^{N-1}\varepsilon_i+\sum_{i=0}^{N-1}\varepsilon_i^2} \tag{4.5}$$

for ε_i given by (4.4). $R_{P/A}$ is equal to 22 for the case of transmitting 10 tones (N = 10) with phases equal to 0. If the phases ϕ_i of the transmitted tones are chosen such that

$$\phi_i = \begin{cases} \pi/2, & i = 0,2,4,6,8, \\ \pi, & i = 1,5,9, \\ 0, & i = 3,7, \end{cases} \tag{4.6}$$

$R_{P/A}$ is equal to 7.4. Although this combination of phase values is not optimal, calculation of the peak to average power ratio for other phase combinations produced greater values of the peak-to-average-power ratio. This suggests that the particular combination in (4.6) produces a near minimum peak-to-average-power ratio value, given the 10 transmitted tones. The top graph of Figure 4.4 is a plot of the digital samples sequence obtained for the 10 transmitted tones when all ϕ_i are zero and the bottom graph displays the sequence obtained if the phases ϕ_i are chosen according to (4.6).

The noise introduced by the transmitter is a combination of quantization noise and the noise present on the printed circuit board where the D/A converter is located. The quantization noise is considered first from a theoretical point of view. Measurements made with a spectrum analyzer of the signal-to-noise ratio of the IF transmit signal are given at the end of this section. The D/A converter is assumed to be a perfectly linear uniform quantizer. Therefore, the error, $q_{D/A}[n_0]$, is the difference between the quantized value, $s_{q,if}[n_0]$, and the actual value of the signal, $s_{if}[n_0]$, for any arbitrary integer n_0. The random variable $q[n_0]$ is uniformly distributed over the interval $(-\Delta_{D/A}/2, +\Delta_{D/A}/2)$, where $\Delta_{D/A}$ is the step size of the quantizer [8]. As the mean and variance of a uniform random variable over an interval (a,b) are respectively equal to $(a+b)/2$ and $(b-a)^2/12$ [14], then with $a = -\Delta_{D/A}/2$ and $b = +\Delta_{D/A}/2$, the mean μ_q and variance σ_q^2 of random

variable $q[n_0]$ are given by

$$E\{q[n_0]\} = \mu_q = 0,$$
$$E\{(q[n_0] - \mu_q)^2\} = \sigma_q^2 = \frac{\Delta_{D/A}^2}{12}, \tag{4.7}$$

for any integer n_0.

As the signal $s_{if}[n]$ contains more than three tones, the quantization errors $q_{D/A}[n]$ are independent [8] and $E\{q_{D/A}[n_1]q_{D/A}[n_2]\} = E\{q_{D/A}[n_1]\}E\{q_{D/A}[n_2]\}$ for $n_1, n_2 \in I$ with $n_1 \neq n_2$. As the quantization errors have zero-mean and constant variance σ_q^2, the autocorrelation function [14] of $q_{D/A}[n]$ is given by

$$E\{q_{D/A}[n_1]q_{D/A}[n_2]\} = \sigma_q^2 \delta[n_1 - n_2], \tag{4.8}$$

for any integers n_1 and n_2. As $E\{q_{D/A}[n_1]q_{D/A}[n_2]\}$ depends only on the difference between n_1 and n_2, $q_{D/A}[n]$ is a wide sense stationary (WSS) process, and (4.8) can be

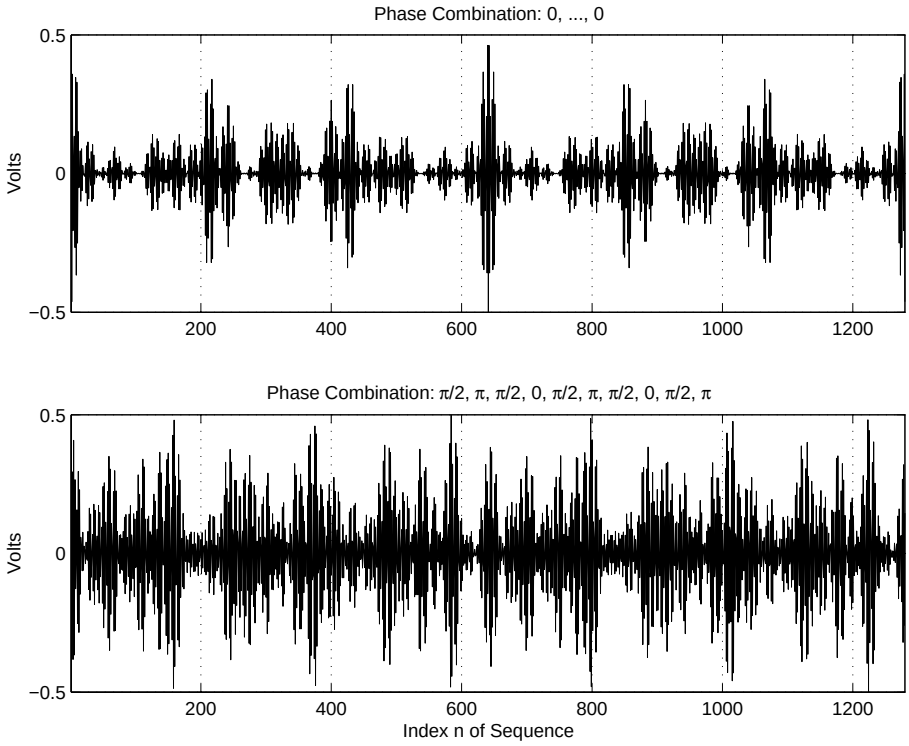

Figure 4.4: Digital Transmit Signal Sequence For Two Different Phase Combinations.

rewritten as

$$R_{qq}[n] = \sigma_q^2 \delta[n], n \in I, \tag{4.9}$$

where $R_{qq}[n]$ is the autocorrelation function of the random sequence $q_{D/A}[n]$. The power spectral density (PSD) of $q_{D/A}[n]$ is given by [14]

$$S_{qq}(e^{j\omega}) = DTFT\{R_{qq}[n]\} = \sigma_q^2, \text{ for } -\pi < \omega \leq +\pi. \tag{4.10}$$

The PSD of the discrete-time quantization noise power is uniform across ω with total power σ_q^2. In case of an analog signal at the output of an ideal lowpass reconstruction filter with cutoff frequency $F_t/2$, the power outside the frequency range $(-F_t/2, +F_t/2)$ is eliminated and the power inside this range is colored by the zero-order hold in the D/A converter. The PSD of the quantization noise in the analog domain is

$$S_{qa,qa} = \begin{cases} \frac{\sigma_q^2}{\Omega^2/4} \sin^2(\Omega/2F_t), & |\Omega| < \pi F_t, \\ 0, & \text{otherwise.} \end{cases} \tag{4.11}$$

The even function $\sin^2(\Omega/2F_t)$ monotonically increases for Ω in $[0, \pi F_t]$ since $0 \leq \Omega/2F_t \leq \pi/2$ on that interval. Thus, for a given Ω in $[0, \pi F_t]$, an increase in F_t decreases the argument of $\sin^2(\Omega/2F_t)$, causing the function to decrease. Therefore, (4.11) shows that increasing F_t to its practical limit minimizes the analog PSD of the quantization noise. The quantization noise within the 6 MHz bandwidth of the signal, $s_{IF}(t)$, will then be minimized. The data sheet of the D/A converter indicates a maximum sampling rate of 165 megasamples/second (MSPS). Due to timing constraint on the board where the D/A converter is located, the maximum sampling rate is 100 MSPS. Therefore, F_t is set to 100 MSPS. Table 4.1 gives measurement of the signal-to-noise ratio (SNR) at the output of the D/A converter for sampling rates of 20 MHz and 100 MHz. The SNR theoretical value is 56.5 dB. The measured values are 32 and 37 dB below the theoretical value. A thorough check of the board showed no stuck bits that could have caused such a drop of the SNR. Thus, a much lower SNR than the theoretical value arises because of the noise on the printed circuit board. The layout of the D/A converter is not perfect. Some of the noise generated by the digital chips of the board gets coupled with the analog signal generated by the D/A converter.

Table 4.1: Signal-to-Noise Ratio Measurements For IF Transmit Signal

F_t	Noise Pwr ($10kHz$ RBW)	Signal Tone Pwr	Total Signal Pwr	Noise Pwr ($6MHz$ BW)	SNR
$100MHz$	$33.5dB\mu V$	$75dB\mu V$	$85.5dB\mu V$	$61.3dB\mu V$	$24.2dB$
$20MHz$	$18dB\mu V$	$54.5dB\mu V$	$65dB\mu V$	$45.8dB\mu V$	$19.2dB$

The measurements indicate that the SNR increases by 5 dB when the sampling rate is increased from 20 MHz to 100 MHz. If the frequency response of the D/A converter is approximated by a rectangular function above the 6 MHz bandwidth of interest, then the noise power due to quantization should be 7 dB lower when the sampling rate is increased from 20 MHz to 100 MHz. An increase of the SNR by 5 dB instead of a 7 dB increase suggests that another source of noise such as transient noise may be increasing as the sampling rate increases.

4.3 The Receiver of The Acquisition System

The sampling rates in the transmitter and receiver need not be equal, but if they are not the spectrum of the receive signal will be a frequency scaled version of the original spectrum. The highest possible sampling rate was chosen for the transmitter. However, there is something to gain by having a lower sampling rate in the receiver. The signal processing can then be done at a lower rate. The lowest sampling rate that can be used is limited by the sampling theorem for bandpass signals [15]. The bandpass sampling theorem states that a bandpass signal with bandwidth B, must be sampled at a rate greater than 2B to retain all the information in the signal. As the transmit signal bandwidth is 6 MHz, the sampling rate in the receiver, F_r, has to be greater than 12 megasamples/second (MSPS). F_r is chosen to be 20 MSPS to create guard band space that will make the filtering easier.

As the reconstruction filter used in the transmitter is centered at 44 MHz, the analog IF frequency, $F_{IF\text{-transmitter}}$, of the transmit signal is set to 44 MHz. This is achieved by setting the digital IF frequency, $f_{if\text{-transmitter}}$, of $s_{if}[n]$ to $\frac{2.2}{5} = 0.44$ cycle/sample since the D/A converter is at $F_t = 100$ MSPS and $F_{IF\text{-transmitter}} = f_{if\text{-transmitter}} \times F_t$. The same

intermediate frequency, $F_{IF\text{-receiver}} = F_{IF\text{-transmitter}} = 44$ MHz, is used in the receiver so that a filter identical to the reconstruction filter in the transmitter can be used.

The top graph of Figure 4.5 shows a characterization of the spectrum of the 44 MHz IF receive signal. A consequence of the bandpass sampling theorem is that sampling this signal at $F_r = 20$ MSPS, produces a digital IF signal whose digital IF frequency, $f_{if\text{-receiver}}$, is equal to

$$\begin{aligned} f_{if\text{-receiver}} &= 44 \text{ MHz } / F_r \\ &= 2 + \frac{1}{5} \text{ cycles/sample} \\ &= \frac{1}{5} \text{ cycles/sample, } \frac{-1}{2} < f < \frac{1}{2}. \end{aligned} \tag{4.12}$$

Due to the inherent periodicity of the spectrum of a digital signal, the convention is to express the digital frequency in the interval $(\frac{-1}{2}, \frac{1}{2})$ cycles/sample or $(-\pi, \pi)$ radians/sample. $f_{if\text{-transmitter}}$ and $f_{if\text{-receiver}}$ are also related by

$$f_{if\text{-receiver}} = f_{if\text{-transmitter}} \frac{F_t}{F_r} - 2 = 5 f_{if\text{-transmitter}} - 2. \tag{4.13}$$

The spectrum of a digital signal is expressed in the interval $(-\pi, \pi)$ radians/sample or $(-0.5, 0.5)$ cycle/sample. The minus 2 constant in (4.13) indicates that the spectrum of the sampled IF receive signal is an aliased copy of the spectrum in the intervals $(-2.5, -2)$ and $(2, 2.5)$ cycles/sample. This is illustrated by the bottom graph of Figure 4.5 that shows the spectrum of the digital IF receive signal obtained after sampling the analog IF receive signal.

The ratio between F_t and F_r is equal to 5. This factor appears in front of $f_{if\text{-transmitter}}$ in (4.13) and results in a scaling of the frequency axis by a factor of 5. This is illustrated in Figure 4.6. The top graph shows a characterization of the spectrum of the IF digital transmit signal, $s_{if}[n]$. The bottom graph shows how this spectrum appears in the receiver after the IF receive signal has been sampled. The expansion of the spectrum due to the frequency scaling by a factor of 5 can be easily seen. To summarize, if the spectrum of the digital signal in the transmitter is denoted $R_t(e^{j\omega})$, and the spectrum of the digital signal in the receiver is denoted $R_r(e^{j\omega})$, then these two spectra are related by the following

equations.

$$R_t(e^{j\omega}) = R_r(e^{j(5\omega-4\pi)}), -\pi \leq \omega < \pi,$$
$$R_r(e^{j\omega}) = R_t(e^{j(\frac{1}{5}(\omega+4\pi)}), -\pi \leq \omega < \pi. \quad (4.14)$$

The frequency scaling by a factor of 5 changes the frequency spacing between the tones. The goal when devising the acquisition system is to have the frequency of the complex exponential tones of the lowpass equivalent receive signal, $r_l[n]$, to be integer multiples of $\frac{1}{L}$ cycle/sample. This is a requirement for the L-point FFT to produce good estimates of the amplitude and phase of the receive tones (Section 3.3). Because of the frequency scaling by a factor of 5, the frequency of the complex exponential tones in the transmitter should be chosen such that they are integer multiples of $\frac{1}{5L}$ cycle/sample. The expression for the digital transmit signal, derived from the results of this section and Section 4.2, is given in the next section.

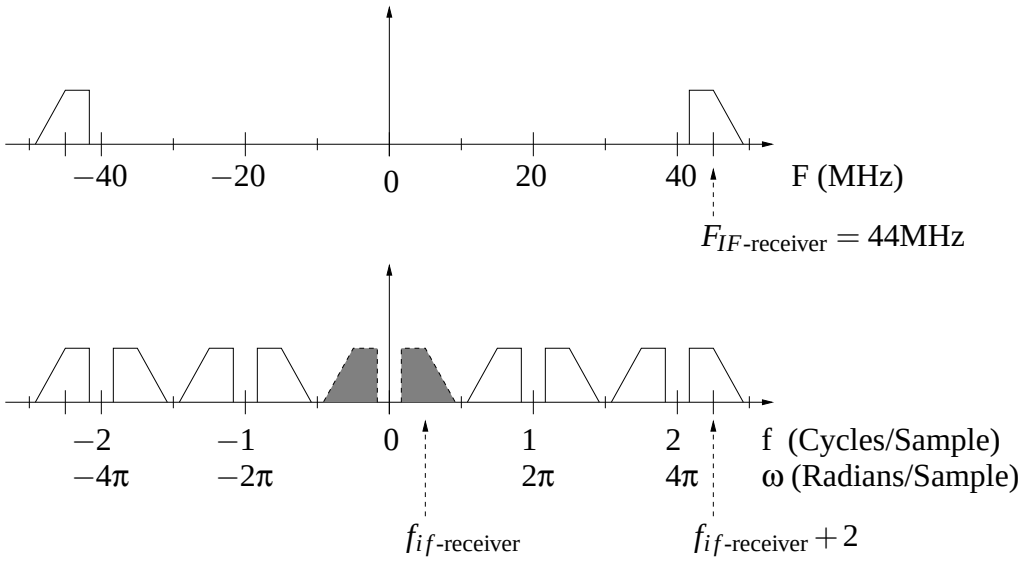

Figure 4.5: Spectrum of Analog & Digital IF Receive Signals: Top - Analog Signal, Bottom - Digital Signal

4.4 The Digital Transmit Signal

The digital IF transmit signal,$s_{if}[n]$, is directly generated in the transmitter. $s_{if}[n]$ is equal to

$$s_{if}[n] = \sum_{i=-\lceil 5L\times 0.03\rceil}^{+\lfloor 5L\times 0.03\rfloor} (1+\varepsilon_i)\cos((\omega_{if\text{-transmitter}} + \frac{2\pi i}{5L})n + \phi_i), \tag{4.15}$$

where $\omega_{if\text{-transmitter}} = 2\pi f_{if\text{-transmitter}}$. The $(1+\varepsilon_i)$ and ϕ_i constants in (4.15) were defined in Section 4.2. The analog IF signal, $s_{IF}(t)$, should be centered at 44 MHz with a 6 MHz bandwidth. This means that the tones of this signal must have analog frequencies comprised between 41 and 47 MHz. The tones of $s_{if}[n]$ must then have digital frequencies comprised between 41 MHz / $F_t = 0.41$ and 0.47 cycle/sample. Thus, the possible values for i in (4.15) must be such that

$$0.41 < f_{if\text{-transmitter}} + \frac{i}{5L} < 0.47, \tag{4.16}$$

which means that the values for i must be comprised in the interval

$$-\lceil 5L\times 0.03\rceil \leq i \leq +\lfloor 5L\times 0.03\rfloor. \tag{4.17}$$

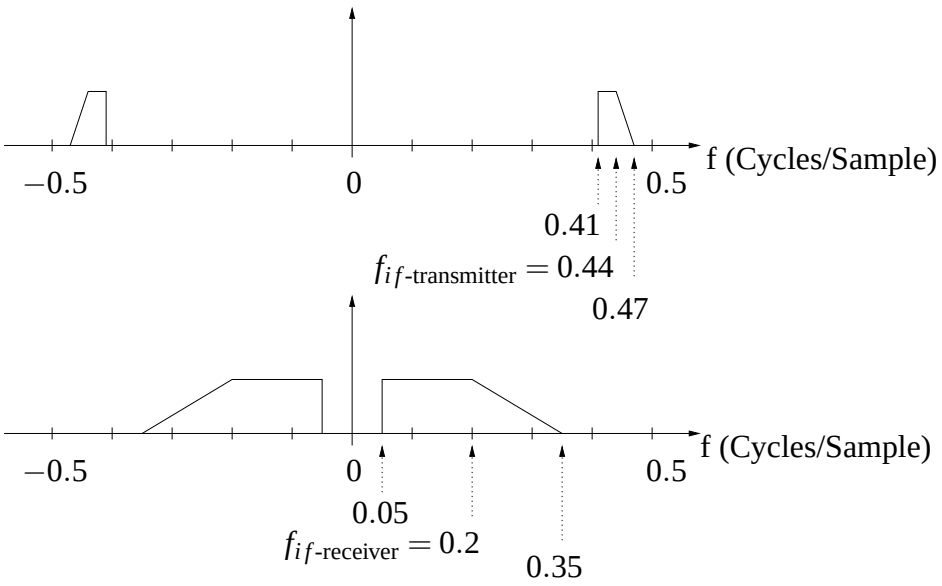

Figure 4.6: Spectrum of Digital IF Transmit & Receive Signals: Top - Transmit Signal, Bottom - Receive Signal

The number of samples, L, for the FFT must be chosen such that $L \times T_r < \Delta T$, where $\Delta T = 5$ ms is the largest interval of time over which the amplitude and phase of the tones are assumed to remain constant, and $T_r = \frac{1}{F_r}$. As $F_r = 20$ MHz, then L can be as high as 100,000 samples. The size of L has implications on the processing time, so L is restricted to

$$L = 256, \tag{4.18}$$

and (4.17) becomes

$$-38 \leq i \leq +38. \tag{4.19}$$

To have an analog IF of 44 MHz, the parameter, $\omega_{if\text{-transmitter}}$, in (4.15) must be set to $2\pi \times 0.44$ rad/sample. However, implementation is made easier if $\omega_{if\text{-transmitter}}$ is chosen to make $s_{if}[n]$ periodic with period $5L = 1280$. The value chosen for $\omega_{if\text{-transmitter}}$ has to be near $2\pi \times 0.44$ because the center frequency of the IF 6 MHz SAW filter is 44 MHz. $s_{if}[n]$ is periodic with period $5 \times 256 = 1280$ if

$$\omega_{if\text{-transmitter}} * 1280 = 2k\pi, \tag{4.20}$$

where k is a positive integer. The closest integer k that satisfies (4.20) with $\omega_{if\text{-transmitter}} \approx 2\pi \times 0.44$ is $k = 563$. $\omega_{if\text{-transmitter}}$ is then set equal to

$$\omega_{if\text{-transmitter}} = 2\pi\frac{563}{1280} = 2\pi \times 0.4398 \text{ rad/sample}. \tag{4.21}$$

This completes the definition of all the parameters in (4.15), and (4.15) can be written as

$$s_{if}[n] = \sum_{i=-38}^{38} (1+\varepsilon_i)\cos((2\pi\frac{563}{1280} + \frac{2\pi i}{1280})n + \phi_i). \tag{4.22}$$

The expression for $s_{if}[n]$ includes all tones that can possibly be sent when $L = 256$. In practice, the number of tones sent will be much less than $2 \times 38 + 1 = 77$. This has to do with the limitation in total transmit power. Decreasing the number of tones increases the power allocated to each tone, which increases the signal-to-noise ratio (SNR) of each tone, and reduces estimation error. Ten tones will be sent when collecting data in the field. To make the post-processing easier, the tone at the center of the band is sent. This tone, denoted the center tone, is at frequency $\omega_{if\text{-transmitter}}$.

4.5 Implementation of The Transmitter and Receiver

The internal ROM of the FPGA in the transmitter contains the 1280 samples representing one digital period of the transmit signal, $s_{if}[n]$ (4.22). These samples are continuously sent to the D/A converter along with a 100 MHz clock. The Verilog code that generates the signal and 100 MHz clock is relatively simple. It includes a counter generating an address for the ROM storing the sample sequence. This counter automatically resets to 0 after reaching 1279.

The FPGA in the receiver is programmed to output a 20 MHz clock for the 12-bit A/D converter. The samples are sign-extended from 12 bits to 16 bits using two's complement format. These samples are then gathered in groups of two for 32-bit transfers between the FPGA and the DAQ board using a 10 MHz clock, which is generated from the 20 MHz clock with a frequency divider.

The LabVIEW Software is used to operate the DAQ board.

5. THE POST-PROCESSING SYSTEM

The post-processing system is a non-real time processing system whose input is a digital signal recorded on a disk by the acquisition system. The objective of the post-processing is to compute estimates, $\hat{a}_i[k]$ and $\hat{\theta}_i[k]$, of the amplitude and phase of the receive tones. This can only be done after correcting any translations or distortions introduced by the acquisition system. The post-processing system was implemented in Simulink. The Matlab and Simulink source files make up Appendix C.

5.1 Distortions Caused by The Acquisition System

The frequencies of the oscillators that control the D/A converter in the transmitter and the A/D converter in the receiver have some error, so the sampling frequencies F_t and F_r are not exactly as they should be, and $F_t \neq 5 \times F_r$. Suppose that the relationship between the sampling rate, F_t, in the transmitter with respect to the sampling rate, F_r, in the receiver is

$$F_t = 5(F_r + \Delta F_r). \tag{5.1}$$

Then from (5.1) and (4.14), a tone with frequency $\frac{1126}{1280}\pi + \frac{2\pi i}{1280}$ at the output of the transmitter will have, after being received and digitized in the receiver, a frequency

$$\begin{aligned}(\frac{1126}{1280}\pi + \frac{2\pi i}{1280})\frac{F_t}{F_r} - 4\pi &= (\frac{1126}{1280}\pi + \frac{2\pi i}{1280})\frac{5(F_r + \Delta F_r)}{F_r} - 4\pi \\ (\frac{1126}{1280}\pi + \frac{2\pi i}{1280})\frac{F_t}{F_r} - 4\pi &= \frac{53}{128}\pi + \frac{2\pi i}{256}(1 + \frac{\Delta F_r}{F_r}) + \frac{1126}{256}\pi(\frac{\Delta F_r}{F_r}).\end{aligned} \tag{5.2}$$

The frequency spacing of the tones in the receiver becomes $(\frac{1}{256}) \times (1 + \frac{\Delta F_r}{F_r})$. If $\Delta F_r = 0$, the receive signal spectrum is as desired, and the center tone is also at the desired frequency, $\frac{53}{128}\pi$ rad/sample. If $\Delta F_r > 0$, then the spacing between the tones is larger than $\frac{1}{256}$ and the spectrum has been expanded. If $\Delta F_r < 0$, then the spectrum has been compressed. A translation of the compressed/expanded spectrum also occurs since the frequency of the center tone is shifted by $\frac{1126}{256}\pi(\frac{\Delta F_r}{F_r})$ rad/sample.

The frequencies of the oscillators of the up and down conversion stages are also in error. This causes an additional frequency shift of the center tone. This frequency shift also varies with time, due to the frequency drift of these oscillators. If the frequency deviation of the center tone from its desired frequency is denoted by $\Delta\omega_{if}[n]$, and $a_i[n]$ and $\theta_i[n]$ are the amplitude and phase of the receive tones, then the digital IF receive signal, $r_{if}[n]$, is given by

$$r_{if}[n] = \sum_{i=-38}^{38} a_i[n] \cos\left((\frac{53}{128}\pi + \Delta\omega_{if}[n] + \frac{2\pi i}{256} \times (1 + \frac{\Delta F_r}{F_r}))n + \theta_i[n] \right) + \eta[n], \quad (5.3)$$

where $\eta[n]$ is zero-mean white additive Gaussian noise.

In summary, the frequencies of the oscillators are imprecise. Imprecision of the frequencies of the oscillators that control the sampling and the up/down-conversion stages causes the spectrum of the sampled receive signal to be shifted and compressed/expanded. The effect of compression/expansion is to change the frequency spacing so that the spacing is $(1/256) * (1 + \Delta F_r/F_r)$ instead of $1/256$. The complex exponential tones of the lowpass-equivalent receive signal are no longer harmonically related with fundamental period 256. Once the harmonic relationship of the tones is destroyed, cross-coupling between the tones will occur when computing the FFT, causing a large error in the amplitude and phase estimates of the tones.

5.2 Post-Processing System Overview

The frequency shift and compression/expansion, which was previously described can be corrected by applying digital signal processing (DSP) techniques. This must be done before the amplitudes and phases of the tones are extracted. Figure 5.1 shows a data flow diagram of the whole post-processing system. This is a four pass system, in which the previously recorded receive signal, $r_{if}[n]$, is processed to extract a parameter, and then reprocessed to extract another parameter, etc.

In the first pass $r_{if}[n]$ is processed to estimate the frequency deviation, $\Delta\omega_{if}[n]$, of the center tone from the desired frequency, $\frac{53}{128}\pi$ rad/sample. The frequency drift of the up/down-conversion stages can be significant over the 5 second measurement interval. In the first pass, a digital phase-lock loop (DPLL) is used to generate estimates of $\Delta\omega_{if}[n]$

over the 5 second duration of the signal. The estimates obtained are then averaged to yield an estimate, $\overline{\Delta\omega}_{if}$, of the frequency deviation, $\Delta\omega_{if}[n]$.

In the second pass, the lowpass equivalent signal, $r_l[n]$, of $r_{if}[n]$ is computed. $r_l[n]$ can be recovered with a baseband down-converter. The baseband down-converter uses an NCO whose frequency is set to $\frac{53}{128}\pi + \overline{\Delta\omega}_{if}$. The down-converted signal, $r_l[n]$, is stored on a disk so it can be used in the third pass. The deviation ΔF_r of the sampling rate F_r is also estimated in this pass for use in the third pass. ΔF_r is estimated from $r_l[n]$.

The third pass consists of restoring the frequency spacing between the tones of $r_l[n]$ to $1/L$. This is done by resampling $r_l[n]$. The resampled lowpass equivalent signal, $r_l^r[n]$, is then temporary stored on disk for use in the fourth pass. The fourth pass consists of computing estimates $\hat{a}_i[k]$ and $\hat{\theta}_i[k]$ of the amplitude $A_i(t)$ and phase $\theta_i(t)$ of the tones.

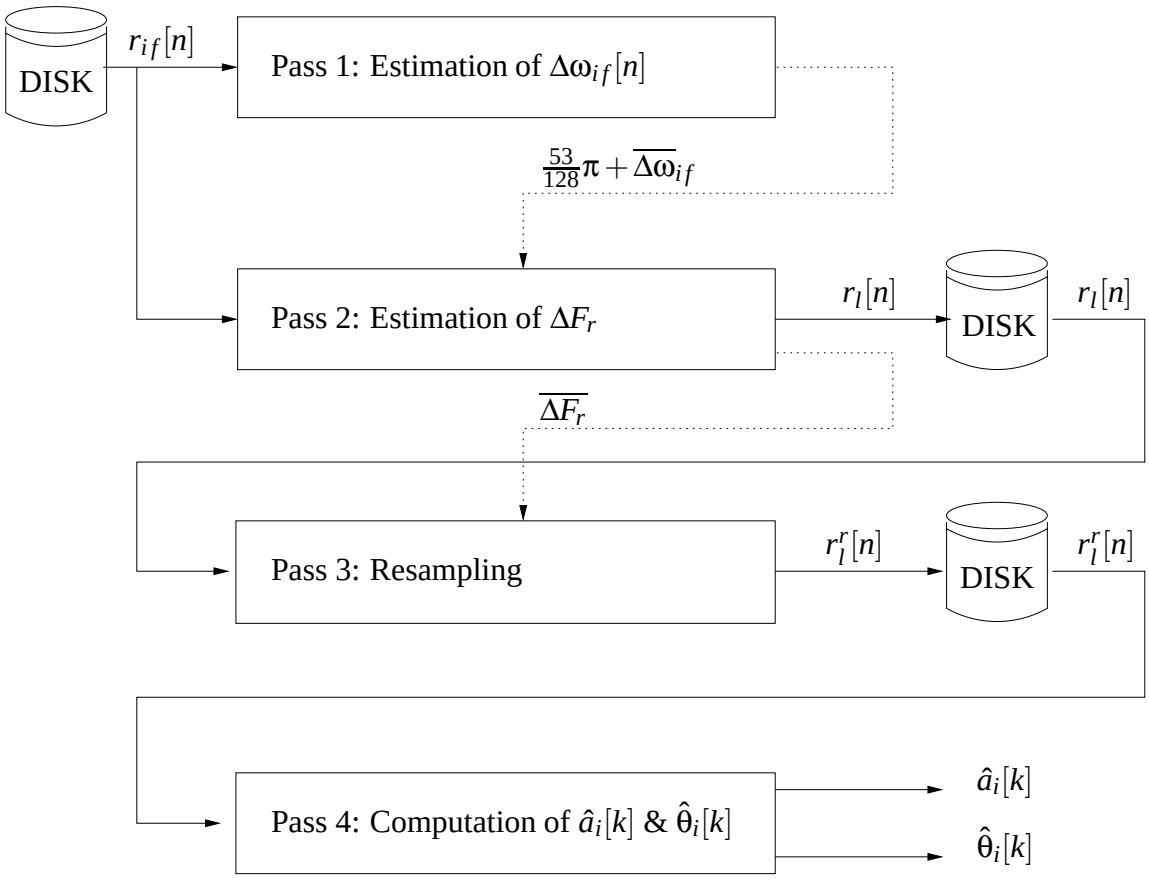

Figure 5.1: Post-Processing System Data Flow Diagram

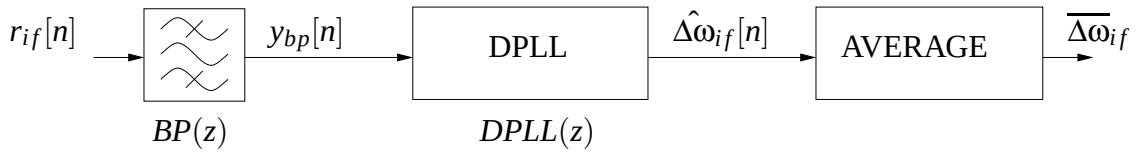

Figure 5.2: System Block Diagram For Pass 1

5.3 Pass 1: Estimation Of $\Delta\omega_{if}[n]$

Figure 5.2 shows a block diagram of the system making up Pass 1. The recorded receive signal, $r_{if}[n]$, is first filtered with a bandpass filter in order to isolate the center tone. The bandwidth of this filter is sufficiently wide to account for the frequency deviation of this tone from its nominal frequency, $\frac{53}{128}\pi$ rad/sample. The bandwidth of this filter was calculated from the knowledge of the tolerances of the oscillators used at the up and down conversion stages. The tolerance of the oscillators at the up and down-conversion stage are ± 2 ppm. Therefore, the tolerance of the combination of the two oscillators is ± 4 ppm. Since the RF frequency is 2.5 GHz, the maximum frequency deviation of the receive signal is $2.5\text{ GHz}\times 4/10^6 = 10$ kHz. A digital 100 kHz bandwidth bandpass filter is obtained with three poles. The transfer function of this filter is

$$BP(z) = \frac{K_{BP}}{\prod_{i=1}^{3}(1-2r\cos(\omega_{p_i})z^{-1}+r^2z^{-2})}, \tag{5.4}$$

where $\omega_{p_1} = \frac{53}{128}\pi$, $\omega_{p_2} = \frac{53}{128}\pi + \frac{5\pi}{1000}$, $\omega_{p_3} = \frac{53}{128}\pi - \frac{5\pi}{1000}$, $r = 0.99$, and $K_{BP} = 10^{-74/20}$. At the output of this filter, the tones adjacent to the center tone are attenuated by about 45 dB. The center tone is amplified 10 times and its phase is changed by ϕ_{bp}. The signal at the output of the bandpass filter is denoted $y_{bp}[n]$. If $a_{ct}[n]$ and $\theta_{ct}[n]$ denote the amplitude and phase of the center tone, then $y_{bp}[n]$ is given by

$$y_{bp}[n] = 10\times a_{ct}[n]\cos((\frac{53}{128}\pi + \Delta\omega_{if}[n])n + \theta_{ct}[n] + \phi_{bp}) + \eta_{bp}[n], \tag{5.5}$$

where $\eta_{bp}[n]$ is the noise resulting from filtering the white additive Gaussian noise present in the recorded signal.

A digital phase-lock loop (DPLL) is used to estimate $\Delta\omega_{if}[n]$ from the incoming signal, $y_{bp}[n]$, after each processed sample. This occurs after the DPLL has achieved phase-

lock with $y_{bp}[n]$. The instantaneous frequency values, $\hat{\Delta\omega}_{if}[n]$, synthesized by the DPLL are averaged to yield an estimate $\overline{\Delta\omega}_{if}$ of $\Delta\omega_{if}[n]$. A brief description and analysis of the DPLL used in this research is given in Appendix B.

Figure 5.3 shows a detailed block diagram of the Pass 1 processor. Two parameters, denoted by "a" and "K" have to be set to configure the DPLL. The DPLL frequency lock range, $|\Delta F_{DPLL}|$ depends on K. It is given by [16]

$$|\Delta F_{DPLL}| = K * F(1) * F_s/2\pi, \tag{5.6}$$

where $F(z)$ is the transfer function of the loop filter and $F(1)$ is its DC response. As indicated in Appendix B, the loop filter was designed such that $F(1) = 1$. The DPLL frequency lock range has to be greater than 10 kHz at all times to guarantee that the DPLL can phase lock on $y[n]$, and also remain locked for the whole duration of the signal. K is set to $8.75 * 10^{-3}$, yielding $|\Delta F_{DPLL}| = 28$ kHz. This assumes that the amplitude of $y_{bp}[n]$ is constant and equal to 1 V.

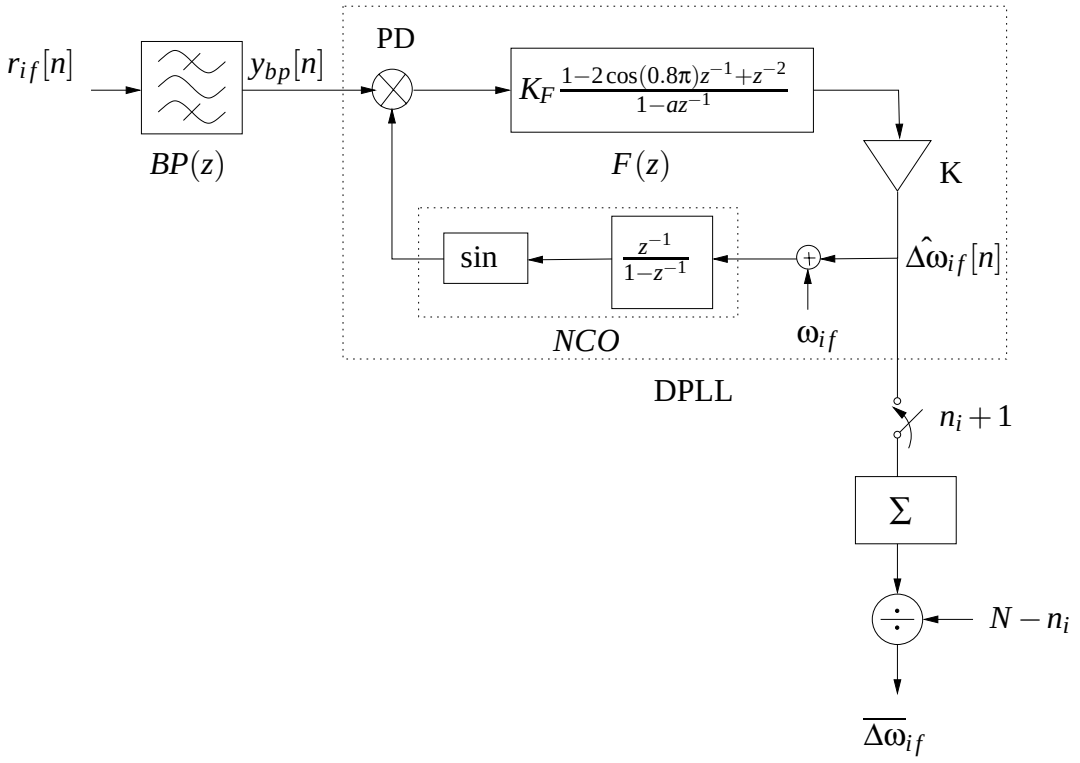

Figure 5.3: Detailed Block Diagram of System For Pass 1

The phase detector is not a true phase detector. The output of the phase detector is the product of the amplitude of $y_{bp}[n]$ and the phase difference between $y_{bp}[n]$ and the NCO. If the amplitude of $y_{bp}[n]$ decreases, then the phase error increases to keep the loop in phase-lock. A variation in the amplitude of $y_{bp}[n]$ by ΔA while the gain K of the DPLL remains constant, can be seen as a variation of K by $\Delta K = \Delta A * K/$amplitude of $y_{bp}[n]$ while the amplitude of $y_{bp}[n]$ remains constant. Therefore, a decrease in amplitude of $y_{bp}[n]$ from 1 V to 0.5 V can be seen as a decrease of K from $8.75 * 10^{-3}$ to $4.375 * 10^{-3}$. If K changes to $4.375 * 10^{-3}$, then the lock-range will change to 14 kHz. Therefore, for the incoming signal, $y_{bp}[n]$, whose amplitude may vary between 0.5 V and 1 V due to tree foliage, the DPLL frequency lock range is between 14 kHz and 28 kHz. This means that the DPLL can achieve phase lock and can remain phase locked if at all times $|\Delta\omega_{if}[n]| < 2\pi\frac{14 \text{ kHz}}{20 \text{ MHz}}$ $= 4.4 * 10^{-3}$ radians/sample.

The parameter "a" of the loop filter is set to 0.999, such that the loop filter pole is placed close to the unit circle, making the rolloff of the filter amplitude response stronger. Figure 5.4 shows the frequency response amplitude of the DPLL for $K = 8.75 * 10^{-3}$. The top plot shows the DPLL frequency response over the frequency range 0 to 10 MHz. The sharp dip in the vicinity of 8 MHz is due to the single zero of the loop filter. This zero is required to filter out the high frequency component generated by the phase detector. In the bottom plot, the DPLL frequency response is shown over the frequency range 0 to 50 kHz.

Variations in $\Delta\omega_{if}[n]$ obviously cause variations in the estimates $\Delta\hat{\omega}_{if}[n]$. Similarly, variations in the phase of $y_{bp}[n]$ (due to the tree foliage and noise, $\eta_{bp}[n]$) cause $\Delta\hat{\omega}_{if}[n]$ to move around its true value, $\Delta\omega_{if}[n]$. A cumulative sum at index n is obtained by summing the $\Delta\hat{\omega}_{if}[n]$ terms produced by the DPLL at discrete-time $0, 1, 2, \ldots, n$. If this cumulative sum is plotted as a function of n, it looks like a ramp function that is not perfectly straight due to the variations in $\Delta\hat{\omega}_{if}[n]$. Figure 5.5 shows the type of ramp function that is obtained by plotting the cumulative sums. In this figure, the ramp function is plotted from $n = 0$ to $n = 5 * 10^4$. This interval expressed in samples corresponds to an interval of time of 2.5 ms. The slope of the straight line approximating this ramp function can be obtained by averaging the $\Delta\hat{\omega}_{if}[n]$ over the 5 second duration of the signal. This

average value is taken as the estimate, $\overline{\Delta\omega}_{if}$, of $\Delta\omega_{if}[n]$. This slope is calculated using two points of this ramp function. To reduce the error on the slope calculation, the two points are taken as far as possible from each other. This is achieved by taking the last point of the waveform and the first point of the waveform after the DPLL has phase-locked to $y_{bp}[n]$. As it can be noticed on Figure 5.5, the slope of the ramp function between $n = 1$ and $n \approx 7000$ is incorrect. This is because the DPLL hasn't phase-locked to the signal yet and is still hunting. If n_i represents the number of samples required for the DPLL to lock, and N is the length of $y_{bp}[n]$, then $\overline{\Delta\omega}_{if}$ is given by

$$\overline{\Delta\omega}_{if} = \frac{1}{N-n_i}\left(\sum_{i=0}^{N}\hat{\Delta\omega}_{if}[n] - \sum_{i=0}^{ni}\hat{\Delta\omega}_{if}[n]\right)$$

$$\overline{\Delta\omega}_{if} = \frac{1}{N-n_i}\sum_{i=n_i+1}^{N}\hat{\Delta\omega}_{if}[n] \tag{5.7}$$

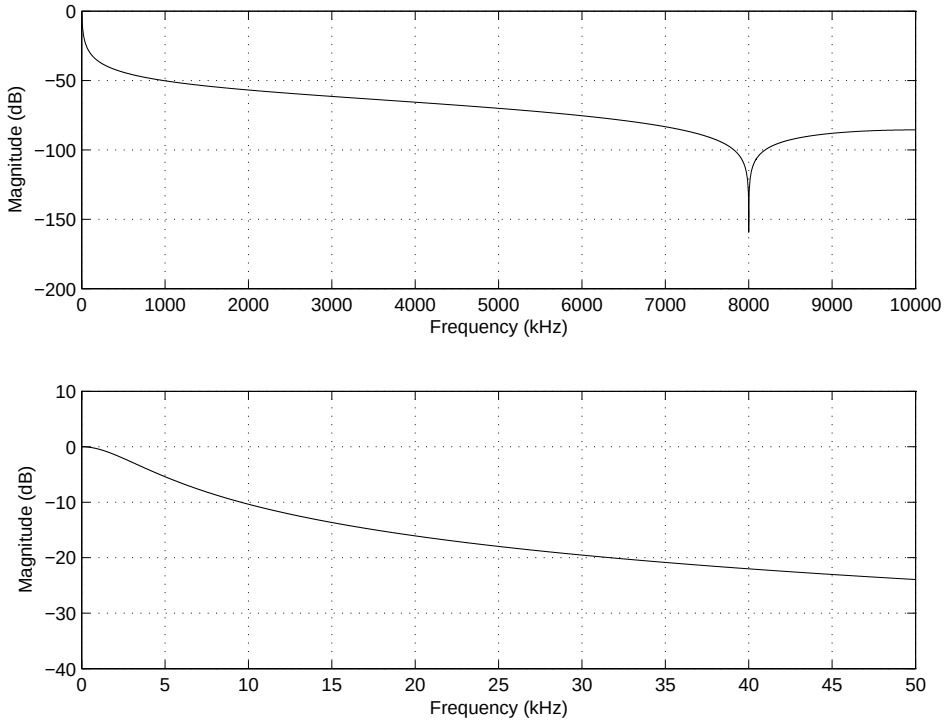

Figure 5.4: DPLL Frequency Response Amplitude for $a = 0.999$ and $K = 8.75 * 10^{-3}$

5.4 Pass 2: Estimation Of ΔF_r

This pass is composed of two processes. The first process is a baseband down-converter that recovers the lowpass equivalent signal, $r_l[n]$, of $r_{if}[n]$. The second process estimates ΔF_r by using a DPLL that phase-lock on one of the tones of $r_l[n]$. These two processes are cascaded, which means that the output of the baseband down-converter is fed to the input of the process estimating ΔF_r. This is illustrated in Figure 5.6.

The NCO frequency of the baseband down-converter is set to $\frac{53}{128}\pi + \overline{\Delta\omega_{if}}$ before the down-conversion starts. It has a phase, ϕ_{nco}, with respect to the incoming signal. ϕ_{nco} can be any value and therefore can be seen as a random variable uniform over $(0, 2\pi)$. Figure 5.7 shows a block diagram of the baseband down-converter. Two low-frequency signals are separately generated by using a mixer and a lowpass filter (LPF). Lowpass filters are used to remove the high frequencies generated by the mixers. These filters are linear phase FIR filters designed using the Matlab Remez function. The mixers used to

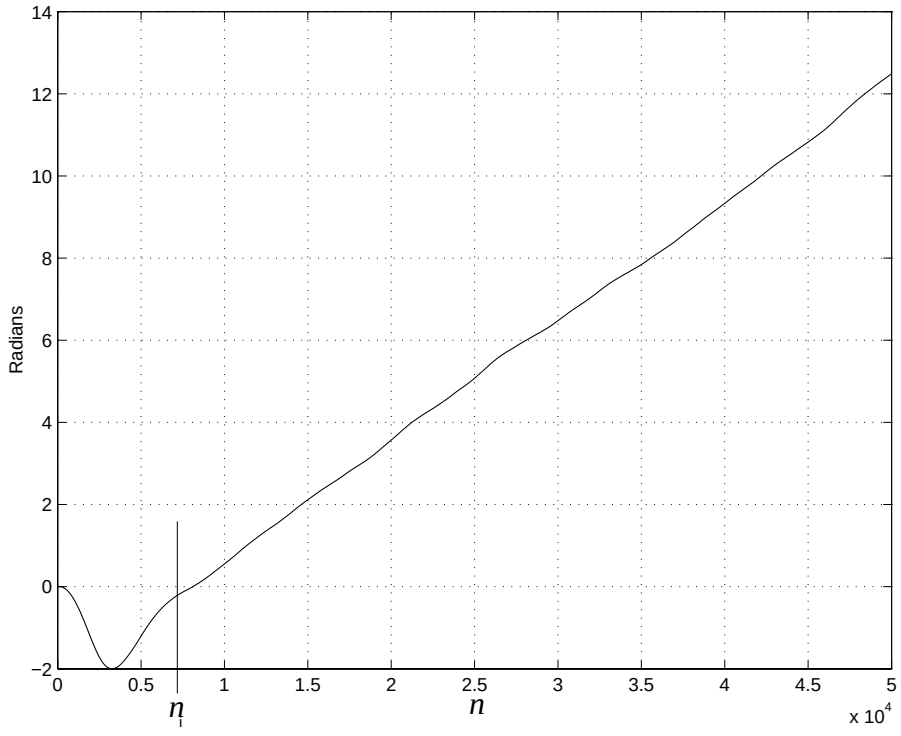

Figure 5.5: Typical Ramp Function Made of The Cumulative Sums of $\hat{\Delta\omega}_{if}[n]$.

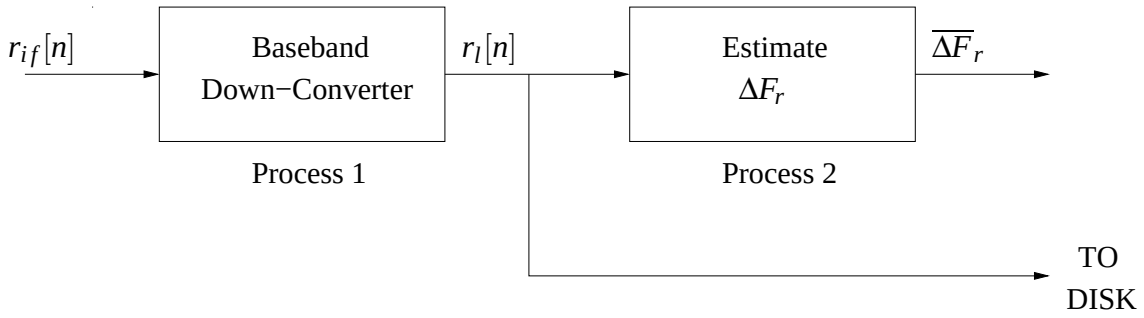

Figure 5.6: System Block Diagram for Pass 2

generate these two signals are set to the same frequency but have their phase separated by $\pi/2$. Depending on which of the two mixers is taken as the reference, one of the low frequency signals is called the in-phase signal and the other one the quadrature signal. In this project, the mixer with the cosine function is taken as the reference. The signal obtained with this mixer after filtering, is denoted $p[n]$. The other signal is denoted $q[n]$. These two signals are combined to yield the baseband signal

$$r_l[n] = p[n] - j * q[n]. \tag{5.8}$$

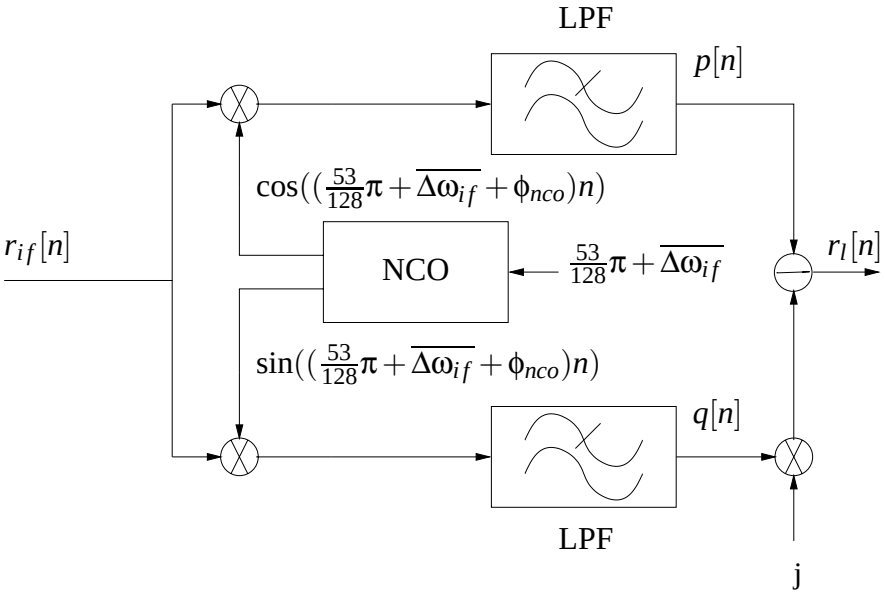

Figure 5.7: System Block Diagram for Process 1 of Pass 2 (Baseband Down-Converter)

It can be demonstrated that $r_l[n]$ is the lowpass equivalent signal of $r_{if}[n]$ (5.3) weighted by 0.5 [9]. $r_l[n]$ is then given by

$$r_l[n] = \frac{1}{2}\sum_{i=-38}^{38} a_i[n]e^{j(\theta_i[n]-\phi_{nco})}e^{j(2\pi i/256)(1+\Delta F_r/F_r)n} + \eta_l[n]. \tag{5.9}$$

Figure 5.8 shows the spectrum of $r_{if}[n]$ and of $r_l[n]$. Recovering $r_l[n]$ from $r_{if}[n]$ consists in the frequency domain of shifting the spectrum of $r_{if}[n]$ to the left by $\omega_{if} + \overline{\Delta\omega}_{if}$ rad/sample, and filtering out the high frequency components of the shifted spectrum.

The problem under discussion in this section is the estimation of ΔF_r. This is done using one of the complex exponential tones. The question is which tone should be used. If tone number i is selected and ω_i denotes its nominal frequency then from (5.3), its actual frequency, denoted ω_i', is equal to

$$\omega_i' = \omega_i(1 + \frac{\Delta F_r}{F_r}). \tag{5.10}$$

ω_i' can also be expressed as

$$\omega_i' = \omega_i + \Delta\omega_i, \tag{5.11}$$

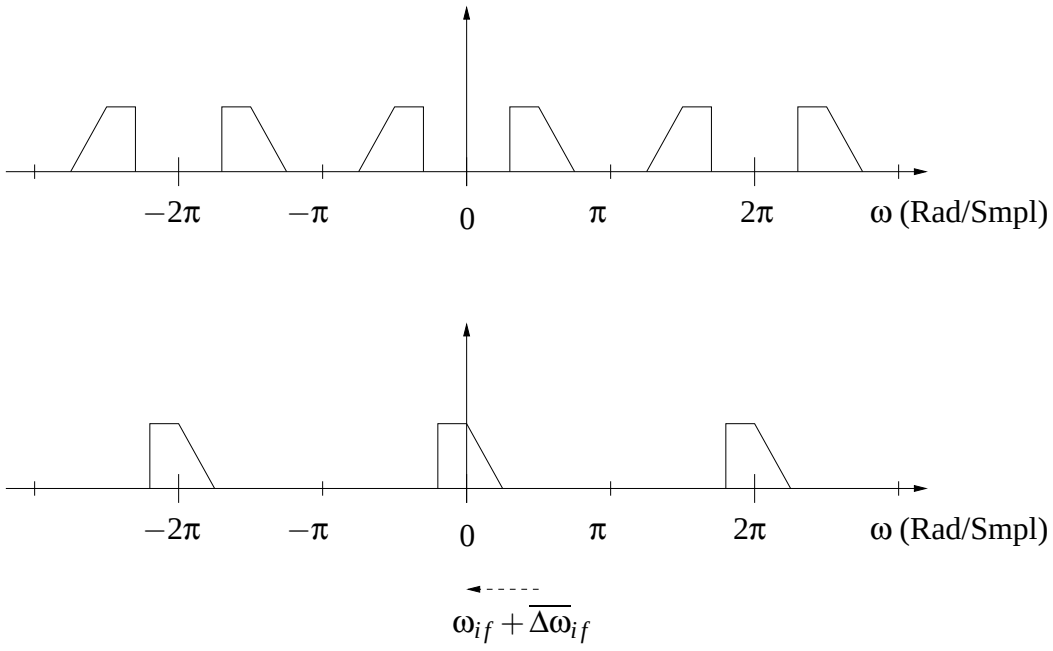

Figure 5.8: Spectrum of Digital IF Receive Signal (Top) & Digital Lowpass Equivalent Receive Signal (Bottom)

where $\Delta\omega_i$ is the frequency deviation from ω_i. From (5.10) and (5.11),

$$\Delta F_r = F_r \frac{\Delta\omega_i}{\omega_i}. \tag{5.12}$$

(5.12) indicates that an estimate of ΔF_r can be obtained from an estimate of $\Delta\omega_i$. If $var_{\Delta F_r}$ denotes the variance of the estimator of ΔF_r, and $var_{\Delta\omega_i}$ denotes the variance of the estimator of $\Delta\omega_i$, then from (5.12)

$$var_{\Delta F_r} = F_r^2 \frac{var_{\Delta\omega_i}}{\omega_i^2}. \tag{5.13}$$

Assuming the variance of the estimator of $\Delta\omega_i$ is the same for all the tones, then from (5.13), the variance of the estimator of ΔF_r is minimized by maximizing ω_i. This is done by selecting the tone with the highest frequency. The second process estimates $\Delta\omega_i$ by using a DPLL that is phased-lock on tone number i.

Figure 5.9 shows a block diagram of the second process. The lowpass equivalent signal, $r_l[n]$, is first filtered with a bandpass filter to isolate the selected tone, which is the complex exponential $e^{j\omega_i}$ with the highest positive frequency. The frequency response of this filter doesn't show the Hermitian symmetry since this filter passes only the complex exponential $e^{j\omega_i}$. Therefore, the impulse response of this filter is complex. It is a three pole filter with a passband gain of 10. It has transfer function

$$BP_c(z) = \frac{K_{BP}}{\prod_{i=1}^{3}(1 - re^{j\omega_{p_i}} z^{-1})}, \tag{5.14}$$

where $\omega_{p_1} = \omega_i$, $\omega_{p_2} = \omega_i + \frac{5\pi}{1000}$, $\omega_{p_3} = \omega_i - \frac{5\pi}{1000}$, $r = 0.99$, and $K_{BP} = 10^{-88/20}$. This filter is similar to the bandpass filter used in Pass 1. In this filter, all the poles are located in the upper-half of the z-plane near $e^{j\omega_i}$. The output of the bandpass filter, z_{bpc}, is fed to a DPLL which is used to estimate $\Delta\omega_i$.

The DPLL that estimates $\Delta\omega_i$ is similar to the DPLL used in Pass 1 except that it operates on a complex input signal. The modified PLL works as follows. A complex exponential $e^{-j\theta_{NCO}[n]}$ is generated from an NCO. This signal is multiplied with $z_{bpc}[n]$. Only the imaginary component of the product is passed to the loop filter. The transfer function of the loop filter is similar to the DPLL loop filter of Pass 1, except that no zeros are required since the product of these two complex exponentials doesn't create a high

frequency component. The transfer function of the loop filter is given by

$$F_2(z) = \frac{1-a}{1-az^{-1}}. \tag{5.15}$$

As for Pass 1, the $\hat{\Delta\omega}_i[n]$ terms generated by the DPLL are averaged to yield an estimate of $\Delta\omega_i$. This estimate is denoted $\overline{\Delta\omega}_i$ and is equal to

$$\overline{\Delta\omega}_i = \frac{1}{N-n_i} \sum_{i=n_i+1}^{N} \hat{\Delta\omega}_{if}[n], \tag{5.16}$$

where n_i is the number of samples required for the DPLL to lock. From (5.12), the estimate, $\overline{\Delta F}_r$, of ΔF_r is then given by

$$\overline{\Delta F}_r = F_r \frac{\overline{\Delta\omega}_i}{\omega_i}. \tag{5.17}$$

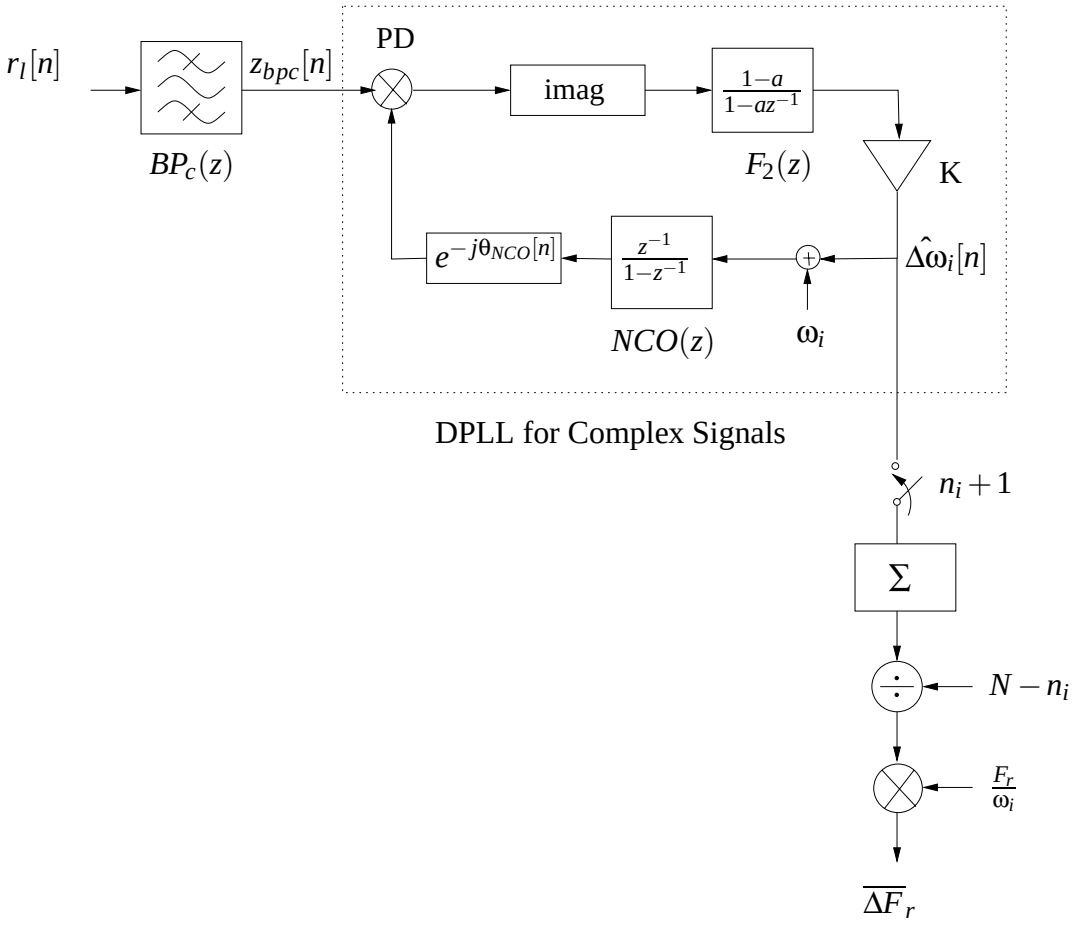

Figure 5.9: System Block Diagram for Process 2 of Pass 2 (Estimate $\Delta F_r[n]$)

5.5 Pass 3: Resampling

The frequency spacing between the complex exponential tones of $r_l[n]$ can be restored to $1/256$ by resampling $r_l[n]$ at a different sampling rate. One way to do this is to first convert the complex digital signal to a complex analog signal using two D/A converters, one for the real and one for the imaginary component, and then resample the analog signals at rate $F_r + \Delta F_r$. Since ΔF_r is not known exactly, the signal is resampled at rate $F_r + \overline{\Delta F}_r$. From (5.9), the resampled signal is then equal to

$$r_l[n] = \frac{1}{2} \sum_{i=-38}^{38} a_i[n] e^{j(\theta_i[n] - \phi_{nco})} e^{j(2\pi i/256) \frac{F_r + \Delta F_r}{F_r} \frac{F_r}{F_r + \overline{\Delta F}_r} n} + \eta_l^r[n],$$

which, if $\overline{\Delta F}_r = \Delta F_r$ is equal to

$$\frac{1}{2} \sum_{i=-38}^{38} a_i[n] e^{j(\theta_i[n] - \phi_{nco})} e^{j(2\pi i/256)n} + \eta_l^r[n]. \tag{5.18}$$

This shows that the operation of resampling does restore the frequency spacing between the tones.

The resampling can be and is more accurately done digitally. The signals, $p[n]$ and $q[n]$, do not have to be physically converted to analog and then back to digital with D/A and A/D converters to perform the resampling.

The digital resampling is performed on real and imaginary parts separately. Digital resampling is carried out by interpolating between the samples of the signal. Interpolation can be achieved by performing piecewise interpolations between the signal samples. Low-order polynomials can be used for these piecewise interpolations. A cubic spline interpolation, which uses 3^{rd} order polynomial such that the first and second derivatives of the piecewise functions on each side of the samples are equal [17], is used as the interpolator. The new sampling period is

$$T_r' = \frac{T_r}{F_r + \overline{\Delta F}_r} = \frac{1}{1 + \frac{\overline{\Delta F}_r}{F_r}}. \tag{5.19}$$

The resampled lowpass equivalent signal, $r_l^r[n]$ is approximately

$$r_l^r[n] \simeq \frac{1}{2} \sum_{i=-38}^{38} a_i[n] e^{j(\theta_i[n] - \phi_{nco})} e^{j(2\pi i/256)n} + \eta_l^r[n]. \tag{5.20}$$

5.6 Pass 4: Computation of $\hat{a}_i[k]$ and $\hat{\theta}_i[k]$

The estimated values, $\hat{a}_i[k]$ and $\hat{\theta}_i[k]$, are obtained by computing a series of 256-point FFT of $r_l^r[n]$ in successive windows of length 256. To do so, $r_l^r[n]$ is truncated with a rectangular window, $w[n-256\times k]$, where

$$w[n] = \begin{cases} 1, & 0 \le n < 256 \\ 0, & \text{otherwise.} \end{cases} \tag{5.21}$$

Using the symbols introduced at the end of Section 3.3, the k$^{\text{th}}$ FFT is performed on data

$$r_l^{rw}[n,k] = \begin{cases} \frac{1}{2}\sum_{i=-38}^{38} a_i[n]e^{j(\theta_i[n]-\phi_{nco})}e^{j(2\pi i/256)n} + \eta_l^r[n], & k\times 256 \le n < (k+1)\times 256 \\ 0, & \text{otherwise.} \end{cases} \tag{5.22}$$

The FFT is a fast implementation of the discrete Fourier Transform (DFT). The 256-point DFT of $r_l^{rw}[n,k]$ is given by

$$R_l^{rw}[i,k] = \sum_{n=0}^{255} r_l^{rw}[n,k]e^{-j\frac{2\pi in}{256}},\ i = 0,\ldots,255. \tag{5.23}$$

The amplitude and phase estimates of $a_i[k]$ and $\theta_i[k]$ are then given by

$$\hat{a}_i[k], \hat{\theta}_i[k] = \begin{cases} \frac{1}{256}|R_l^{rw}[i,k]|, \angle R_l^{rw}[i,k] - \phi_{nco}, & 0 \le i \le 38 \\ \frac{1}{256}|R_l^{rw}[i+256,k]|, \angle R_l^{rw}[i+256,k] - \phi_{nco}, & -38 \le i \le -1. \end{cases} \tag{5.24}$$

6. ESTIMATION OF THE ERROR ASSOCIATED WITH THE MEASUREMENTS

The previous chapters described the measuring system along with the method used to compute estimates of the amplitude and phase of the tones. Because of the noise generated by the acquisition system and the noise impinging on the receive antenna, measurements of the amplitude and phase of the tones will be in error. This chapter deals with the estimation of the variance (mean square of the error) associated with these measurements. The next chapter shows how these measurements can be further processed to reduce the error and obtain better estimates of the amplitude and phase of the tones.

6.1 Effect of White Additive Gaussian Noise

As indicated in Chapter 3, the noise corrupting the receive signal can be represented by zero-mean, stationary, white additive Gaussian noise. The receive signal is filtered with a 6 MHz bandpass SAW filter and then sampled. For the analysis, this filter is assumed to be an ideal bandpass filter. The spectral constant of the noise, after sampling, is denoted σ_η^2. The purpose of this section is to first derive equations, (6.12) and (6.15), to determine the variance of the amplitude and phase estimates of the tones, due to the noise. The second part of this section consists of verifying the validity of these equations with an experiment.

Equations (6.12) and (6.15) are based on the assumption that σ_η^2 is known. This means that in order to use these equations, σ_η^2 will have to be determined. The top graph of Figure 6.1 shows a characterization of the power spectrum of the noise in the sampled receive signal, $r_{if}[n]$, which is an IF signal. The post-processing system recovers the complex baseband signal, $r_l[n]$, by multiplying $r_{if}[n]$ with a complex exponential with amplitude 1, and filtering to remove the image at twice the IF. For the noise, this operation has the effect of shifting to baseband the noise power spectrum and removing the high-frequency component. The bottom graph of Figure 6.1 shows a characterization of the

noise power spectrum in $r_l[n]$. The spectral constant of the noise remains unchanged. A resampling of $r_l[n]$ also occurs to restore the correct frequency spacing between the tones. The resampled signal is denoted $r_l^r[n]$. The noise introduced by the resampling operation is negligible. The spectral constant, σ_η^2, can then be determined by computing estimates at several frequencies of the noise power spectrum in $r_l^r[n]$, and averaging these estimates.

Let $S_{xx}(e^{j\omega})$ denote the power spectrum of the noise sequence, $x_l[n]$, in $r_l[n]$. The first step in deriving (6.12) and (6.15) is to find the value of the average power in $X_l[i]$ which is the i^{th} term of an L-point ($L = 256$) DFT of $x_l[n]$

$$X_l[i] = \sum_{n=0}^{L-1} x_l[n] e^{-j2\pi \frac{i}{L} n}. \tag{6.1}$$

The average power in $X_l(i)$ can be determined by taking the expectation of $|X_l[i]|^2$, yielding

$$E\left[X_l[i] X_l^*[i]\right] = E\left[\sum_{n=0}^{L-1}\sum_{m=0}^{L-1} x_l[n] x_l^*[m] e^{-j2\pi \frac{i}{L}(n-m)}\right], \tag{6.2}$$

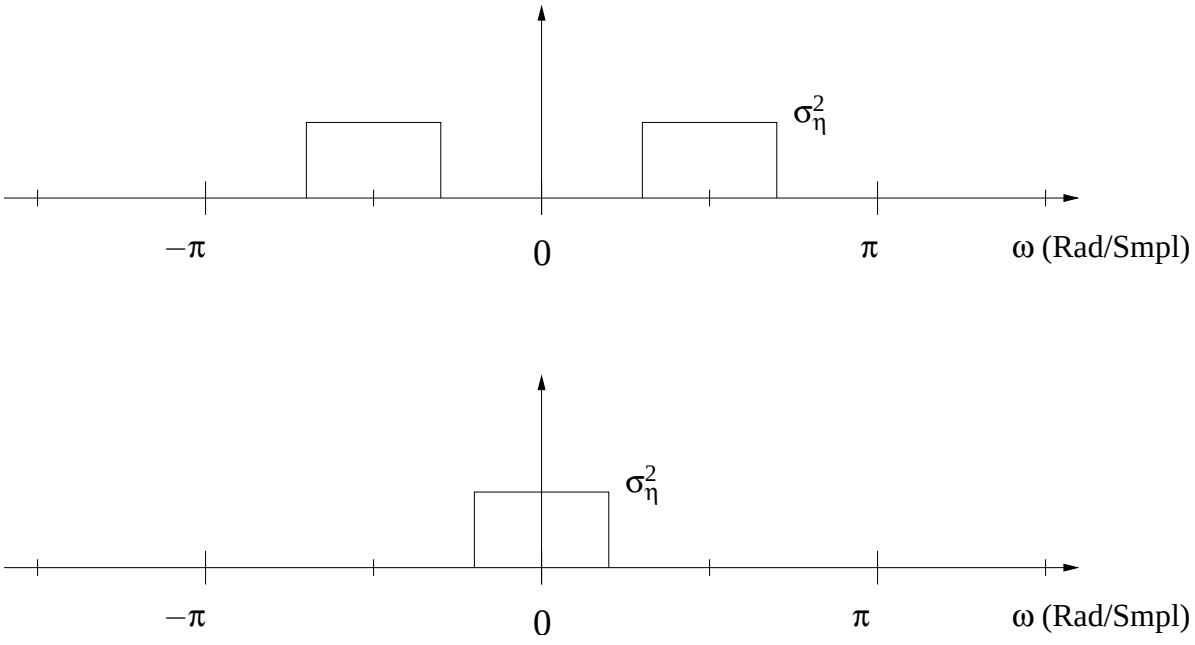

Figure 6.1: Noise Power Spectrum Before And After Post-Processing.

where $X_l^*(i)$ denotes the conjugate of $X_l(i)$. If $k = m - n$, equation (6.2) becomes

$$E\left[X_l[i]X_l^*[i]\right] = E\left[\sum_{n=0}^{L-1}\sum_{k=-n}^{L-1-n} x_l[n]x_l^*[n+k]e^{j2\pi\frac{i}{L}k}\right]$$
$$E\left[X_l[i]X_l^*[i]\right] = \sum_{n=0}^{L-1}\sum_{k=-n}^{L-1-n} R_{xx}[k]e^{j2\pi\frac{i}{L}k}, \tag{6.3}$$

where $R_{xx}[k]$ is the autocorrelation function of the noise and is equal to [14]

$$R_{xx}[k] = E[x_l[n]x_l^*[n+k]] = \frac{1}{2\pi}\int_{-\pi}^{\pi} S_{xx}(e^{j\omega})e^{j\omega k}d\omega. \tag{6.4}$$

Replacing 6.4 in 6.3 yields

$$E\left[X_l[i]X_l^*[i]\right] = \sum_{n=0}^{L-1}\sum_{k=-n}^{L-1-n}\frac{1}{2\pi}\int_{-\pi}^{\pi} S_{xx}(e^{j\omega})e^{j\omega k}d\omega e^{j2\pi\frac{i}{L}k}$$
$$E\left[X_l[i]X_l^*[i]\right] = \frac{1}{2\pi}\int_{-\pi}^{\pi} S_{xx}(e^{j\omega})\sum_{n=0}^{L-1}\sum_{k=-n}^{L-1-n} e^{j(\omega+2\pi\frac{i}{L})k}d\omega. \tag{6.5}$$

Using the fact that for two integers p and q with $q > p$, $\sum_{n=p}^{q-1} e^{an} = \frac{e^{ap}-e^{aq}}{1-e^a}$, (6.5) becomes

$$E\left[X_l[i]X_l^*[i]\right] = \frac{1}{2\pi}\int_{-\pi}^{\pi} S_{xx}(e^{j\omega})\left(\frac{1-e^{j(\omega+\frac{2\pi i}{L})L}}{1-e^{j(\omega+\frac{2\pi i}{L})}}\right)^*\left(\frac{1-e^{j(\omega+\frac{2\pi i}{L})L}}{1-e^{j(\omega+\frac{2\pi i}{L})}}\right)d\omega$$
$$E\left[X_l[i]X_l^*[i]\right] = \frac{1}{2\pi}\int_{-\pi}^{\pi} S_{xx}(e^{j\omega})\left(\frac{\sin(\frac{(\omega+\frac{2\pi i}{L})}{2}L)}{\sin(\frac{(\omega+\frac{2\pi i}{L})}{2})}\right)^2 d\omega. \tag{6.6}$$

Most of the area obtained by integrating the function $(\frac{\sin L\omega}{\sin\omega})^2$ belongs to its main lobe. This lobe can be approximated by a rectangle of height L^2 and width $\frac{2\pi}{L}$. The area of this rectangle is then equal to $2\pi L$, and the average power, $E\left[X_l[i]X_l^*[i]\right]$, of the DFT of the noise at $\frac{2\pi i}{L}$ rad/sample is approximately equal to

$$E\left[X_l[i]X_l^*[i]\right] \simeq \frac{1}{2\pi}\int_{-\pi}^{\pi} 2\pi L\delta(\omega+\frac{2\pi i}{L})S_{xx}(e^{j\omega})d\omega \tag{6.7}$$
$$E\left[X_l[i]X_l^*[i]\right] \simeq L\sigma_\eta^2.$$

It is convenient at this point to use the symbols of Section 5.6. The k^{th} FFT performed on the noise sequence $x_l^{rw}[n,k]$ is denoted by $X_l^{rw}[i,k]$, and

$$E\left[|X_l^{rw}[i,k]|^2\right] \simeq L\sigma_\eta^2, i = [0,\ldots,L-1] \tag{6.8}$$

Also from Section 5.6, $\hat{a}_i[k]$ and $\hat{\theta}_i[k]$ are the amplitude and phase estimates of tone number i, that are obtained by taking the DFT, $R_l^{rw}[i,k]$, of $r_l^{rw}[n,k]$. Because the noise is additive, Figure 6.2 shows that $R_l^{rw}[i,k]$ can be viewed as a phasor equal to the sum of two phasors, $V[i,k]$ with magnitude $La_i[k]$ and phase $\theta_i[k]-\phi_{nco}$ and $X_l^{rw}[i,k]$, where $X_l^{rw}[i,k]$ makes an angle $\alpha[i,k]$ with $V[i,k]$. This angle can be any value in $(0,2\pi)$, and can then be seen as a random variable independent of $X_l^{rw}[i,k]$ and uniform over $(0,2\pi)$.

The effect of the noise on the magnitude of $R_l^{rw}[i,k]$ can be measured by projecting $X_l^{rw}[i,k]$ onto $V[i,k]$, yielding

$$|R_l^{rw}[i,k]| = La_i[k] + X_l^{rw}[i,k]\cos(\alpha[i,k]). \tag{6.9}$$

The mean of $|R_l^{rw}[i,k]|$ is equal to

$$\begin{aligned} E\left[|R_l^{rw}[i,k]|\right] &= E\left[La_i[k]\right] + E\left[X_l^{rw}[i,k]\cos(\alpha[i,k])\right] \\ E\left[|R_l^{rw}[i,k]|\right] &= La_i[k] \end{aligned} \tag{6.10}$$

since $E\left[X_l^{rw}[i,k]\cos(\alpha[i,k])\right] = E\left[X_l^{rw}[i,k]\right]E\left[\cos(\alpha[i,k])\right] = 0$. The variance of $|R_l^{rw}[i,k]|$

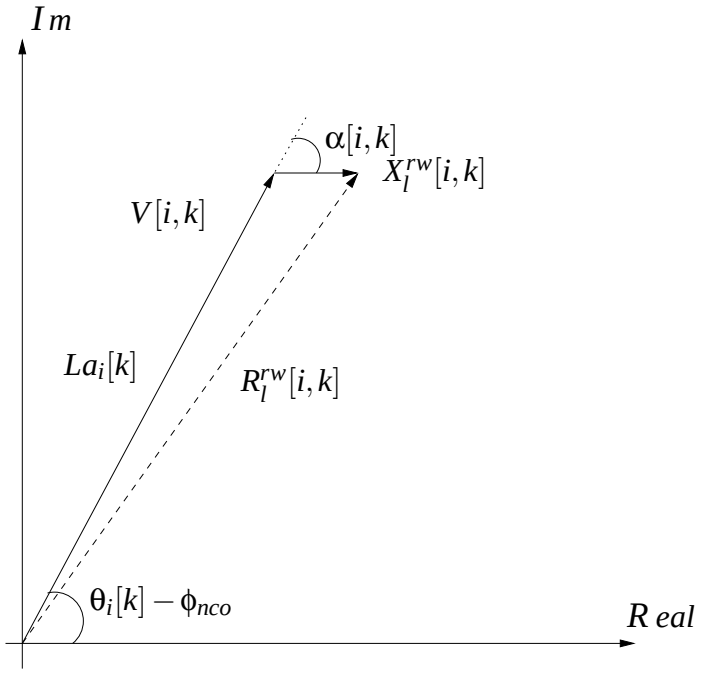

Figure 6.2: Effect of Noise on Amplitude And Phase Estimates.

is given by

$$\begin{aligned}\mathrm{Var}\left(|R_l^{rw}[i,k]|\right) &= E\left[|X_l^{rw}[i,k]|^2\right] E\left[\cos^2(\alpha[i,k])\right] \\ \mathrm{Var}\left(|R_l^{rw}[i,k]|\right) &\simeq \frac{1}{2}L\sigma_\eta^2. \end{aligned} \tag{6.11}$$

From (5.24) and 6.11, the variance of the amplitude estimates, $\hat{a}_i[k]$, due to the noise is then given by

$$\mathrm{Var}\left(\hat{a}_i[k]\right) \simeq \frac{1}{2L}\sigma_\eta^2. \tag{6.12}$$

The effect of the noise on the phase of $R_l^{rw}[i,k]$ can be measured as follows. The phasor component $X_l^{rw}[i,k]\sin(\alpha[i,k])$ is perpendicular to $V[i,k]$, and therefore only affects the phase. As the change in phase due to $X_l^{rw}[i,k]\sin(\alpha[i,k])$ is small, then the phase of $R_l^{rw}[i,k]$ is given by

$$\angle R_l^{rw}[i,k] = \theta_i[k] - \phi_{nco} + \frac{X_l^{rw}[i,k]\sin(\alpha[i,k])}{La_i[k]}. \tag{6.13}$$

The mean of $\angle R_l^{rw}[i,k]$ is equal to $\theta_i[k]-\phi_{nco}$, and the variance of $\angle R_l^{rw}[i,k]$ is given by

$$\begin{aligned}\mathrm{Var}\left(\angle R_l^{rw}[i,k]\right) &= \frac{E\left[|X_l^{rw}[i,k]|^2\right] E\left[\sin^2(\alpha[i,k])\right]}{L^2 a_i^2[k]} \\ \mathrm{Var}\left(\angle R_l^{rw}[i,k]\right) &\simeq \frac{1}{2La_i^2[k]}\sigma_\eta^2. \end{aligned} \tag{6.14}$$

From (5.24) and (6.14), the variance of the phase estimates, $\hat{\theta}_i[k]$, due to the noise is then given by

$$\mathrm{Var}\left([\hat{\theta}_i[k]\right) \simeq \frac{1}{2La_i^2[k]}\sigma_\eta^2. \tag{6.15}$$

The method used to show that (6.12) and (6.15) are valid involves a direct computation and an indirect computation of the variance of $\hat{a}_i[k]$ and $\hat{\theta}_i[k]$. These computations are made on the measured signal. If the signal has traveled through foliage than the tones will vary in amplitude and phase. It then becomes very difficult to estimate the variance of the amplitude and phase estimates due to the noise in the system. The action of the tree foliage on the signal can be eliminated by directly connecting the transmitter to the receiver with a coaxial cable and an attenuator. In this configuration, the amplitude and

phase of each tone remain constant during the acquisition period, and any variation in the amplitude and phase estimates is then only due to the noise. The acquired signal is fed to the post-processing system to generate the amplitude and phase estimates, $\hat{a}_i[k]$ and $\hat{\theta}_i[k]$.

The direct computation consists of computing the variance of the sequences, $\hat{a}_i[k]$ and $\hat{\theta}_i[k]$. The indirect method uses (6.12) and (6.15) to estimate the variance of these sequences after computing an estimate for σ_η^2. The results obtained with both computations are then compared.

For the direct computation, best results are obtained if the variance of $\hat{a}_i[k]$ and $\hat{\theta}_i[k]$ is computed from independent observations. Before the SAW filter in the receiver, the noise can be considered white. The SAW filter and the low-pass filter of the baseband down-converter in the post-processing stage color the noise. To determine the amount of correlation introduced by the filtering, the combination of these filters is modeled as an ideal low-pass filter, with bandwidth equal to $2\pi\frac{38}{256}$ rad/sample (4.19) and the autocorrelation sequence of the noise, $x_l[n]$, at the output of this filter is calculated. It is equal to

$$\frac{1}{2\pi}\sigma_\eta^2\int_{-2\pi\frac{38}{256}}^{2\pi\frac{38}{256}} e^{j\omega n}d\omega = \sigma_\eta^2\frac{\sin(\frac{38\pi}{128}n)}{\pi n}. \tag{6.16}$$

For $n > 650$, the autocorrelation sequence is less than $0.005\times\sigma_\eta^2$. It can be assumed that $x_l[650\times n]$ is made of independent samples. Since $X_l^{rw}[i,k]$ is computed with 256 consecutive elements of $x_l[n]$, then $X_l^{rw}[i,p]$ and $X_l^{rw}[i,q]$ (p and q integers) will be independent if there are at least 650 values between the values used in $X_l^{rw}[i,q]$ and the values used in $X_l^{rw}[i,p]$. Therefore, the values of $X_l^{rw}[i,5\times k]$ are independent, and the values of $R_l^{rw}[i,5\times k]$ can be assumed independent.

For the signal used in this experiment, 10 tones are sent. They are separated in frequencies by $\frac{6}{256}$ cycle/sample, and correspond in (4.19) to $i=-30, i=-24,\ldots,i=0,\ldots,i=24$. For the direct computation, 500 values along index k of $R_l^{rw}[i,5\times k]$ are used to compute the variance of $\hat{a}_i[k]$ and $\hat{\theta}_i[k]$, for each of the 10 tones ($i=-30,-24,\ldots$). For the indirect computation, index k covers the same range and the values, $|R_l^{rw}[i,5\times k]|^2$, are averaged along index k to estimate σ_η^2. A total of 57 values are obtained by varying i from -31 to 25 and are displayed with stars in Figure 6.3. These values, except the ones

for $i = -30, -24, \ldots$ (set to 0 in the plot), are averaged to yield the estimate of σ_η^2 which is shown in Figure 6.3 with a horizontal line.

Figure 6.4 shows the results obtained for both computations. The top graph shows with stars the values obtained with the direct computation for the variance of $\hat{a}_i[k]$, and the horizontal line corresponds to the estimate of the variance of $\hat{a}_i[k]$ obtained using (6.12). For 5 out of the 10 tones, the results are similar since they differ by less than 0.8 dB (bottom graph). For the other tones, the results are not as close since they differ by up to 2 dB. A closer look with a spectrum analyzer reveals the presence of several spurious tones in the band. Spurious tones are present in the vicinity of the tones for which the results differ. The error on the amplitude estimates calculated using (6.12) is found to range between 4.3% and 5.4% of the actual amplitude of the tones. When the variance is computed from 500 independent amplitude estimates, the error on the amplitude estimates is found to range between 3.5% and 5.7%. This shows that (6.12) is a valid equation to accurately estimate the variance of $\hat{a}_i[k]$ due to the Gaussian noise.

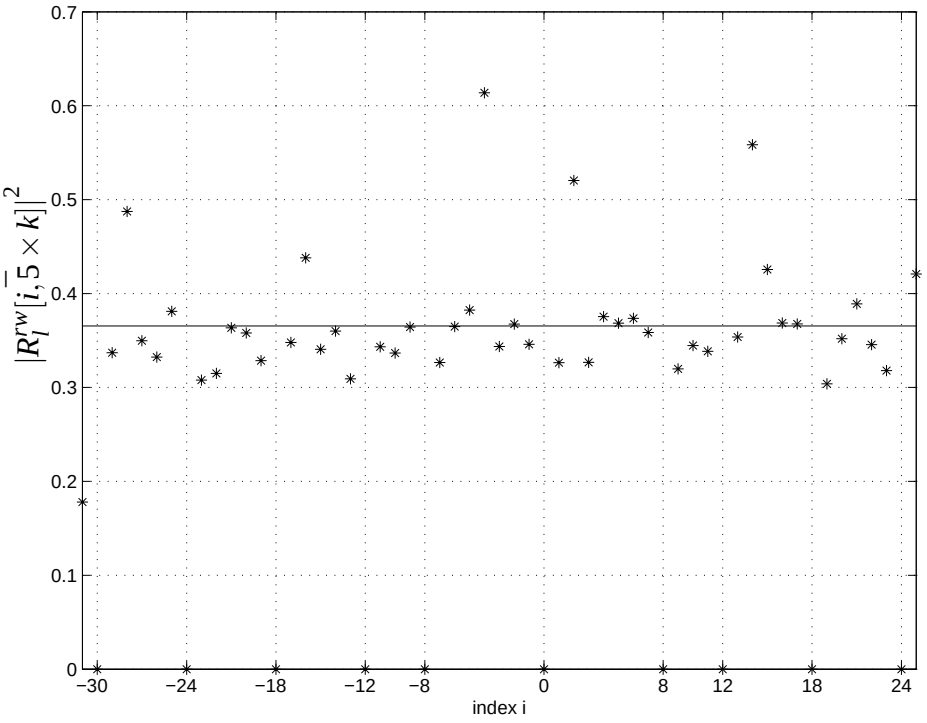

Figure 6.3: Noise Power Spectrum Estimates.

The top graph of Figure 6.5 shows the 500 independent estimates used to compute the variance of $\hat{a}_{24}[k]$, along with horizontal lines corresponding to the mean of these 500 estimates plus or minus the square root of the variance of $\hat{a}_{24}[k]$ that was estimated using (6.12). The middle graph shows the results obtained for $i = -24$, and the bottom graph for $i = 18$. For the top graph, 68% of the 500 estimates are within the horizontal lines, 55% of the estimates for the middle graph, and 81% of the estimates for the bottom graph.

The results obtained to estimate the variance of $\hat{\theta}_i[k]$ are shown in Figure 6.6. The results obtained with the direct computation are shown with stars, and the results obtained with the indirect computation are shown with circles. The results obtained with the direct computation are 10 times higher. This suggests that an extra source of noise is present in the system. This noise source prevents us from accurately computing the variance of $\hat{\theta}_i[k]$ due to the Gaussian noise. However, (6.15) can be used to accurately estimate this variance, as illustrated by the bottom graph of Figure 6.6. This graph shows the 500 estimates

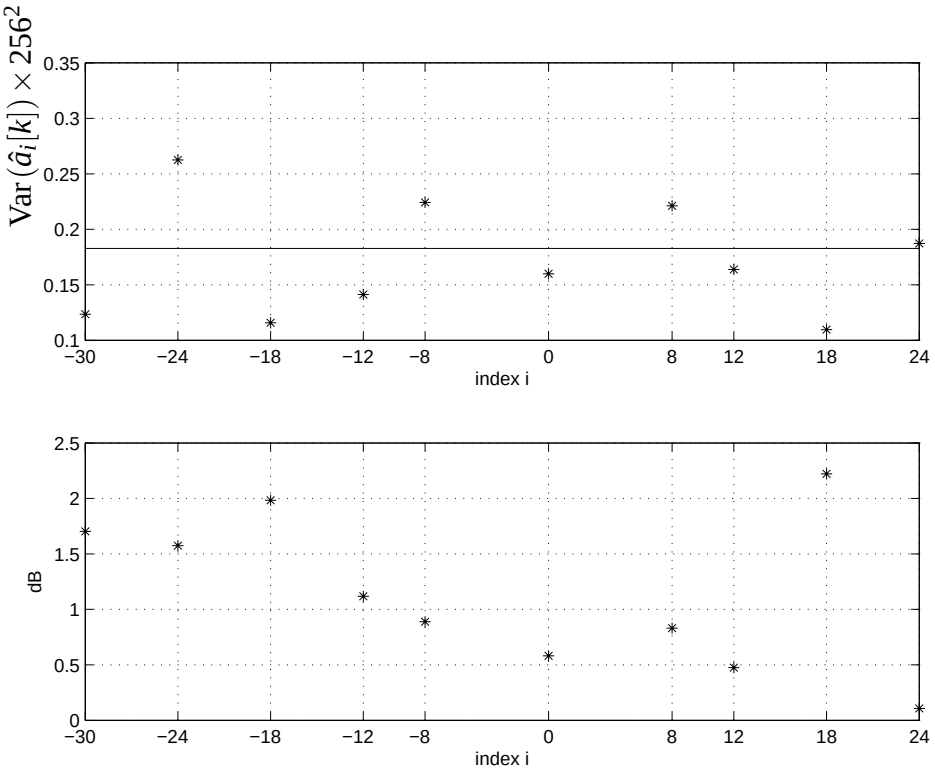

Figure 6.4: Direct & Indirect Computation Results For The Variance Amplitude Estimates.

that were used to compute the variance of $\hat{\theta}_0[k]$, along with horizontal lines corresponding to the mean of these 500 estimates plus or minus the square root of the variance of $\hat{\theta}_0[k]$ calculated using (6.15). These lines surround quite well the measurements for k between 210 and 240, suggesting that the value calculated with (6.15) is quite accurate.

It is shown next that this extra source of noise is introduced by the IF up-converter and corresponds to an angle modulation of the tones.

6.2 Imperfections in Up-Converter

Experiments in the lab showed that the commercial up-converter used to translate the frequency from IF to RF does not work perfectly. It introduces unwanted phase modulation. The effect is the phase of the tones are modulated with a low-frequency sinusoid plus harmonics whose amplitude varies with time. This was observed by feeding a single tone at 44 MHz to the up-converter with a signal generator, and measuring the RF output of

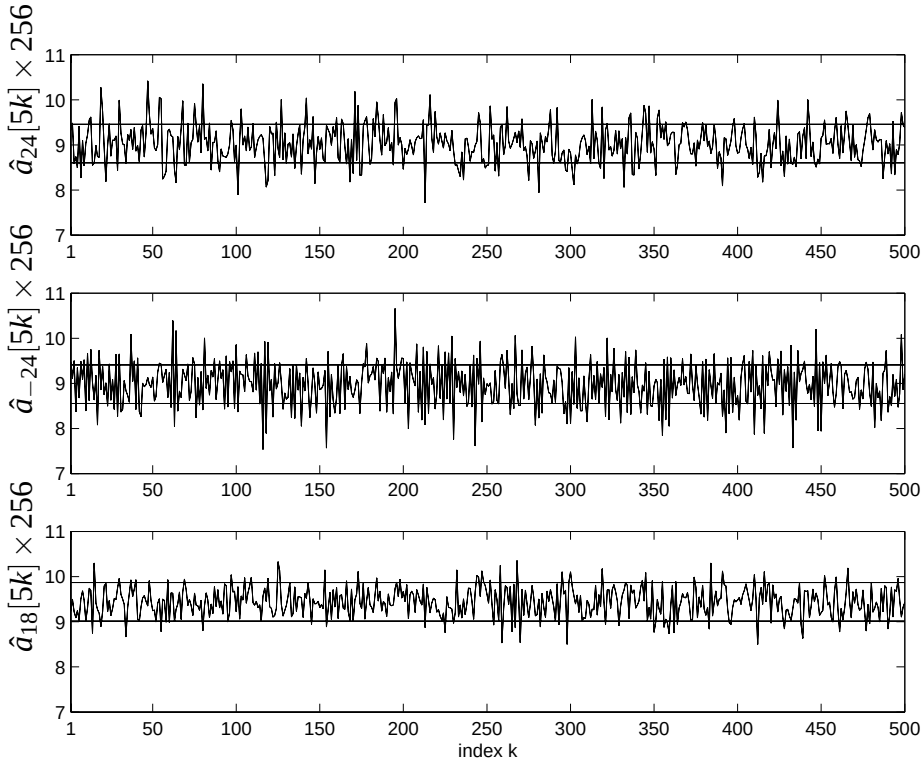

Figure 6.5: Plots of amplitude sequence estimates, $\hat{a}_i[5 \times k]$ (top i = 24, middle i = -24, bottom i = 18), along with lines at one standard deviation from the mean.

the up-converter with a spectrum analyzer.

For the measurements described in this section, a signal made of 10 tones is generated by the transmitter and up-converted to a RF frequency of 2.5457 GHz. The RF output of the transmitter is connected to the RF input of the receiver with a coaxial cable and a 50 dB attenuator. The adjustable gain in the receiver is manually set such that the power level of the tones at IF is $95 dB\mu V$. Some of the sideband peaks shown in Figures 6.7 and 6.8 may be caused by non linearities in the amplifiers. However, only the sideband peaks contributing to this unwanted phase modulation are considered in this section.

To analyze this phase modulation, two types of measurements are made. The first measurement uses the HP 4195A network/spectrum analyzer [18] connected to the input of the A/D converter, in the receiver. It is set to scan a region of 1.2 kHz around one of the tones which is located in the center of the band. Figure 6.7 shows the spectrum analyzer display for one of the scans. The tone of interest appears in the middle of the display. The scaling along the frequency axis is 120 Hz/div. The resolution bandwidth is 3 Hz and the

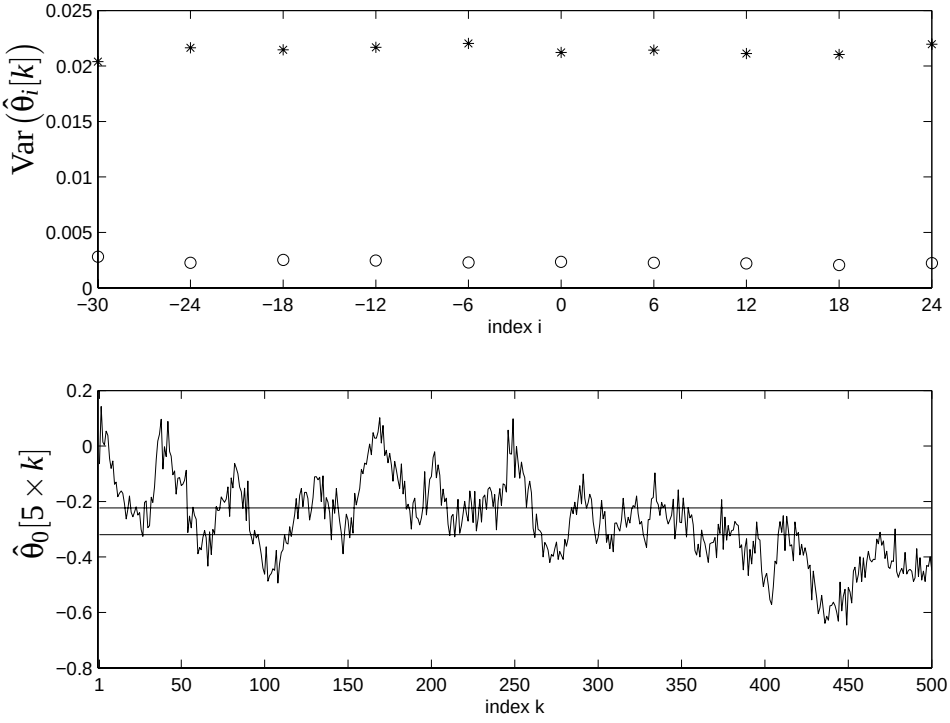

Figure 6.6: Direct & Indirect Computation Results For The Variance Phase Estimates.

time to span 1.2 kHz with this spectrum analyzer is 37.9 minutes. The vertical scale is 6 dB per division.

A digital measurement is performed by computing phase estimates of the tone with a 256-point FFTs. A sequence of phase estimates is then obtained. This sequence is denoted by $\hat{\theta}_s[k]$. Figure 6.8 shows a plot of the spectrum amplitude of $\hat{\theta}_s[k]$. This plot was obtained by performing a 32768-point FFT of $\hat{\theta}_s[k]$. The frequency resolution for this FFT expressed in Hz is $\frac{F_r}{256*32768} = 2.38$ Hz. This plot shows several peaks. Five of these peaks correspond to analog frequencies of approximately 116 Hz, 181 Hz, 233 Hz, 467 Hz, and 493 Hz. Peaks at 120 Hz, 180 Hz, 240 Hz, and 480 Hz away from the frequency of the tone can also be seen in Figure 6.7. A peak at DC is also visible in Figure 6.8. This suggests that frequencies below 2 Hz are present in $\hat{\theta}_s[k]$. There should be corresponding sideband peaks at less than 2 Hz from the tone but these peaks are not visible in Figure 6.7. A possible explanation is that the low-frequency variations in $\hat{\theta}_s[k]$

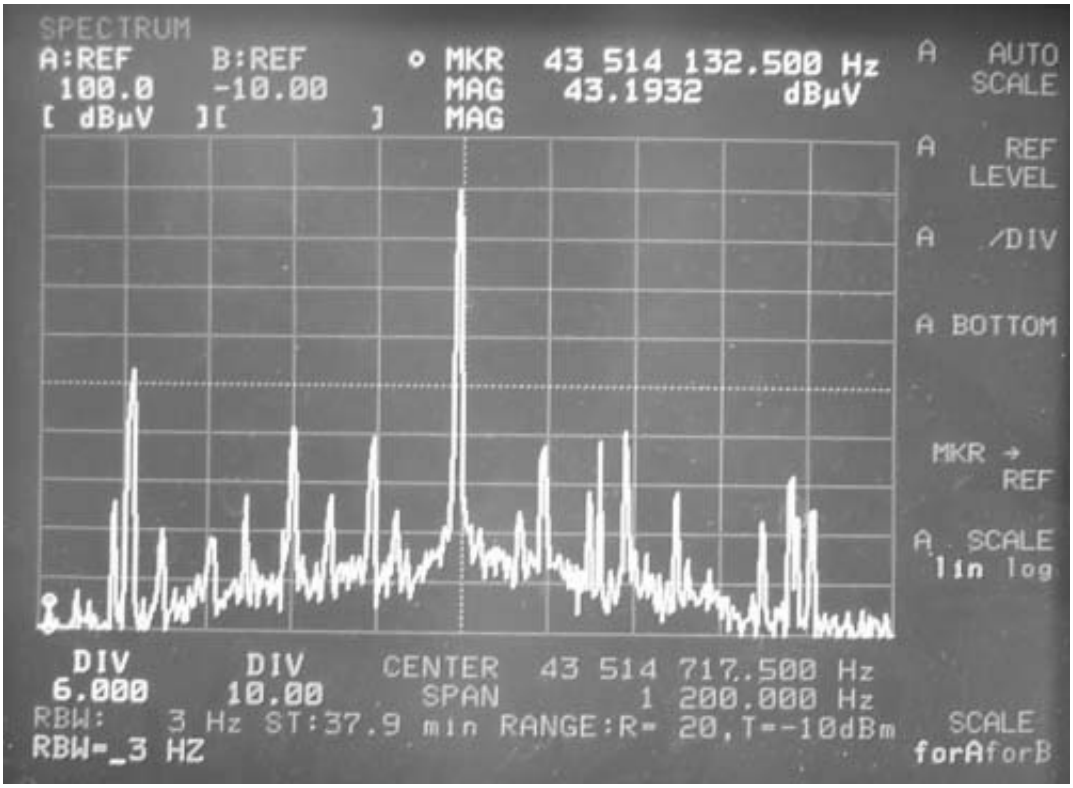

Figure 6.7: Spectrum Analyzer Display

are due to the frequency drift of the oscillators in the up/down converters.

In order to show how the peaks in Figure 6.8 are related to the secondary peaks in Figure 6.7, it is convenient at this point to derive some mathematical expressions for the signal corresponding to the tone. From Figure 6.7, if $\Omega_1, \Omega_2, \ldots, \Omega_n$ denote the analog frequencies of the sideband peaks, and Ω_0 is the nominal analog frequency of the tone, then a possible expression for the time waveform of the tone is

$$x_a(t) = A_0 \cos(\Omega_0 t) + \sum_{i=1}^{n} (A_i(t) \cos((\Omega_0 + \Omega_i)t) + B_i(t) \cos((\Omega_0 - \Omega_i)t)). \qquad (6.17)$$

Because the larger peak in Figure 6.7 could also be seen in Figure 6.8, then from that figure, another possible expression for the time waveform of the tone is

$$x_d(t) = A \cos(\Omega_0 t + \sum_{i=1}^{n} \beta_i(t) \sin(\Omega_i t)). \qquad (6.18)$$

The form of the second expression is that of angle modulation. Equations (6.17) and (6.18) describe the same signal and are related as follows. Equation (6.18) can also be

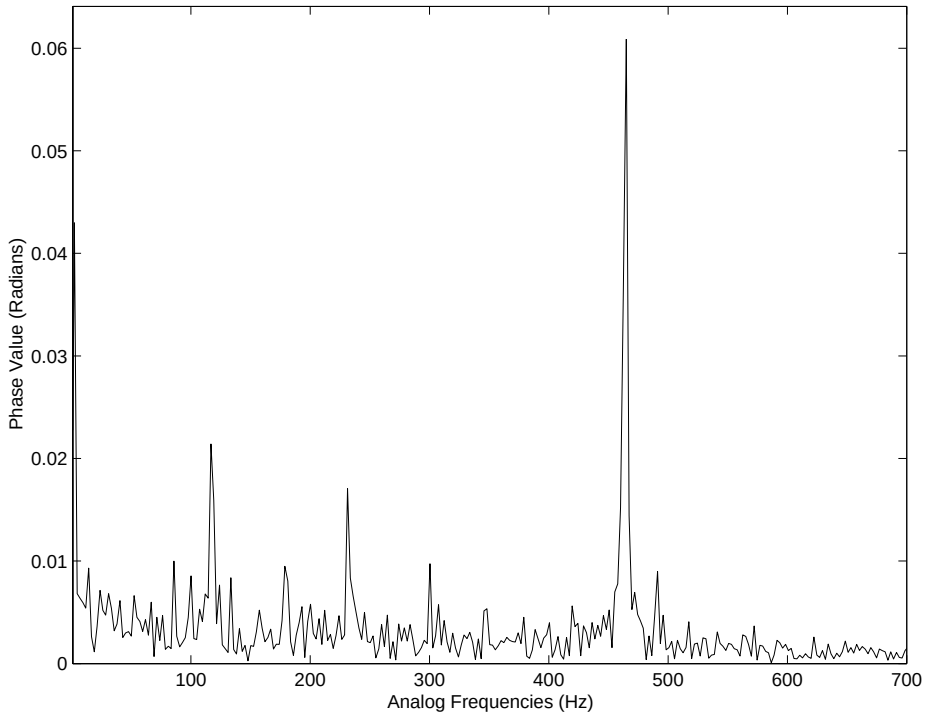

Figure 6.8: Amplitude Spectrum of $\hat{\theta}_s[k]$

rewritten as

$$x_d(t) = AR\, e\{e^{j\Omega_0 t} \prod_{i=1}^{n} e^{j\beta_i(t)\sin(\Omega_i t)}\}. \tag{6.19}$$

From Figure 6.8, $\beta_i \leq 0.062$. The terms in the product of (6.19) can then be approximated by the first two terms of the exponential Taylor series $e^x \approx 1 + x$, yielding

$$x_d(t) = AR\, e\{e^{j\Omega_0 t} \prod_{i=1}^{n} (1 + j\beta_i(t)\sin(\Omega_i t))\}. \tag{6.20}$$

Since $\beta_i(t) \ll 1, i = 1, \ldots, n$, then $\beta_i(t)\beta_j(t) \approx 0$ for $i \neq j$, and (6.20) becomes

$$\begin{aligned}
x_d(t) &= AR\, e\{e^{j\Omega_0 t}(1 + \sum_{i=1}^{n} j\beta_i(t)\sin(\Omega_i t))\} \\
x_d(t) &= AR\, e\{e^{j\Omega_0 t}(1 + \sum_{i=1}^{n} (\frac{\beta_i(t)}{2} e^{j\Omega_i t} - \frac{\beta_i(t)}{2} e^{-j\Omega_i t}))\} \\
x_d(t) &= A\cos(\Omega_0 t) + \sum_{i=1}^{n} (\frac{A\beta_i(t)}{2} cos((\Omega_0 + \Omega_i)t) - \frac{A\beta_i(t)}{2} cos((\Omega_0 - \Omega_i)t))
\end{aligned} \tag{6.21}$$

As $x_d(t) = x_a(t)$ then $A = A_0$, $A_i(t) = A\beta_i(t)/2$, and $B_i(t) = -A\beta_i(t)/2$ for $i = 1, \ldots, n$. The average power of the sideband peaks is then equal to

$$\frac{A_i^2(t)}{2} = \frac{A^2}{4}\frac{\beta_i^2(t)}{2}, i = 1, \ldots, n. \tag{6.22}$$

From (6.22), the average power of the sideband peaks is equal to half of the average power of the tone times a factor, equal to $\frac{\beta_i^2(t)}{2}$, where $\beta_i(t)$ is the value of the corresponding peak in Figure 6.8. The sideband peaks are the results of a narrowband angle modulation of the tones.

Estimates of the spectrum amplitude of $\hat{\theta}_s[k]$ at different instants k, indicate that the values $\beta_i(t)$ of the peaks shown in Figure 6.8 vary with time. This causes the sideband peaks to also vary with time, according to (6.21). However, (6.21) also indicates that the sideband peaks at same distance from the tone should have the same average power at the same time. This is not the case in Figure 6.7 since the sideband peak 467 Hz below the frequency of the tone has a power that is 24 dB less than the power of the tone, and the corresponding sideband peak above the tone has a power that is 36 dB less than the tone. The difference in power between these two sideband peaks arises because the amplitude of the sideband peaks varies with time and the spectrum analyzer doesn't measure the power

of all these sideband peaks at the same time. Figure 6.9 displays a plot of 3125 consecutive values of the phase estimate sequence, $\hat{\theta}_s[k]$, of the tone. Peak-to-peak variations of 0.5 radian, occurring in 1 ms can be observed. These variations can significantly be reduced by filtering out with notch filters the sideband peaks at frequencies 116 Hz, 181 Hz, 233 Hz, 467 Hz, and 493 Hz. The variance of the sequence before filtering was estimated to be 0.021. After notching the main sideband peaks, the variance of the filtered sequence is estimated to be 0.0076.

This angle modulation is nearly identical on all the tones. To verify this statement, two out of the 10 tones are randomly selected. Their phase estimates sequence are subtracted to yield a new sequence. The variance of the new sequence is estimated to be 0.0033.

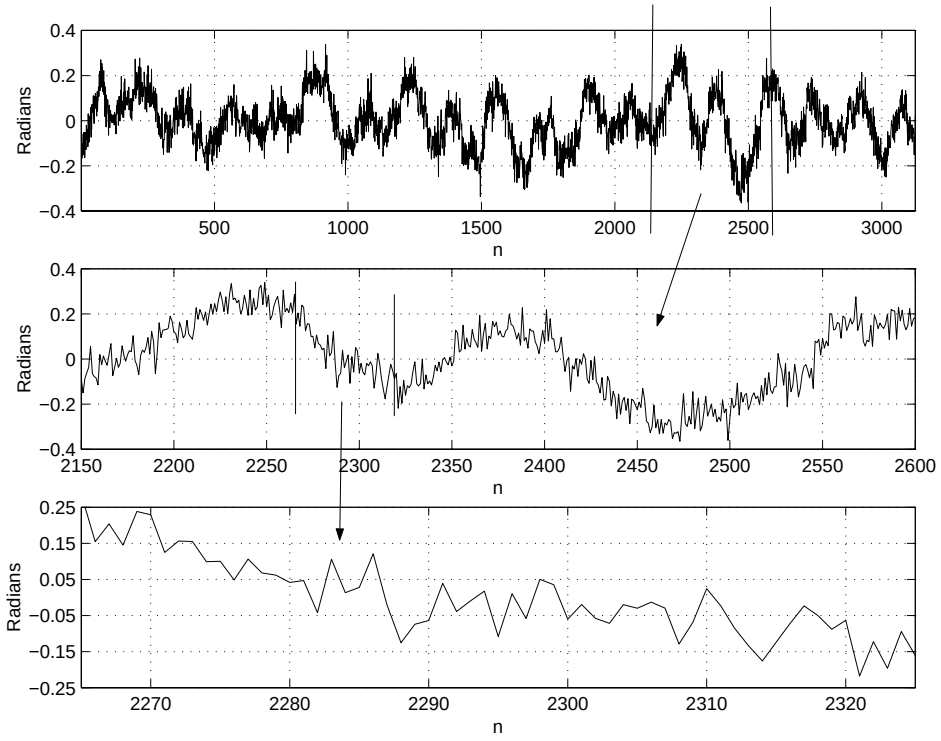

Figure 6.9: Sequence of Phase Estimates, $\hat{\theta}_s[n]$

6.3 Summary

The amplitude measurements are in error due to the Gaussian noise. It was shown that the variance of the amplitude measurements can be accurately estimated using (6.12). For the signal acquired in the lab by connecting the RF output of the transmitter to the RF input of the receiver with a coaxial cable and a 50 dB attenuator, the standard deviation of the amplitude estimates was calculated, using (6.12), to be 4.8% of the actual amplitude of the tones. In the next chapter, it is shown that this error can be significantly reduced.

The phase measurements are also in error due to the Gaussian noise. Equation (6.15) can be used to accurately estimate the variance of the phase estimates due to the Gaussian noise. For the signal acquired in the lab, the variance computed by using 500 phase estimates was largely in error due to the angle modulation introduced by the IF up-converter and the frequency drift of the oscillators of the measuring system. However, (6.15) could be used to accurately estimate the variance of the phase estimates due to the Gaussian noise. The standard deviation on the phase estimates calculated with (6.15) was found to be 0.046 radian or 2.6 degrees. In the next chapter, it is shown that this error can be significantly reduced.

This angle modulation causes some 0.5 radian peak-to-peak ripple at about 500 Hz and is common to all the tones. It is expected that the phase variations due to tree foliage are larger than 0.5 radian and the effect of the angle modulation should be negligible. Slow variations of higher magnitude occur due to the frequency drift of the oscillators. Some of these variations can be removed, as shown in the next chapter.

7. PROCESSING THE AMPLITUDE AND PHASE MEASUREMENTS

As seen in Chapter 6, the measuring system will report variations in the phase of the tones even if the channel remains invariant. Variations in the phase of the tones are mainly caused by the frequency drift of the oscillators in the up/down converters. The presence of Gaussian noise in the system also introduces an error in the measurements. The amplitude and phase estimates can be further processed to reduce the effect of the noise generated by the system.

7.1 Amplitude Measurement

The measuring system makes an amplitude measurement every 12.8 μs. The frequency response of NLOS channel is time-variant, but it changes very slowly. It has been established in Chapter 3 that the channel remains essentially constant over a 5 ms interval. This implies that 390 consecutive measurements at 12.8 μs intervals could then be averaged to get a good estimate of the amplitude and phase of the tones for the center of the interval. A new sequence, denoted $\overline{a}_i[k]$, is generated by averaging 250 consecutive amplitude measurements. The interval of time separating the values of $\overline{a}_i[k]$ becomes equal to 12.8 μs $*250 = 3.2$ ms. For the signal acquired in the lab by connecting the RF output of the transmitter to the RF input of the receiver with a coaxial cable and a 50 dB attenuator, the standard deviation on the amplitude estimates was found to be 4.8% of the actual amplitude of the tones (Chapter 6). After averaging, the standard deviation on the amplitude estimates is computed to be 0.3% of the actual amplitude of the tones. The signal-to-noise ratio of the receive signal is about 20 dB.

The same computation is applied to the sequence of phase estimates, $\hat{\theta}_i[k]$. The new sequence of phase estimates is denoted by $\overline{\theta}_i[k]$, and the interval of time separating the values of $\overline{\theta}_i[k]$ is also equal to 3.2 ms.

7.2 Phase Measurement

It is possible to filter out some of the variations due to the frequency drift of the oscillators in the transmitter and receiver. Some of these variations can be estimated because of the deterministic behavior of these components, and can then be removed from the phase measurements. The approach taken to accomplish this is described next.

The imprecision in the frequency of the oscillators of the up and down-conversion stages causes the tones to all deviate from their nominal frequency by the same amount, $\Delta\omega[n]$. Furthermore, $\Delta\omega[n]$ does not remain constant over the duration of the signal but varies due to variations in the frequency generated by the oscillators. For example, changes in ambient temperature cause the oscillators to drift in frequency. The frequency of an oscillator may also slowly vary around its nominal value. However, over the 5 second period during which the signal is acquired, it can be assumed that the drift in frequency of the oscillators remains constant. The frequency deviation, $\Delta\omega[n]$, of the tones can then be expressed as $\Delta\omega[n] = \alpha_1 n + C$, where α_1 can be positive, negative, or zero over the 5 second interval. If the frequency of each oscillator remains constant, then the frequency difference between any two oscillators is a constant, C, and $\alpha_1 = 0$. If $\alpha_1 \neq 0$, then the N receive tones will have phase that is a parabolic function of time, i.e. $\Delta\omega[n] * n = \alpha_1 n^2 + C * n + D_i$, where D_i is a constant that depends on the phase of tone number i, $(i = 1, \ldots, N)$ at the beginning of the 5 second interval.

The post-processing system estimates $\Delta\omega[n]$ from the center tone and uses that value to convert the IF receive signal to baseband. This action causes the phase of the down-converted tones to vary along parabolic curves given by

$$\begin{cases} p_1[n] & = \alpha_1(n - 781 - \alpha_2)^2 + k_1 \\ p_2[n] & = \alpha_1(n - 781 - \alpha_2)^2 + k_2 \\ \quad \ldots & \\ p_N[n] & = \alpha_1(n - 781 - \alpha_2)^2 + k_N. \end{cases} \tag{7.1}$$

where k_i is a constant that depends on the phase of down-converted tone number i at the beginning of the 5 second interval, and α_2 is a constant. This is explained as follows. A perfect down-conversion to baseband is obtained when the down-converted center tone

is at 0 Hz. The way the system has been designed, in case of a constant drift of the oscillators frequency over the 5 second interval, the down-converted center tone will vary in frequency but will be equal to 0 Hz exactly at the center of the 5 second interval. But because of noise and additional phase variations caused by tree foliage, the down-converted center tone will not be equal to 0 exactly at the center of the interval. This is illustrated in Figure 7.1. This figure shows a plot of the phase estimates, $\overline{\theta}_i[k]$, obtained for each of the tones when 10 tones are sent and the receiver is connected to the transmitter with a coaxial cable and a 50 dB attenuator. The phase varies similarly for all the tones. The phase mainly decreases between 0 and 2 seconds, suggesting that the frequency of the down-converted center tone is negative, then remains relatively constant between 2 and 3 seconds (the frequency of the down-converted center tone is about 0 Hz), and mainly increases between 3 and 5 seconds (the frequency of the down-converted center tone is positive). The phase variation of the 10 tones can be approximated with parabolic curves, given by (7.1), where $N = 10$. This can be achieved by deriving a system of equations

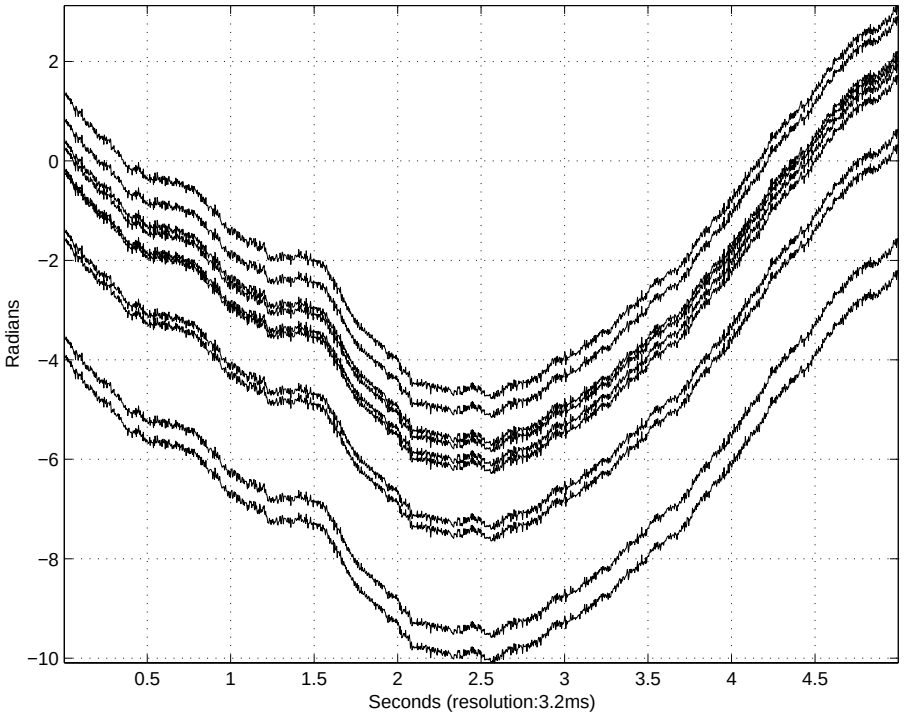

Figure 7.1: Plot of Tones Phase Estimates, $\overline{\theta}_i[k]$, $i = 1, \ldots, 10$.

from (7.1) and finding the values for the parameters that minimize the error between the phase measurements and the parabolic curves in the least-squares sense. This system of equations is derived as follows. (7.1) can be rewritten as (with N = 10)

$$\begin{cases} p_1[n] & = \alpha_1(n-781)^2 - 2\alpha_1\alpha_2(n-781) + \alpha_1\alpha_2^2 + k_1 \\ p_2[n] & = \alpha_1(n-781)^2 - 2\alpha_1\alpha_2(n-781) + \alpha_1\alpha_2^2 + k_2 \\ \cdots & \\ p_{10}[n] & = \alpha_1(n-781)^2 - 2\alpha_1\alpha_2(n-781) + \alpha_1\alpha_2^2 + k_{10}. \end{cases} \tag{7.2}$$

This system of equations is also equal to

$$\begin{cases} p_1[n] & = c_1(n-781)^2 + c_2(n-781) + c_3 \\ p_2[n] & = c_1(n-781)^2 + c_2(n-781) + c_4 \\ \cdots & \\ p_{10}[n] & = c_1(n-781)^2 + c_2(n-781) + c_{12}, \end{cases} \tag{7.3}$$

where the parameters, $c_1, \ldots, c_{12}$ are equal to $c_1 = \alpha_1$, $c_2 = -2\alpha_1\alpha_2$, $c_3 = \alpha_1\alpha_2^2 + k_1$, $c_4 = \alpha_1\alpha_2^2 + k_2$, …, $c_{12} = \alpha_1\alpha_2^2 + k_{10}$. The Matlab function "lsqcurvefit" is used to estimate these parameters. Figure(7.2) shows the parabolic curves obtained, displayed on the same plot as the phase estimates, $\overline{\theta}_i[n]$, of the tones. The parabolic curves can then be subtracted from the phase estimates of the tones, yielding new sequences, $\overline{\theta}_i^p[n]$, equal to

$$\overline{\theta}_i^p[n] = \overline{\theta}_i[n] - p_i[n]. \tag{7.4}$$

Figure 7.3 shows a plot of $\overline{\theta}_1^p[n]$ at the top and a plot of $\overline{\theta}_6^p[n]$ at the bottom. The 2 radian peak-to-peak low-frequency ripple is probably due to the oscillators. The waveforms shown on the figure are very similar. To verify this, one of the waveform taken as the reference is subtracted from all the waveforms, $\overline{\theta}_i^p[n]$ $(i = 1, \ldots, 10)$. $\overline{\theta}_6^p[n]$ is the waveform arbitrary chosen to be the reference. The waveforms obtained are denoted by $\overline{\Delta\theta}_i^p[n]$, where

$$\overline{\Delta\theta}_i^p[n] = \overline{\theta}_i^p[n] - \overline{\theta}_6^p[n], i = 1, \ldots, 10. \tag{7.5}$$

Only the variations due to Gaussian noise should be left. This is not the case, as shown in Figure 7.4. In this figure, each waveform has the shape of a straight line whose slope is

proportional to the digital frequency of the down-converted tone the waveform represents. The slopes are also proportional to each other. These variations are due to a residual error in the resampling. They can be approximated with straight lines equal to

$$\begin{cases} st_1[n] & = -30\alpha_3 n \\ st_2[n] & = -24\alpha_3 n \\ \quad \dots & \\ st_6[n] & = 0 \\ \quad \dots & \\ st_{10}[n] & = 24\alpha_3 n, \end{cases} \tag{7.6}$$

where α_3 is a constant. Equation (7.6) can be combined with (7.1) to produce a new system of equations that is similar to (7.3). The parameters of this new system of equations are estimated with "lsqcurvefit". The waveforms, $\overline{\Delta\theta}_i^p[n]$, are then generated. This time, they look like noise, with a standard deviation that is estimated to be 0.004 radian or 0.23

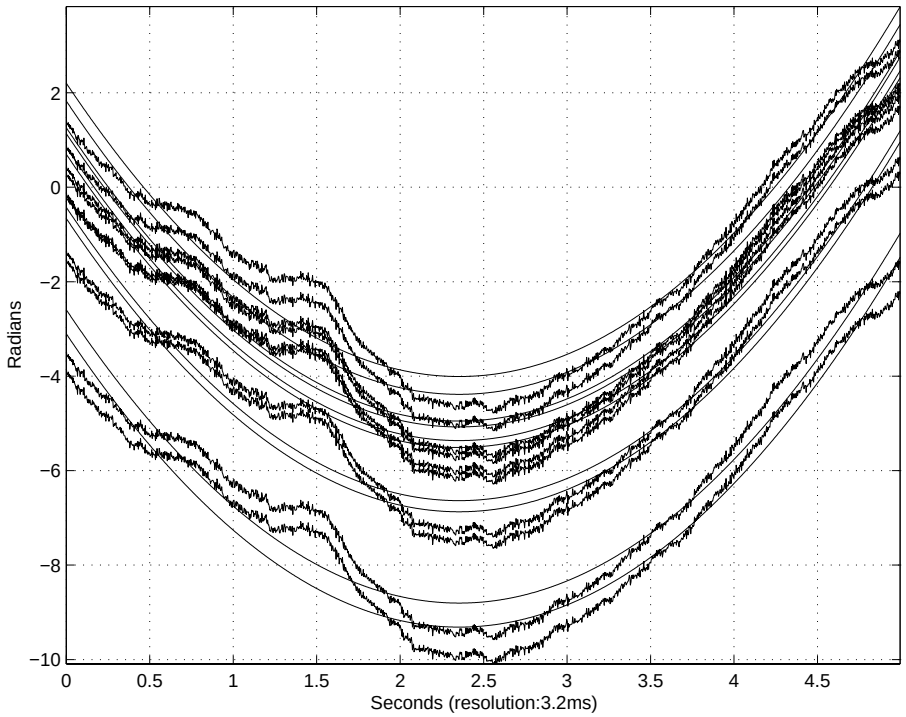

Figure 7.2: Plot of Tones Phase Estimates, $\overline{\theta}_i[k]$, Along With Parabolic Curves, $p_i[n]$, $i = 1, \dots, 10$.

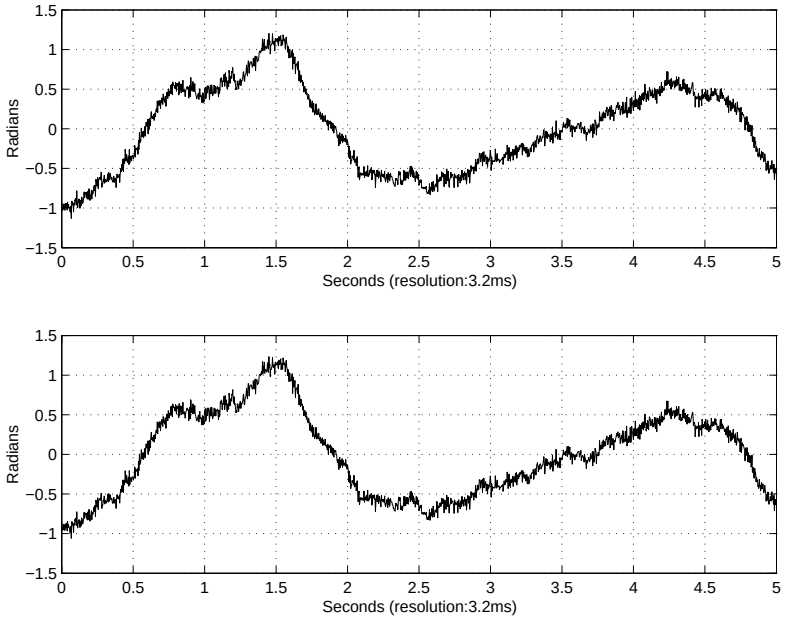

Figure 7.3: Plot of Tones Phase Estimates, $\overline{\theta}_1^p[n]$, and $\overline{\theta}_6^p[n]$

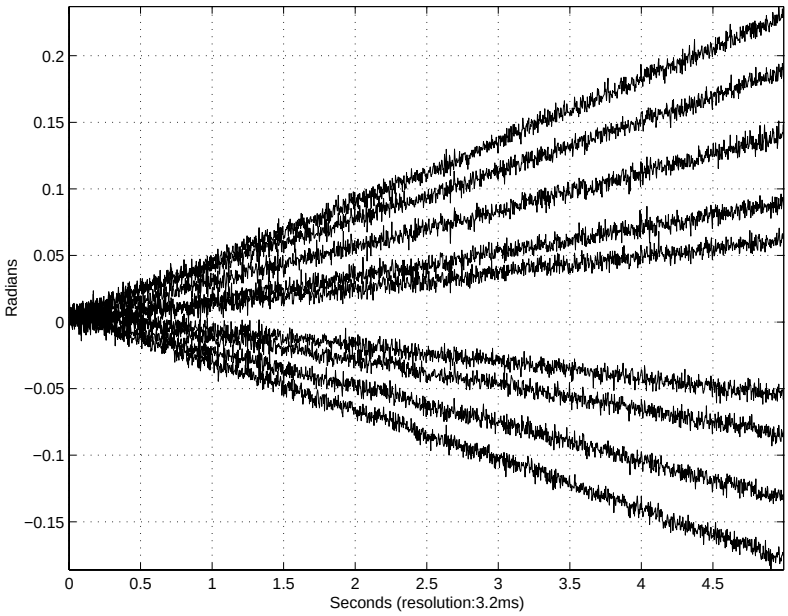

Figure 7.4: Plot of Tones Phase Estimates, $\overline{\Delta\theta}_i^p[n]$, $i = 1,\ldots,10$.

degrees.

7.3 Summary

Two types of sequences are obtained for phase. The first type of sequence represents phase estimates of the tones, 3.2 ms apart, after some of the variations due to the oscillators have been removed. The variations left appear as low-frequency ripple and are probably due to the oscillators. The second type of sequence represents the variation in the phase estimates of the tones with respect to the variation in the phase estimates of one of the tone taken as the reference. Only noise could be seen on the signal acquired in the lab. The standard deviation of these sequences was calculated to be about 0.23 degrees. This means that any variation in phase caused by tree foliage that is not common to all the tones can be accurately measured with this system.

Any variation in amplitude that is common to all the tones or any variation in amplitude that is frequency selective can also be accurately measured with this system since the standard deviation of the amplitude estimates for the signal acquired in the lab was calculated to be 0.3% of the actual amplitude of the tones.

8. OUTDOOR MEASUREMENTS AND ANALYSIS

8.1 Fall 2002 Measurements

The selected site was the north east end of the TR*Labs* building parking lot. The TR*Labs* building is situated at the north end of Innovation Place, on the University of Saskatchewan campus. The receive antenna was placed behind one of the Poplar trees planted at the edge of the parking lot. Figure 8.1 shows the 25-ft tall Poplar tree that was selected. The rail road track showing at the bottom of the figure is the CP line that runs west and east. As shown in the figure, the receive antenna was placed at 80ft from the tree and was 12 feet high from the ground. Figure 8.2 is an aerial view of the site. This photo was taken from the roof of the TR*Labs* building where the transmit antenna was installed. The white ar-

Figure 8.1: Line-of-sight Obstruction With a Single Poplar Tree.

row in the Figure points to the tree that was shown in Figure 8.1. Although this system configuration wasn't very realistic because of the closeness of the transmit antenna to the receive antenna and the presence of only a single tree in the line-of-sight, the setup revealed many of the problems that needed to be overcome in order to collect good real-time data.

The first set of measurements taken in the wind showed strong variations that were attributed to the motion of the antennas. The transmit antenna was then fixed for the measurements that followed. Some of the data acquired are shown next.

8.1.1 Line-Of-Sight Measurement

The receive antenna was placed in front of the Poplar tree such that there was no obstacle between the transmit and receive antennas. Figure 8.3 shows the amplitude variation of the tones. These curves were obtained by converting the sequences of amplitude estimates, $\overline{a}_i[k]$, to dBV, and rescaling such that at the beginning of the plot, the curves are separated by 0.5 dB. They were also organized such that the curves are in the same order as the tones in the band, with the one corresponding to the lowest frequency tone shown at the bottom of the plot. The oscillation at about 1.5 Hz that can be seen on all the tones is due to the motion of the receive antenna. The wind was less than 6 km/h, suggesting that the receive antenna should also be fixed.

Figure 8.4 shows the amplitude variation of each tone relative to the amplitude varia-

Figure 8.2: Aerial Views of The Poplar Tree Obstructing The Line-Of-Sight.

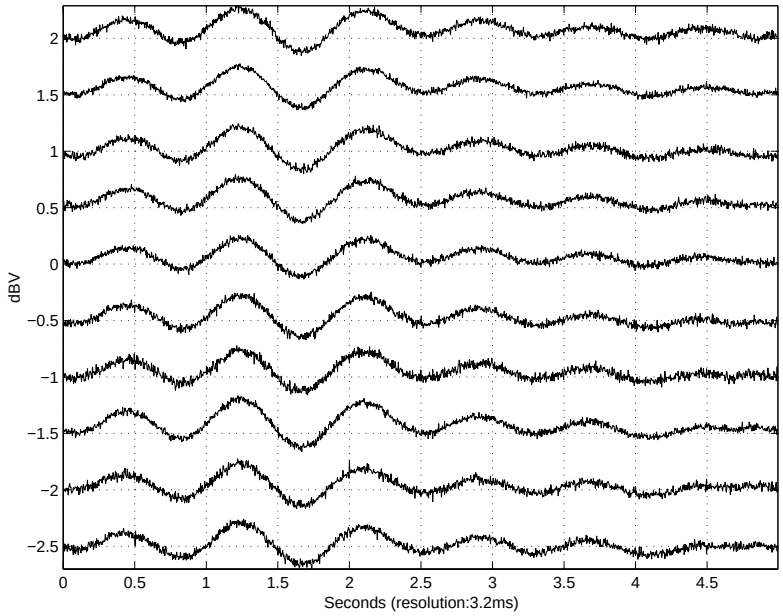

Figure 8.3: Line-Of-Sight: Amplitude Variation of The Tones.

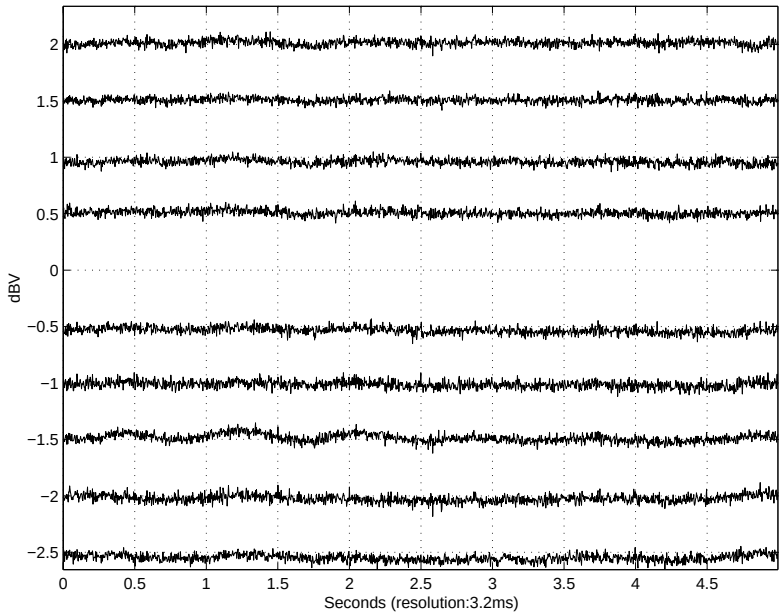

Figure 8.4: Line-Of-Sight: Amplitude Variation of the Tones Relative To Amplitude Variation of The Center Tone.

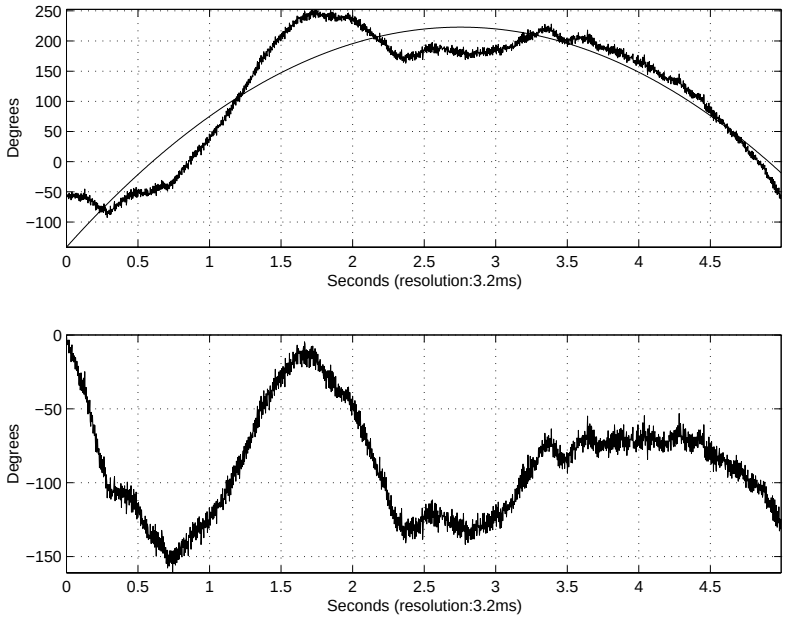

Figure 8.5: Line-Of-Sight: Phase Measurements of The Center Tone Before And After Correction.

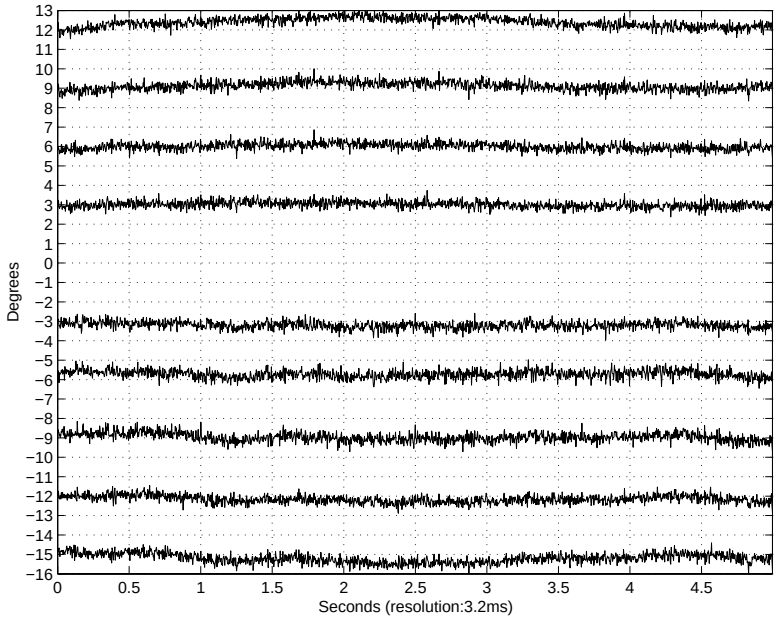

Figure 8.6: Line-Of-Sight: Phase Variation of The Tones Relative To Phase Variation of The Center Tone.

tion of the tone at the center of the band. A 0.2 dB peak-to-peak oscillation at 1.5 Hz on the third curve and lasting for the first three seconds of the acquisition can be seen. The motion of the receive antenna gives rise to variations among the tones, which suggests that multipath independent of the trees exists in the channel. This multipath propagation appeared to be quite strong when the receive antenna was moved back and forth by hand, and was likely due to the roof edge in the proximity of the transmit antenna. When the receive antenna is placed behind the tree, this multipath may cause severe frequency selective fades that make it difficult to tell what type of distortions actually originate from the tree.

The top graph of Figure 8.5 is the sequence of phase estimates, $\overline{\theta}_i[k]$, obtained for the tone at the center of the band (center tone), along with a parabolic approximation to that curve. The bottom graph of that figure is the phase variation of the center tone after removing the parabolic variation. Figure 8.6 shows the phase variation of the tones relative to the phase variation of the center tone. The peak-to-peak variations are less than 1 degree. As for amplitude, the curves are in the same order as the tones in the band, and the curve corresponding to the lowest frequency tone is shown at the bottom of the plot.

8.1.2 Measurements During Windy and Rainy Conditions

The antenna was placed 80 ft behind the tree, beside the rail road track (Figure 8.1). The wind was blowing at 35 km/h, gusting to 50 km/h. The rainfall amount for that day was about 20 mm. Variations of 2 dB in the amplitude of the tones can be seen in Figure 8.7. These variations are caused by changes in the foliage density with the swaying of the branches in the wind. However, some of these variations may be due to the motion of the receive antenna. The signal loss through the tree was measured to be 7 dB.

In Figure 8.8, the relative amplitude variations are 0.5 dB or less, and occur in 250ms. Some variations larger than 0.5 dB can be seen. Variations of 1 dB over a period of time between 250 and 500 ms are visible at 0.5 seconds (tone number 9), and 2.25 seconds (tones number 1 and 3).

The phase measurements obtained for the center tone are shown in Figure 8.9. The variations are similar to the variations of the line-of-sight measurements, suggesting that

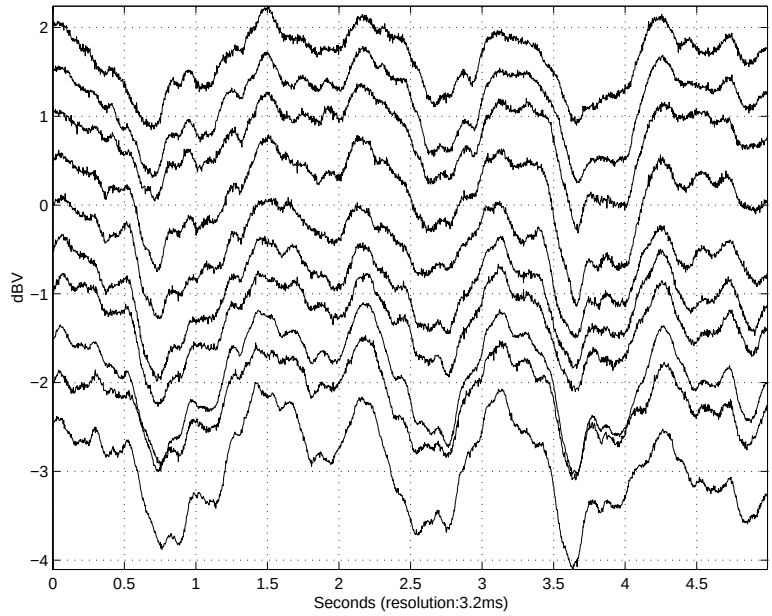

Figure 8.7: Wind And Rain Measurement (Fall 2002): Amplitude Variation of The Tones.

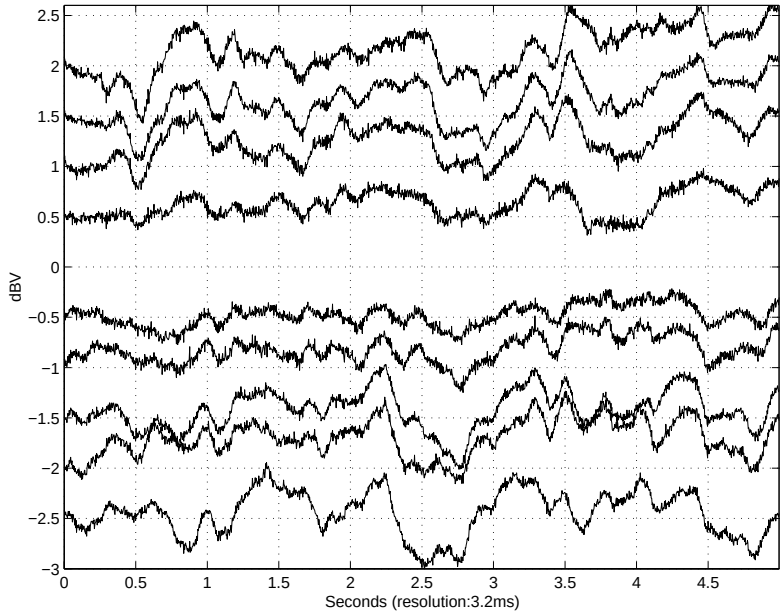

Figure 8.8: Wind And Rain Measurement (Fall 2002): Amplitude Variation of The Tones Relative To Amplitude Variation of The Center Tone.

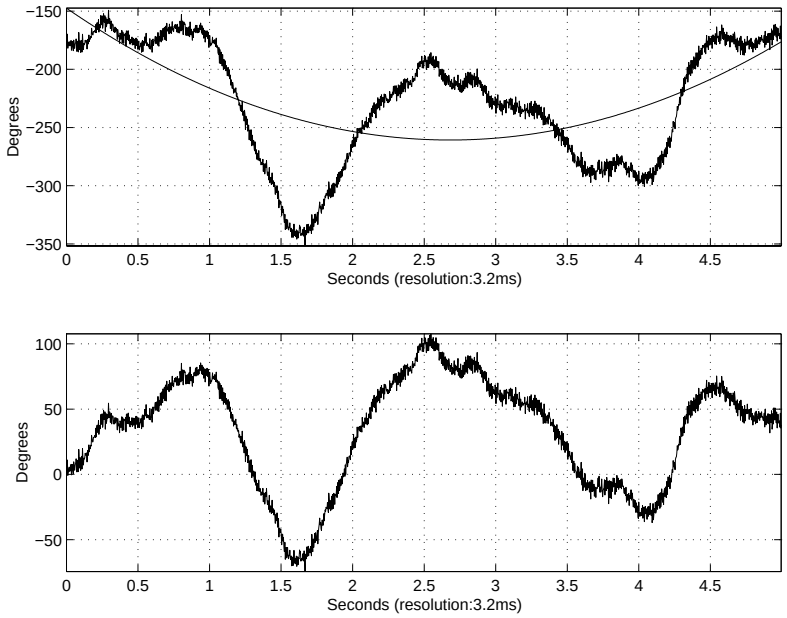

Figure 8.9: Wind And Rain Measurement (Fall 2002): Phase Measurements of The Center Tone Before And After Correction.

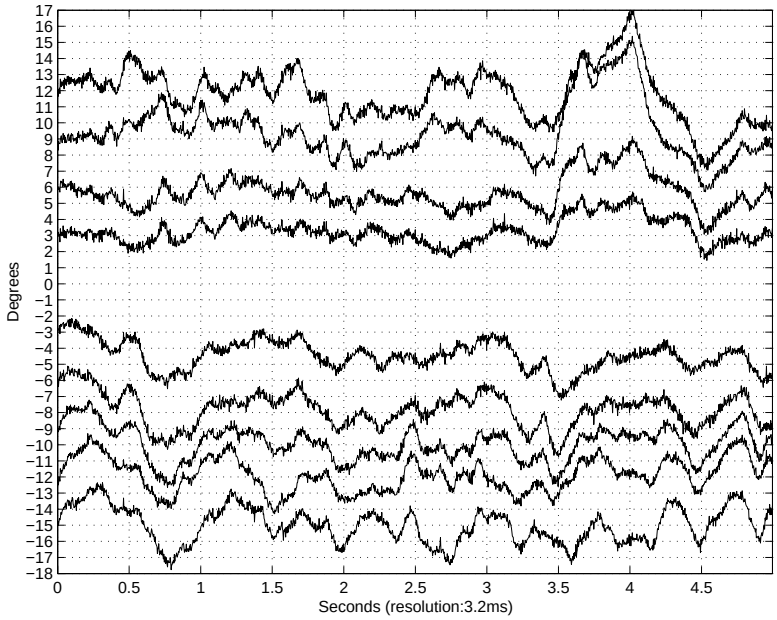

Figure 8.10: Wind And Rain Measurement (Fall 2002): Phase Variation of The Tones Relative To Phase Variation of The Center Tone.

the phase variations due to the Doppler shift induced by the motion of the branches are in the same range as the variations caused by the frequency drift of the oscillators in the up/down converters. In Figure 8.10, the relative phase variations are 3 degrees or less, and occur in 250 ms. Some variations much larger than 3 degrees can be seen. There is a 7 degree variation in 125 ms for tone number 9 at 3.5 seconds, and a 9 degree increase over a period of 500 ms for tones 9 and 10, at 4 seconds.

8.2 Summer 2003 Measurements

The measurements took place on an acreage located on Valley road, 12km southwest of Saskatoon. The 110 degree sectoral transmit antenna was mounted on the side of a barn, 20 feet above the ground. The receive antenna was placed 10 feet behind a clump of 25-foot tall Poplar trees. Figure 8.11 shows a view of the trees obstructing the line-of-sight. This clump was located northwest of the barn, at a distance of 292 meters (958 feet) from the barn. A southeast wind blew in the same direction as the line-of-sight. A southwest

Figure 8.11: A Clump of 25-Feet Tall Poplar Trees Obstructing The Line-Of-Sight.

wind blew in the direction normal to the line-of-sight.

The ground elevation was 25 feet lower at the bush than at the barn. The receive antenna was mounted on a 16 feet poll, buried 2 feet in the ground, placing the receive antenna at an elevation 30 feet lower than the transmit antenna. The angle between the signal path and the normal to the transmit antenna was then 1.7 degrees. As the transmit antenna had a vertical angle of 10 degrees, then the receive signal was well within the main lobe of the transmit antenna. A water level was used to set the poll vertical and the receive antenna was visually aimed at the barn by rotating the poll. A finer adjustment was obtained by slightly rotating the poll and measuring the amount of power received with a spectrum analyzer.

The RF transmit signal power was 30 dBmW and the gain of the transmit antenna was 13.5 dBi. The power of the receive signal when the antenna was placed in front of the bush was measured to be -58 dBmW. The amount of multipath in the channel was measured by moving the antenna 5 feet sideway. This test showed that the channel exhibited little amount of multipath since the variations among the tones were less than 0.5 dB for amplitude and less than 10 degrees for phase. The receive power decreased to -71 dBmW when placing the antenna 10 feet behind the clump, indicating that the attenuation of the RF signal through the clump was 13 dB.

A wind meter was used to perform signal acquisition with different wind conditions. The largest fades were seen with gust winds. Data acquired under little and strong wind, with and without rain are presented next. Measurements of the depth and rate of the fades seen on the data are also given.

8.2.1 Measurements During Windy Conditions

Figure 8.12 shows the amplitude variation of the tones when the wind speed was measured to be varying from 8.6 to 5.8km/h during the 5 second acquisition of the signal. The curve at the bottom corresponds to the lowest frequency tone, the curve in the middle to the tone at the center of the band, and the curve at the top to the highest frequency tone. For display purposes, the spacing between the curves was arbitrarily set to 2dB. Figure 8.13 shows the amplitude variation of the tones relative to the amplitude variation of the lowest

frequency tone. The curves are in the same order as the tones in the band. The curve for the lowest frequency tone is a straight line equal to 0dBV. The spacing between the curves was arbitrarily set to 1dB. The variations among the tones are less than 1dB.

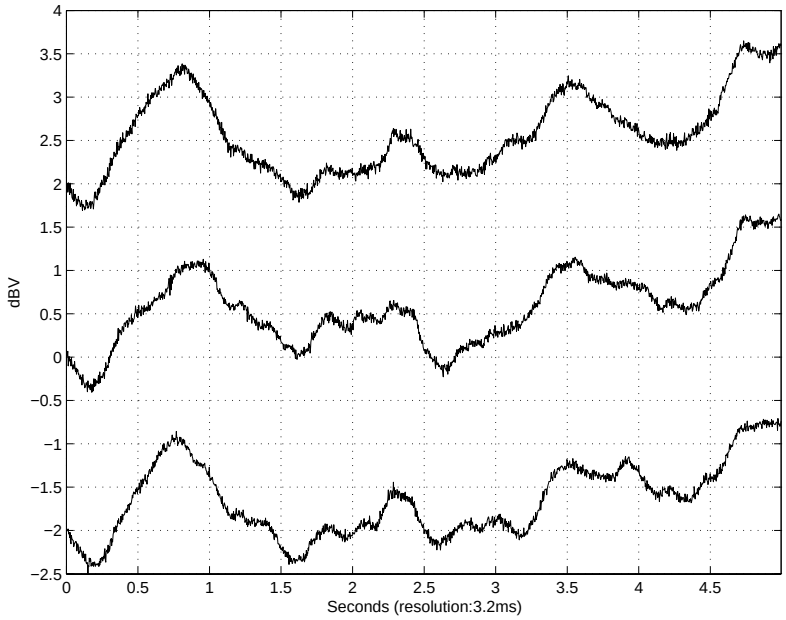

Figure 8.12: 8.6 To 5.8 km/h South East Wind, No Rain: Amplitude Variation of The Tones.

The variation in phase due to tree foliage that is common to all the tones is masked by the variation in phase caused by the frequency drift of the oscillators. Therefore, there is no figure to show the phase variation of the tones. Figure 8.14 shows the phase variation of the tones relative to the phase variation of the lowest frequency tone. The variations among the tones are less than 9 degrees. The peak-to-peak variation of the curves given in Figure 8.12, 8.13, and 8.14 are reported in Table 8.1.

Figure 8.15 shows the amplitude variation of the tones when the wind varied from 24 to 9.6km/h. Guard wires were used to keep the receive antenna poll still. As in Figure 8.12, the curve at the bottom corresponds to the lowest frequency tone, the curve in the middle to the center tone, and the curve at the top to the highest frequency tone. For

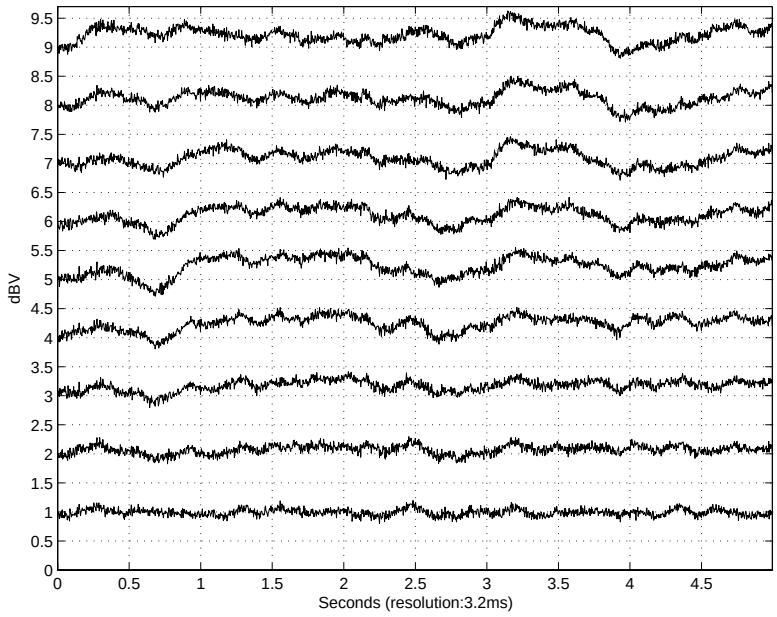

Figure 8.13: 8.6 To 5.8 km/h South East Wind, No Rain: Amplitude Variation of The Tones Relative To Amplitude Variation of The Lowest Frequency Tone.

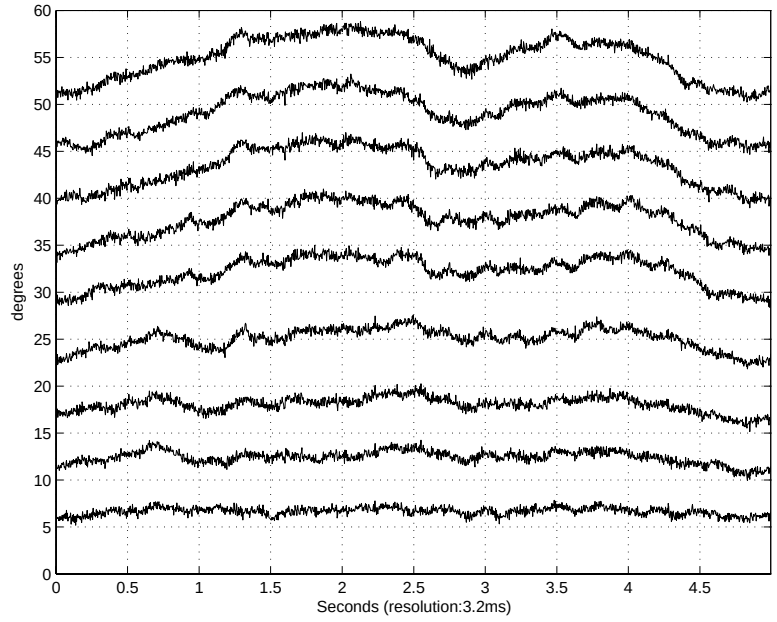

Figure 8.14: 8.6 To 5.8 km/h South East Wind, No Rain: Phase Variation of The Tones Relative To Phase Variation of The Lowest Frequency Tone.

Table 8.1: 8.6 To 5.8 km/h South East Wind, No Rain: Peak-to-peak Variations for Amplitude & Phase Measurements.

Tone #	**1**	**2**	**3**	**4**	**5**	**6**	**7**	**8**	**9**	**10**
Amp. (dB)	**1.8**	**1.7**	**1.8**	**1.9**	**1.9**	**2.1**	**2**	**2**	**2**	**2**
Rel. Amp. (dB)	**0**	**0.4**	**0.5**	**0.6**	**0.7**	**0.8**	**0.7**	**0.7**	**0.8**	**0.8**
Abs. Pha. (Deg)	**417**	**419**	**421**	**423**	**425**	**427**	**428**	**431**	**433**	**435**
Rel. Pha. (Deg)	**0**	**2.7**	**4.3**	**5.1**	**5.7**	**6.6**	**7.8**	**8**	**8.7**	**8.6**

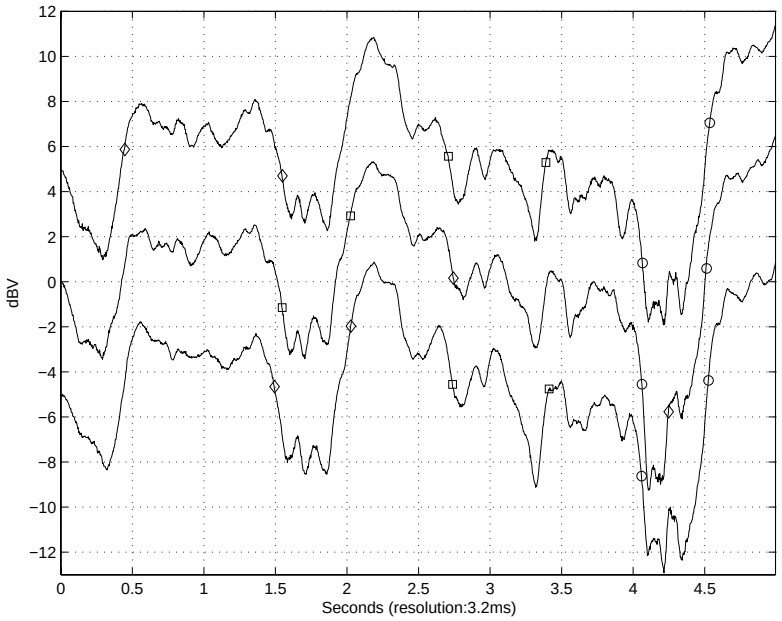

Figure 8.15: 24 To 9.6 km/h South East Wind, No Rain: Amplitude Variation of The Tones.

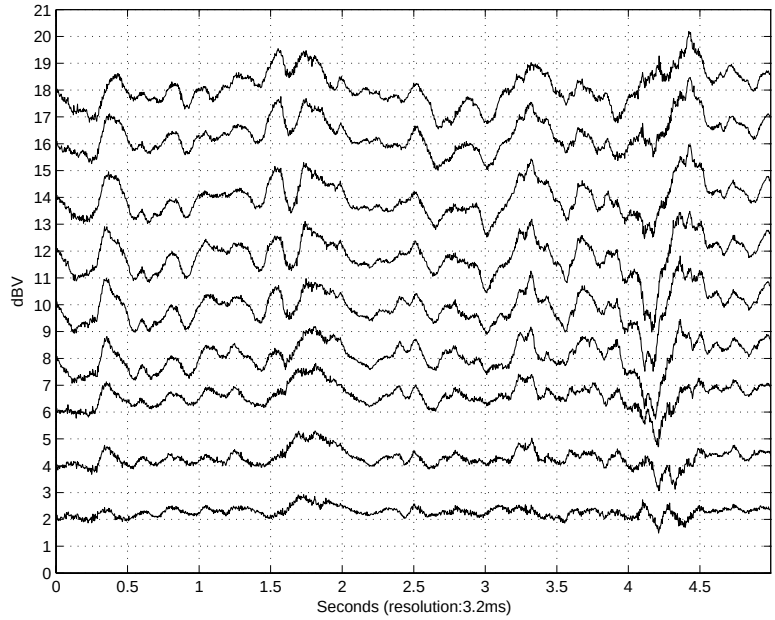

Figure 8.16: 24 To 9.6 km/h South East Wind, No Rain: Amplitude Variation of The Tones Relative To Amplitude Variation of The Lowest Frequency Tone.

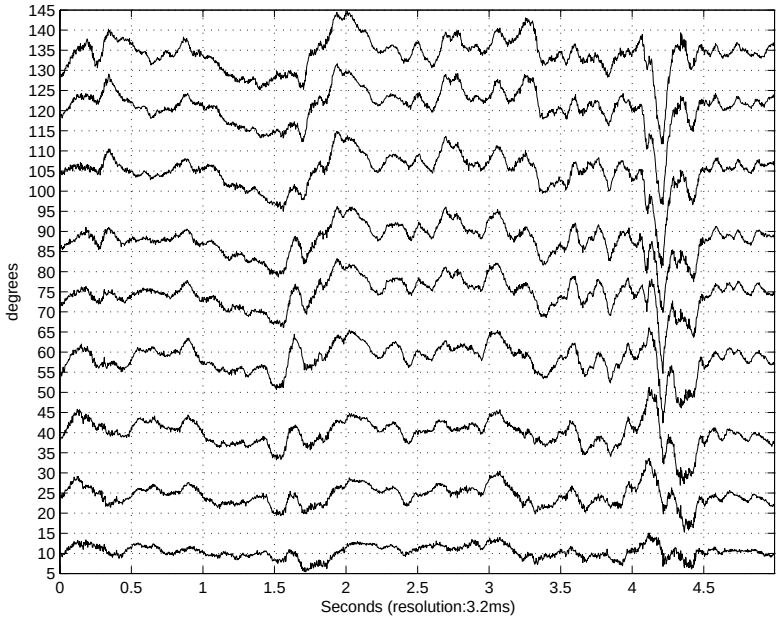

Figure 8.17: 24 To 9.6 km/h South East Wind, No Rain: Phase Variation of The Tones Relative To Phase Variation of The Lowest Frequency Tone.

display purposes, the spacing between the curves was arbitrarily set to 5dB. The variations are much stronger than on the previous plots, with three strong fades occurring over the 5 second period. An algorithm was developed in Matlab to locate these fades, and compute the depth of the fades and the fading rate. The fades are located by extracting the variations with the strongest slope. These variations are identified with little circles, squares, and diamonds on the curves shown in Figure 8.15. Table 8.3 gives for each of them the amount of variation in dB, the duration of the variation, the rate in dB/s, and the location of the variation in the curve.

Figure 8.16 shows the amplitude variation of the tones relative to the amplitude variation of the lowest frequency tone. The strongest variations were extracted and measurements of these variations are reported in table 8.4. No data were available for the cells of the table that are empty. Figure 8.17 shows the phase variation of the tones relative to the phase variation of the lowest frequency tone. The strongest variations were also extracted and measurements of these variations are reported in table 8.5. Finally, the peak-to-peak variation of the curves given in Figure 8.15, 8.16, and 8.17 are reported in Table 8.2.

Table 8.2: 24 To 9.6 km/h South East Wind, No Rain: Peak-to-peak Variations for Amplitude & Phase Measurements.

Tone #	**1**	**2**	**3**	**4**	**5**	**6**	**7**	**8**	**9**	**10**
Abs. Amp. (dB)	**13.8**	**14.5**	**14.9**	**15.7**	**15.7**	**15.7**	**15.9**	**14.8**	**14.4**	**13.3**
Rel. Amp. (dB)	**0**	**1.4**	**2.2**	**3.1**	**3.7**	**4.3**	**4.5**	**3.5**	**3.5**	**3.6**
Abs. Pha. (Deg)	**330**	**333**	**333**	**334**	**324**	**321**	**318**	**314**	**318**	**323**
Rel. Pha. (Deg)	**0**	**9.7**	**18.4**	**24.3**	**23.7**	**28.5**	**26.4**	**33.9**	**35**	**32.8**

The deepest fade can last 500 milliseconds. Severe frequency selective distortions to the signal can occur during that time.

Table 8.3: 24 To 9.6 km/h South East Wind, No Rain: Instantaneous Amplitude Variations.

Circles / Squares / Diamonds								
Tone #	Var. (dB)	Dur. (s)	Rate (dB/s)	Loc. (s)	Var. (dB)	Dur. (s)	Rate (dB/s)	Loc. (s)
1	**11.5**	**0.33**	**34.5**	**4.5**	**-5.6**	**0.13**	**-42**	**4.0**
6	**10.4**	**0.32**	**32**	**4.5**	**-6.6**	**0.13**	**-51.5**	**4.0**
10	**11.3**	**0.36**	**30.1**	**4.5**	**-4.9**	**0.12**	**-40.4**	**4.0**
1	**4.4**	**0.17**	**26.6**	**3.4**	**-3.5**	**0.16**	**-21.6**	**2.7**
6	**8.1**	**0.33**	**24.5**	**2**	**-3.9**	**0.15**	**-26.6**	**1.5**
10	**3.7**	**0.11**	**31.8**	**3.4**	**-3.5**	**0.17**	**-20.5**	**2.7**
1	**9.3**	**0.34**	**27.4**	**2**	**-5.2**	**0.23**	**-23**	**1.5**
6	**4**	**0.11**	**36.4**	**4.2**	**-2.9**	**0.17**	**-17.4**	**2.7**
10	**6.7**	**0.26**	**25.9**	**0.4**	**-3.7**	**0.16**	**-23.7**	**1.5**

Table 8.4: 24 To 9.6 km/h South East Wind, No Rain: Instantaneous Amplitude Variations Relative to Amplitude Variations of Lowest Frequency Tone.

Tone #	Var. (dB)	Dur. (s)	Rate (dB/s)	Loc. (s)	Var. (dB)	Dur. (s)	Rate (dB/s)	Loc. (s)
1	**0.5**	**0.08**	**6.9**	**4.3**	**0.8**	**0.19**	**4.1**	**1.6**
2	**0.5**	**0.11**	**4.5**	**4.4**	**0.7**	**0.12**	**5.7**	**1.7**
3	**1.1**	**0.09**	**12.3**	**4.3**	**0.9**	**0.1**	**9.1**	**1.6**
4	**3.2**	**0.18**	**17.7**	**4.3**	**1.1**	**0.15**	**7.5**	**1.7**
5	**3.6**	**0.19**	**19.2**	**4.3**	**1.1**	**0.1**	**11.7**	**1.7**
6	**4.3**	**0.2**	**22**	**4.3**	**1.6**	**0.1**	**16.6**	**1.7**
7	**2.4**	**0.22**	**10.9**	**4.3**	**1.6**	**0.1**	**15.8**	**1.7**
8					**1.2**	**0.09**	**13.7**	**1.7**
9	**1.6**	**0.16**	**10.1**	**4.4**				

8.2.2 Measurements During Windy and Rainy Conditions

Figure 8.18 shows the amplitude variation of the tones when the wind speed was measured to be varying from 21 to 15.5 km/h during the 5 second acquisition of the signal. It was raining. The total amount of precipitation for that day was 25 millimeters. The Measurements for the variations identified with small circles, squares, and diamonds are reported in table 8.7. Figure 8.19 shows the amplitude variation of the tones relative to the amplitude variation of the lowest frequency tone. Figure 8.20 shows the phase variation of the tones relative to the phase variation of the lowest frequency tone. The peak-to-peak variation of the curves given in Figure 8.18, 8.19, and 8.20 are reported in Table 8.6.

Table 8.5: 24 To 9.6 km/h South East Wind, No Rain: Instantaneous Phase Variations Relative to Phase Variations of Lowest Frequency Tone.

Tone #	Var. (Deg)	Dur. (s)	Rate (Deg/s)	Loc. (s)	Var. (Deg)	Dur. (s)	Rate (Deg/s)	Loc. (s)
1	**-3.8**	**0.06**	**-62.7**	**4.2**				
2	**-10**	**0.12**	**-84.8**	**4.2**				
3	**-12.3**	**0.1**	**-124**	**4.2**				
4	**-15.5**	**0.1**	**-156.7**	**4.2**	**6**	**0.05**	**110.4**	**4.3**
5	**-15.5**	**0.08**	**-186.1**	**4.2**	**7.7**	**0.08**	**100.2**	**4.3**
6	**-12.3**	**0.09**	**-137.1**	**4.2**	**7.6**	**0.08**	**91.1**	**4.3**
7	**-15.4**	**0.09**	**-178.7**	**4.2**	**19.2**	**0.1**	**187.7**	**4.3**
8	**-15.5**	**0.09**	**-173.5**	**4.2**	**24.9**	**0.14**	**176.8**	**4.3**
9	**-17.2**	**0.1**	**-173.6**	**4.2**	**20.3**	**0.12**	**171.5**	**4.3**

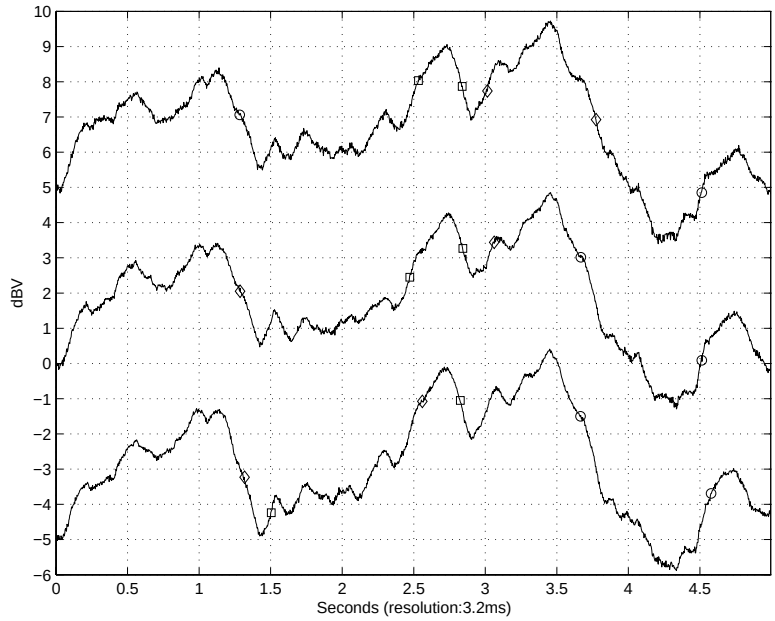

Figure 8.18: 21 To 15.5 km/h South West Wind, Rain: Amplitude Variation of The Tones.

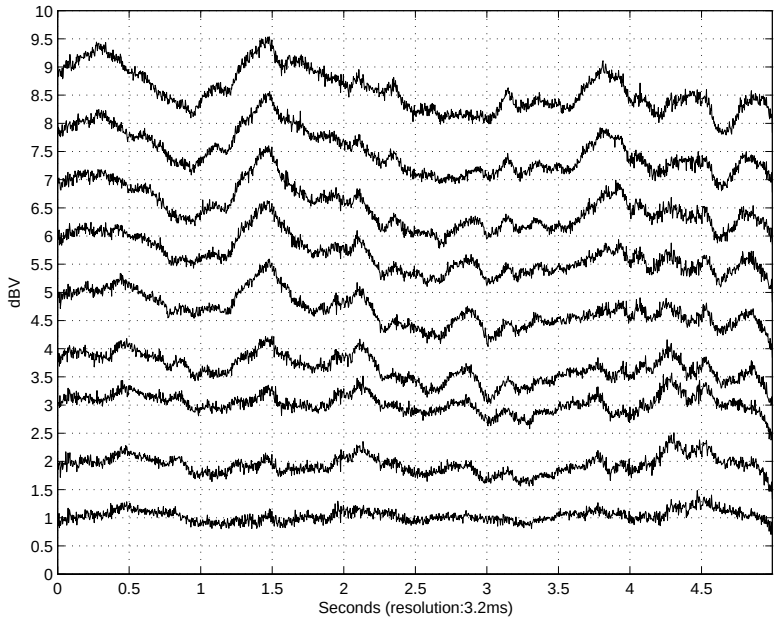

Figure 8.19: 21 To 15.5 km/h South West Wind, Rain: Amplitude Variation of The Tones Relative To Amplitude Variation of The Lowest Frequency Tone.

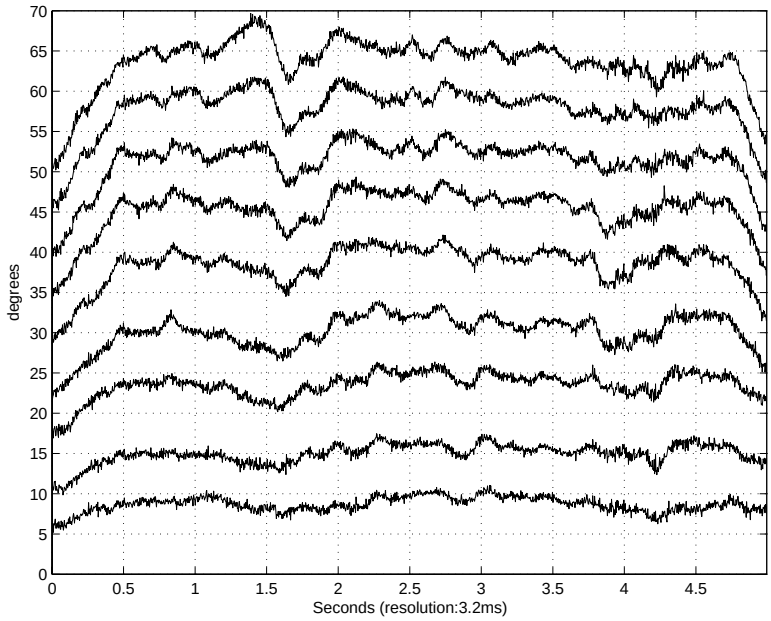

Figure 8.20: 21 To 15.5 km/h South West Wind, Rain: Phase Variation of The Tones Relative To Phase Variation of The Lowest Frequency Tone.

Table 8.6: 21 To 15.5 km/h South West Wind, Rain: Peak-to-peak Variations for Amplitude & Phase Measurements.

Tone #	**1**	**2**	**3**	**4**	**5**	**6**	**7**	**8**	**9**	**10**
Abs. Amp. (dB)	**6.3**	**6.1**	**5.8**	**5.9**	**5.9**	**6.1**	**6.1**	**6**	**6.2**	**6.3**
Rel. Amp. (dB)	**0**	**0.8**	**1.2**	**1.2**	**1.2**	**1.7**	**1.8**	**1.8**	**1.8**	**1.7**
Abs. Pha. (Deg)	**475**	**471**	**467**	**466**	**466**	**464**	**465**	**464**	**465**	**464**
Rel. Pha. (Deg)	**0**	**5.8**	**7.6**	**9.4**	**12.2**	**13.5**	**15**	**15.9**	**16.5**	**19.5**

Figure 8.21 shows the amplitude variation of the tones when the wind speed was measured to be varying from 14 to 15.5 km/h during the 5 second acquisition of the signal. This signal was acquired shortly after the previous signal. The Measurements for the variations identified with small circles and squares are reported in table 8.9. Figure 8.22 shows the amplitude variation of the tones relative to the amplitude variation of the lowest frequency tone. Figure 8.23 shows the phase variation of the tones relative to the phase variation of the lowest frequency tone. The strongest variations of these curves were extracted and measurements of these variations are reported in table 8.10. Finally, the peak-to-peak variation of the curves given in Figure 8.21, 8.22, and 8.23 are reported in Table 8.8.

From the measurements, the wind seems to be the major factor causing signal fading.

Table 8.7: 21 To 15.5 km/h South West Wind, Rain: Instantaneous Amplitude Variations.

Circles / Squares / Diamonds								
Tone #	Var. (dB)	Dur. (s)	Rate (dB/s)	Loc. (s)	Var. (dB)	Dur. (s)	Rate (dB/s)	Loc. (s)
1	**2.2**	**0.26**	**8.7**	**4.6**	**-4.2**	**0.4**	**-10.3**	**3.7**
6	**1.6**	**0.13**	**12**	**4.5**	**-4**	**0.4**	**-10.2**	**3.7**
10	**1.2**	**0.13**	**9.2**	**4.5**	**-2.6**	**0.31**	**-8.6**	**1.3**
1	**0.9**	**0.11**	**8.4**	**1.5**	**-1.9**	**0.19**	**-9.8**	**2.8**
6	**1.7**	**0.18**	**9.3**	**2.5**	**-1.7**	**0.18**	**-9.4**	**2.8**
10	**1.9**	**0.25**	**7.8**	**2.5**	**-1.9**	**0.18**	**-10.6**	**2.8**
1	**2.6**	**0.32**	**8.1**	**2.5**	**-3.3**	**0.27**	**-12**	**1.3**
6	**0.9**	**0.11**	**7.7**	**3**	**-2.9**	**0.31**	**-9.3**	**1.3**
10	**1.4**	**0.18**	**7.8**	**3**	**-2.1**	**0.19**	**-11.6**	**3.8**

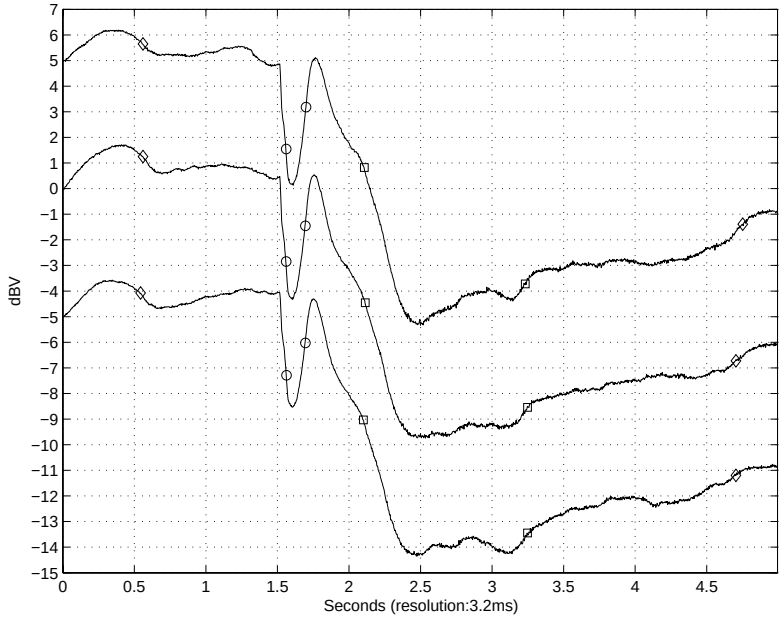

Figure 8.21: 14 To 15.5 km/h South West Wind, Rain: Amplitude Variation of The Tones.

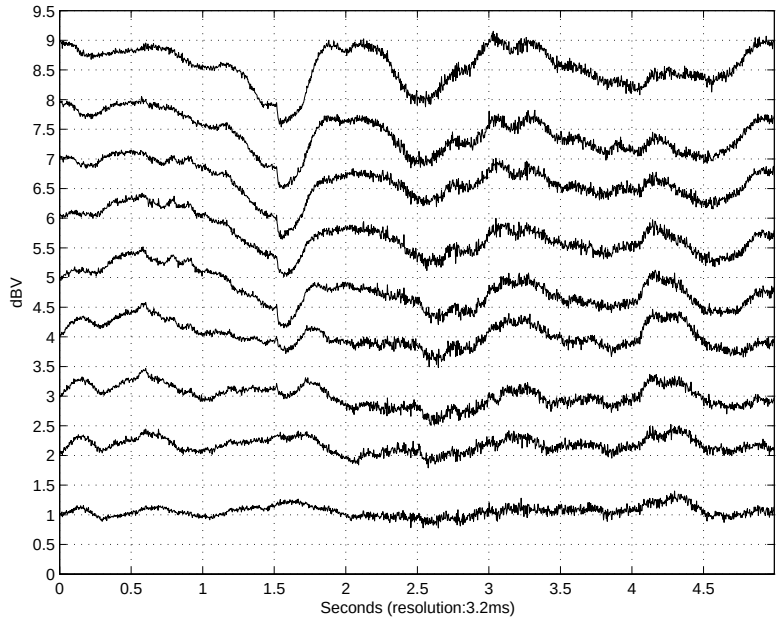

Figure 8.22: 14 To 15.5 km/h South West Wind, Rain: Amplitude Variation of The Tones Relative To Amplitude Variation of The Lowest Frequency Tone.

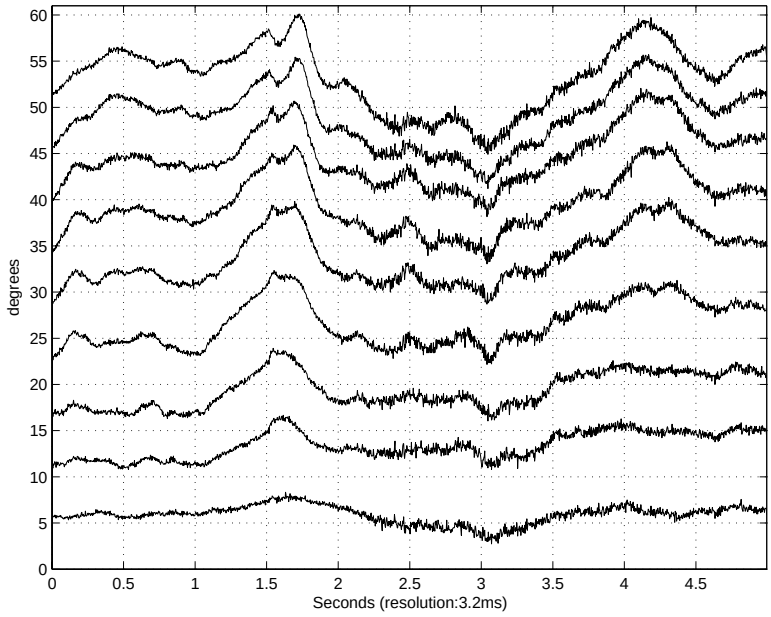

Figure 8.23: 14 To 15.5 km/h South West Wind, Rain: Phase Variation of The Tones Relative To Phase Variation of The Lowest Frequency Tone.

Table 8.8: 14 To 15.5 km/h South West Wind, Rain: Peak-to-peak Variations for Amplitude & Phase Measurements.

Tone #	**1**	**2**	**3**	**4**	**5**	**6**	**7**	**8**	**9**	**10**
Abs. Amp. (dB)	**10.8**	**10.8**	**10.8**	**11.1**	**11.2**	**11.5**	**11.6**	**11.5**	**11.7**	**11.5**
Rel. Amp. (dB)	**0**	**0.6**	**0.7**	**1**	**1.1**	**1.4**	**1.4**	**1.5**	**1.5**	**1.6**
Abs. Pha. (Deg)	**324**	**326**	**328**	**330**	**333**	**333**	**333**	**333**	**335**	**338**
Rel. Pha. (Deg)	**0**	**5.6**	**5.9**	**7.9**	**10.2**	**11.6**	**13.2**	**13.9**	**14.5**	**15.2**

Table 8.9: 14 To 15.5 km/h South West Wind, Rain: Instantaneous Amplitude Variations.

Circles / Squares / Diamonds								
Tone #	Var. (dB)	Dur. (s)	Rate (dB/s)	Loc. (s)	Var. (dB)	Dur. (s)	Rate (dB/s)	Loc. (s)
1	**4.1**	**0.15**	**27**	**1.7**	**-4.4**	**0.12**	**-36.2**	**1.6**
6	**4.6**	**0.16**	**29.5**	**1.7**	**-4.6**	**0.12**	**-39**	**1.6**
10	**4.8**	**0.17**	**28.8**	**1.7**	**-4.6**	**0.12**	**-38.9**	**1.6**
1	**1.1**	**0.23**	**5**	**3.2**	**-9.8**	**0.67**	**-14.8**	**2.1**
6	**0.7**	**0.1**	**7.5**	**3.2**	**-10.1**	**0.68**	**-14.8**	**2.1**
10	**1.1**	**0.19**	**5.8**	**3.2**	**-10.2**	**0.65**	**-15.7**	**2.1**
1	**0.5**	**0.13**	**3.8**	**4.7**	**-0.9**	**0.19**	**-4.5**	**0.5**
6	**0.5**	**0.13**	**4.2**	**4.7**	**-0.9**	**0.16**	**-5.6**	**0.6**
10	**0.8**	**0.16**	**5**	**4.7**	**-0.7**	**0.16**	**-4.6**	**0.6**

Table 8.10: 14 To 15.5 km/h South West Wind, Rain: Instantaneous Phase Variations Relative to Phase Variations of Lowest Frequency Tone.

Tone #	Var. (Deg)	Dur. (s)	Rate (Deg/s)	Loc. (s)	Var. (Deg)	Dur. (s)	Rate (Deg/s)	Loc. (s)
1	**1.7**	**0.07**	**25.8**	**3.1**				
2	**1**	**0.06**	**17.4**	**3.1**				
3	**1.4**	**0.06**	**21.9**	**3.1**				
4	**2.3**	**0.1**	**23.2**	**3.1**	**-2.2**	**0.07**	**-33.4**	**1.8**
5	**2.6**	**0.07**	**38**	**3.1**	**-4.9**	**0.13**	**-37.7**	**1.8**
6	**2.2**	**0.1**	**22**	**3.1**	**-6.2**	**0.16**	**-38**	**1.8**
7	**1.5**	**0.06**	**23.2**	**3.1**	**-6.1**	**0.16**	**-37.6**	**1.8**
8	**1.7**	**0.09**	**18.5**	**3.1**	**-6.6**	**0.13**	**-50**	**1.8**
9	**1.2**	**0.07**	**17.8**	**3.1**	**-6.5**	**0.13**	**-49.8**	**1.8**

9. CONCLUSION

9.1 Summary

Signal distortions caused by tree foliage obstructions to a RF line-of-sight 6 MHz channel could be accurately measured. A system constructed as part of the research was able to estimate the amplitude of the receive tones with a standard deviation of 0.3% of the actual amplitude and the phase of the tones with a standard deviation of 0.23 degrees. This accuracy was achieved when the signal-to-noise ratio of the receive signal was greater than 20 dB.

The trees cause fast and large variations in the strength of the receive signal with frequency selective distortion. The sites selected for the measurements had significant foliage obstructions since 4 trees were present on the line-of-sight path. For fades greater than 10 dB, the variation in amplitude that is common to all the tones is found to be about 3 times larger than the variation in amplitude among the tones. This indicates that the operation of the system could be improved by adding a fast automatic gain controller (AGC) to the front-end of the modem.

It is noticed that the position of the receive antenna is very critical. Some branches not on the line-of-sight path on a calm day may cause large temporal signal variation on a windy day as they pass through the line-of-sight path from time to time. The tree trunk may pass through the line-of-sight path when bending under the action of the wind.

The fades are deep, can last less than 100 ms, and the variation in the amplitude of the tones can reach rates of 50 dB/s. This strongly suggests that these amplitude variations are due to changes in the multipath structure of the channel caused by the motion of the trees present in the line-of-sight path. The multipath is likely to be caused by the scattering of the RF signal by the leaves. The number of multipath propagation paths increase with

the number of leaves. Therefore, the more foliage there is on the line-of-sight path, the deeper the fades are. Another explanation for the deep fades could be due to changes in the ground reflected signal reaching the receive antenna and/or the line-of-sight signal, when traveling through the tree foliage.

9.2 Results

On a calm day with less than 5 km/h wind, the presence of tree foliage did not cause the strength of the line-of-sight signal to change significantly. The variation in the amplitude of the tones was measured to be less than 1 dB. The presence of wind causes the branches to sway. The motion of the branches gives rise to large variations in the amount of power received, producing signal fading. The fades affect all the tones. They mainly occur when the wind blows at varying velocity. The deepest fades are seen in presence of gust wind. For a wind of 10 km/h, gusting to 25 km/h, a 22 dB variation in the amplitude of the tones reached a rate of 57 dB/second.

Rain in presence of wind doesn't seem to cause stronger amplitude variations of the tones. The signal power loss through the foliage is also measured to be about the same with and without rain. However, under intense rainfall and no wind, enough water can accumulate on the tree to cause heavy signal attenuation. Such a situation was witnessed when recording data on a rainy day. Signal attenuation by the tree foliage before the rain picked up was measured to be 13 dB. Five minutes after the beginning of a shower, the receive signal power decreased by more than 20 dB, bringing to 33 dB the signal attenuation caused by the foliage. Five minutes after the shower stopped, the signal attenuation was again 13 dB.

Although the tones seem to have large common variation in amplitude, some variations do exist among the tones, indicating that the signal fading is frequency selective. To extract these frequency selective variations, the lowest frequency tone was taken as a reference. Variations in the amplitude of the other tones were then computed with respect to the variation in the amplitude of the reference tone. For a 16 dB fade, the maximum frequency selective variation was measured to be 5 dB. For a 22 dB fade, the maximum frequency selective variation was measured to be 10 dB.

The effect of tree foliage is not sufficiently pronounced to be identified on the curves showing the absolute phase measurements. Some variations, in the 20-30 radians range, common to all the curves, do appear. However, similar variations could be seen on the measurements obtained when directly connecting the RF output of the transmitter to the RF input of the receiver, and were likely due to the frequency drift of the oscillators in the up/down converters. Any phase variation, common to all the tones, that could be caused by tree foliage, appears to be masked or exacerbated by the variations caused by the frequency drift of the oscillators. It is then impossible to extract these variations. Yet, this result confirms that the maximum Doppler shift caused by the swinging of the branches in the wind is very likely to be less than 2 Hz [2].

The variations in phase that differ between the tones can be precisely measured with this system. As for amplitude, these frequency selective variations are extracted by using the lowest frequency tone as a reference and computing the variation in phase of the other tones with respect to the variation in phase of the reference tone. They are the strongest when deep fades occur, and can reach 40 degrees at a rate of 190 degrees / second for a 16 dB fade.

9.3 Future Research

The effect of tree foliage on the RF signal could be thoroughly characterized with this measuring system, and the data collected in the summer of 2003. The next step would be to design an equalizer that can compensate for some of these distortions. A solution to improve the operation of the system would be to place a pilot tone at one edge of the band. This would permit correction for the fast flat variation across the band but also to correct for the phase variation due to Doppler shift caused by the motion of the tree and the frequency drift of the oscillators. Only the variations that are frequency selective would remain.

The frequency selective variations may be assessed by placing a pilot tone at the other end of the band. However, more investigation is required to determine how to efficiently compensate for these distortions.

REFERENCES

[1] Commitee on Broadband Last Mile Technology, National Research Council, *et al.*, *Broadband: Bringing Home the Bits*, ch. 4. The National Academies Press, Washington DC, 2002.

[2] V. Erceg, K. Hari, M. Smith, D. Baum, *et al.*, "Channel models for fixed wireless applications," *IEEE 802.16.3 Task Group Contributions*, July 2001.

[3] F. Schwering, E. Violette, and R. Espeland, "Millimeter-wave propagation in vegetation: Experiments and theory," *IEEE Transactions on Geoscience and Remote Sensing*, vol. 26, pp. 355–367, May 1988.

[4] A. Kajiwara, "Foliage attenuation characteristics for lmds radio channel," *IEEE International Conference on Communications*, vol. 3, pp. 2130–2134, September 2000.

[5] V. Erceg, D. Michelson, S. Ghassemzadeh, L. Greenstein, *et al.*, "A model for the multipath delay profile of fixed wireless channels," *IEEE Journal on Selected Areas in Communications*, vol. 17, pp. 399–410, March 1999.

[6] M.R. Hinds, G. J. Sofko, A. G. Wacker, and J. A. Koehler, "Ku-band polarization characteristics of crops and fallow," *SPIE Radar Polarimetry*, vol. 1748, pp. 47–58, July 1992.

[7] E. Hecht, *Optics*, ch. 8. Addison-Wesley, 3 ed., 1998.

[8] A. V. Oppenheim, R. W. Schafer, and J. R. Buck, *Discrete-Time Signal Processing*. Prentice Hall, 2 ed., 1999.

[9] J. G. Proakis, *Digital Communications*. Mc Graw-Hill, 4 ed., 2001.

[10] G. Wells, *Apex FPGA - DSP Development Board Operating Instructions*. TR*Labs* Saskatoon, rev 1.0 ed., January 2002.

[11] SAWTEK Incorporated, *P/N 855079: 44MHz VSB Filter 6.0MHz Bandwidth*, October 1999.

[12] WaveCom Electronics Inc., *Agile MMDS Upconverter MA4061, Power Amplifier MA4070B, Installation and Operation Guide for System Operators*, man1l2301 rev04 ed., August 2002.

[13] National Instruments, *PCI-6534: 653X User Manual*, January 2001.

[14] A. Papoulis and S. U. Pillai, *Probability, Random Variables, and Stochastic Processes*. Mc Graw-Hill, 4 ed., 2001.

[15] L. W. Couch II, *Digital and Analog Communication Systems*. Prentice Hall, 5 ed., 1997.

[16] E. E. Lee and D. G. Messerschmitt, *Digital Communication*, ch. 15. Kluwer Academic Publishers, 2 ed., 1993.

[17] A. Ralston and P. Rabinowitz, *A First Course in Numerical Analysis*. Dover Publications, Inc., 2 ed., 2001.

[18] Hewlett Packard, *HP 4195A Network / Spectrum Analyzer*, November 1989.

APPENDIX A. SOUNDING THE CHANNEL WITH A BAND-LIMITED RF PULSE

One type of system that is used to characterize a wireless channel consists of transmitting a band-limited RF pulse. This appendix gives a short overview of this type of system and briefly shows how the impulse response of the channel can be estimated.

A.1 System Overview

Figure A.1 shows a block diagram of the measuring system. It is composed of a transmitter and a receiver. In the transmitter, a carrier at F_c is modulated with a very narrow pulses $p(t)$ of width $\Delta\tau$ and amplitude A. The pulse $p(t)$ is defined by:

$$p(t) = \begin{cases} A, & 0 \leq t \leq \Delta\tau \\ 0, & \text{otherwise.} \end{cases} \tag{A.1}$$

The Fourier transform of $p(t)$ is

$$P(j\Omega) = \int_0^{\Delta\tau} Ae^{-j\Omega\tau} d\tau = A\Delta\tau \frac{\sin \Omega\Delta\tau/2}{\Omega\Delta\tau/2} e^{-j\Omega\Delta\tau/2}, -\infty < \Omega < +\infty. \tag{A.2}$$

Ideally, the $\Delta\tau$ should approach 0 and A should approach infinity so that $p(t)$ is an impulse. In which case the output of the channel filter will have a flat energy spectrum. This ideal pulse is impractical. A practical pulse has some width but it can be made sufficiently narrow such that the output of the channel filter has a nearly flat energy spectrum inside the filter bandwidth. The energy spectrum of the pulse $p(t)$ is

$$S_p(j\Omega) = |P(j\Omega)|^2 = A^2\Delta\tau^2 (\frac{\sin \Omega\Delta\tau/2}{\Omega\Delta\tau/2})^2. \tag{A.3}$$

The energy spectrum of $p(t)$ has a null-to-null bandwidth of $2/\Delta\tau$ Hertz. For a channel filter with a bandwidth equal to 2W Hertz and centered at F_c, $\Delta\tau$ must be chosen sufficiently small such that $2/\Delta\tau$ is greater than 2W or $\Delta\tau < 1/W$. For example, if the bandwidth of the channel filter is 6MHz, then $\Delta\tau$ must be less than 333ns long. By proceeding this

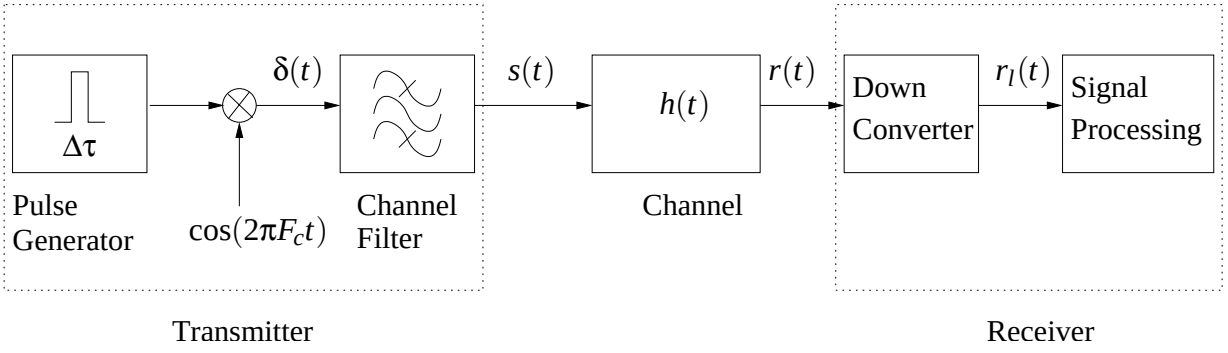

Figure A.1: Measuring System Block Diagram

way, the generated RF pulse approximates an impulse, $\delta(t)$, for the channel to be measured since the output of the channel filter will have a nearly flat energy spectrum inside the bandwidth of the channel of interest. At the output of the channel filter, the transmit signal is given by

$$s(t) = \frac{\sin 2\pi W t}{\pi t} \cos 2\pi f_c t. \tag{A.4}$$

In summary, this signal is a band-limited RF pulse that approximates an impulse for the channel to be characterized.

In the block diagram of the measuring system, $h(t)$ represents the impulse response of the channel. The RF receive signal, $r(t)$, is the signal obtained after the RF transmit signal, $s(t)$, has traveled through the channel from the transmit to the receive antenna. In the receiver, a down-converter is used to generate from $r(t)$, the lowpass equivalent receive signal, $r_l(t)$ [9]. Signal processing can then be applied to extract parameters for characterizing the wireless channel.

A.2 Estimating the Impulse Response of The Channel

Because the transmit signal, $s(t)$, has a nearly flat energy spectrum inside the the bandwidth of the channel of interest, the lowpass equivalent receive signal, $r_l(t)$, is an estimate of the lowpass equivalent impulse response of the channel. If $s(t)$ is transmitted at time $t = t_0$, then $r_l(t)$ is an estimate of the lowpass equivalent impulse response of the channel at time $t = t_0$. An estimate of the lowpass equivalent frequency response of the channel

at time $t = t_0$ can be obtained by sampling $r(t)$, computing the lowpass equivalent signal, and performing a FFT of that signal.

To measure the impulse response of the channel at several instants of time, the measuring system can be modified to send a train of band-limited RF pulses, where the pulses are separated in time by ΔT. ΔT should be sufficiently large to guarantee that the impulse response of the channel at instant t_0 is received before receiving the impulse response of the channel at instant $t_0 + \Delta T$.

APPENDIX B. ANALYSIS OF A SECOND ORDER TYPE I DIGITAL PHASE-LOCK LOOPS (DPLL)

B.1 Principle of Operation

A second order type I DPLL achieves frequency lock if the frequency offset $\Delta\omega_{if}$ of the input recorded signal, $r_{if}[n]$, with the DPLL local oscillator frequency ω_{if} is within the lock range. However, frequency lock is accompanied with a constant phase error with the input signal. This phase error is required for the DPLL to synthesize the instantaneous frequency $\Delta\omega_{if}$ at each iteration or clock cycle.

Figure B.1 shows a block diagram of a second order type I DPLL. It is composed of a phase detector (PD), a loop filter (LF), a gain K, and a numerical control oscillator (NCO). The NCO generates the signal $y[n]$. $x[n]$ and $y[n]$ are mixed by the phase detector. The important pieces of this block diagram are the loop filter and the gain K. These entities generate an instantaneous frequency $\Delta\omega'[n]$ from the phase detector output. The instantaneous phase $\theta_{NCO}[n+1]$ of the NCO output at the discrete instant of time $(n+1)*T_r$

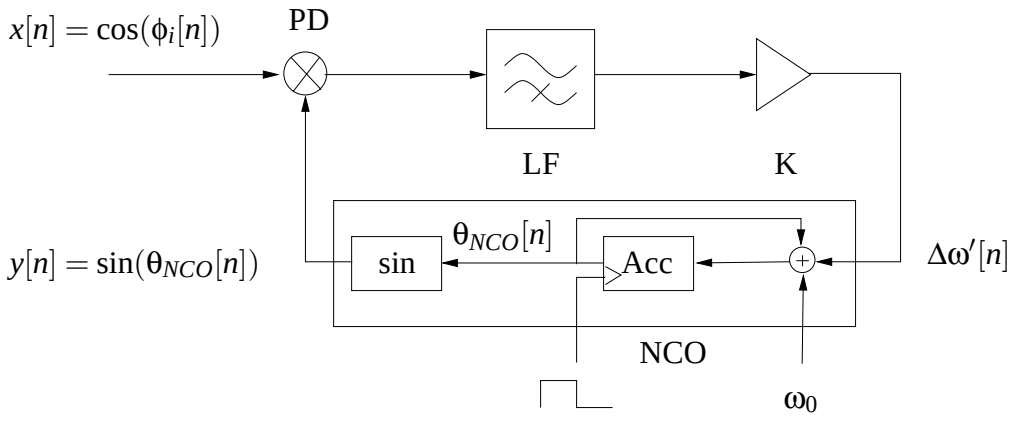

Figure B.1: DPLL Block Diagram

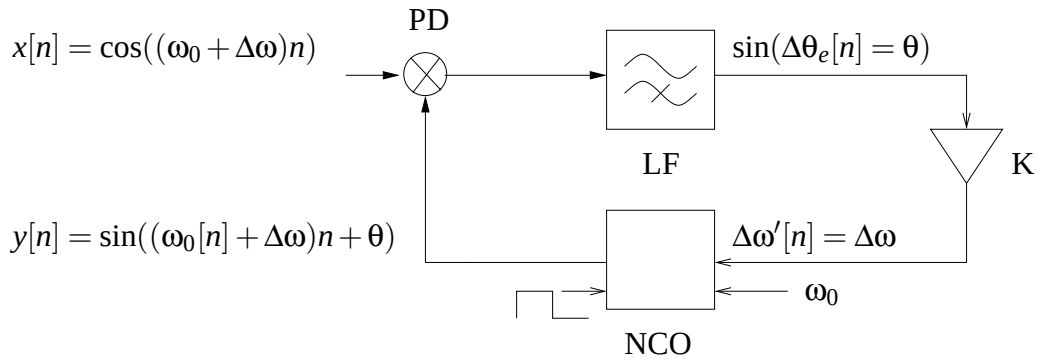

Figure B.2: DPLL Block Diagram (In Lock)

where T_r is the sampling period, is obtained by adding ω_0 and $\Delta\omega'[n]$ to the NCO built-in integrator that was set to $\theta_{NCO}[n]$ at the discrete instant of time $n * T_r$. $\theta_{NCO}[n+1]$ is then loaded into the NCO integrator at the discrete instant of time $(n+1) * T_r$ occurring at the next clock cycle.

The loop filter provides some noise immunity by acting as a second gain that is simultaneously very small for the high frequencies of the signal and that approaches $F(1)$ as $\Delta\theta_e[n]$ becomes constant equal to θ (see Figure B.2) for the frequency the DPLL has achieved frequency lock.

B.2 The Linearized Z-Transform Model of The DPLL

The linearized Z-transform model of the DPLL is based on an approximation of the difference of instantaneous phases $\Delta\theta_e[n]$ between $x[n]$ and $y[n]$ by $\sin(\Delta\theta_e[n]) \approx \Delta\theta_e[n]$. This model is based on taking the Z-transform of the output phase of the NCO, $\theta_{NCO}[n]$, that is defined by (see Figure B.1)

$$\theta_{NCO}[n+1] = \theta_{NCO}[n] + \omega_0 + \Delta\omega'[n]. \tag{B.1}$$

Taking the Z-transform of B.1 yields

$$\Theta_{NCO}(z) = \omega_0 \frac{z^{-1}}{(1-z^{-1})^2} + \frac{z^{-1}}{(1-z^{-1})} \Delta\omega'(z). \tag{B.2}$$

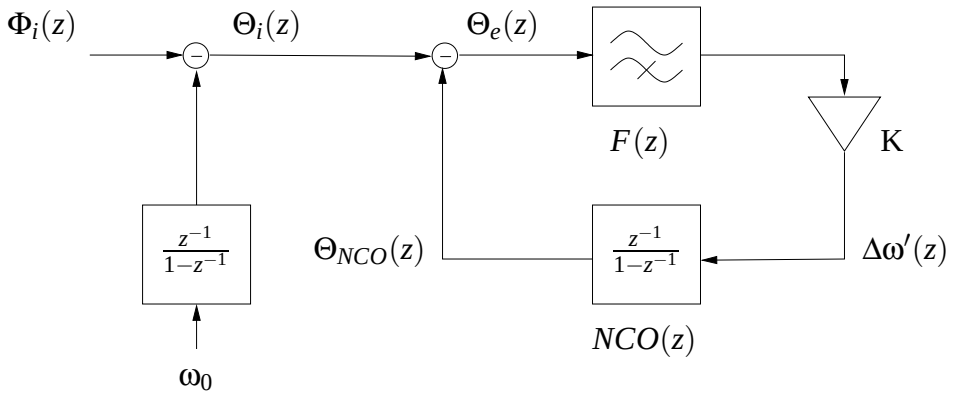

Figure B.3: DPLL Z-Transform Linearized Model

The inverse Z-transform of the first term is a ramp function equal to $\omega_0 * n$. This ramp function can be moved out of the feedback loop of the model, yielding

$$\Theta_{NCO}(z) = \frac{z^{-1}}{(1-z^{-1})}\Delta\omega'(z) = NCO(z)\Delta\omega'(z). \tag{B.3}$$

The Z-transform model of the DPLL is shown on Figure B.3 where $\Phi_i(z)$ denotes the Z-transform of the instantaneous phase $\phi_i[n]$ of $x[n]$, and $\frac{z^{-1}}{(1-z^{-1})}$ represents the Z-transform of the NCO.

The loop filter of a general second-order DPLL has one real pole that is placed close to the unit circle. The phase detector produces a term at frequencies in the neighborhood of $2 * \omega_{if}$. This frequency can be easily filtered by adding a complex conjugate pair of zeros at location $2 * \omega_{if}$. If a denotes the value of the pole, then $F(z)$ is given by

$$F(z) = K_F \frac{1 - 2\cos(0.8\pi)z^{-1} + z^{-2}}{1 - az^{-1}}. \tag{B.4}$$

where K_F is a constant. K_F is set such that the DC response of the loop filter is equal to 1, yielding

$$K_F = \frac{1-a}{2-2\cos(0.8\pi)}. \tag{B.5}$$

The transfer function of the DPLL is equal to

$$\begin{aligned} DPLL(z) &= \frac{K * F(z) * NCO(z)}{1 + K * F(z) * NCO(z)} \\ DPLL(z) &= \frac{KK_F(z^2 - 2\cos(0.8\pi)z + 1)}{z^3 - (1 + a - KK_F)z^2 + (a - 2KK_F\cos(0.8\pi))z + KK_F} \end{aligned} \tag{B.6}$$

APPENDIX C. MATLAB AND SIMULINK SOURCE FILES FOR THE POST-PROCESSING SYSTEM

The implementation of Pass 1 to Pass 4 in Simulink includes the following Matlab and Simulink files that must be run in the same order as they are given below to obtain the estimates $\hat{a}_i[k]$ and $\hat{\theta}_i[k]$ of $A_i(t_k)$ and $\Theta_i(t_k)$.

"S1_run.m" is the program corresponding to Pass 1. This program calls the Simulink program, "S1.mdl". The file that stores $r_{if}[n]$ is too large to be processed in one block through Simulink. $r_{if}[n]$ is processed in portions of 40ms duration. Performing this way requires saving the internal states of the Simulink blocks after processing one block of the signal. The internal states of the Simulink blocks are then reloaded before processing the next signal block. This is easily implemented by using the environment variables defined by Simulink. These variables are used to retrieve the internal states of the Simulink blocks in order to reload these values when running the simulation on the next segment of data. However, in order to function correctly, the next portion of data to be processed must have its first value equal to the last value of the previous segment of data. This is because Simulink doesn't update the internal states of the Simulink blocks after processing the last sample of the segment. "S2_run" is the program corresponding to Pass 2. This program calls the Simulink program, "S2.mdl". "Compute_interpol.m" is the program corresponding to Pass 3. This program uses the Matlab function "spline" to resample $r_l[n]$. "Compute_fft.m" is the program corresponding to Pass 4. This program uses the Matlab function, "fft"."Compute_fft.m" creates two files. One of the file contains the estimates, $\hat{a}_i[k]$, and the other file contains the estimates, $\hat{\theta}_i[k]$, of the amplitude and phase of the tones. These files can then be read to generate the waveforms showing the amplitude and phase estimates of the tone as a function of time.

C.1 Simulink And Matlab Source Files For Pass 1

```
clear;
% S1_run.m
```

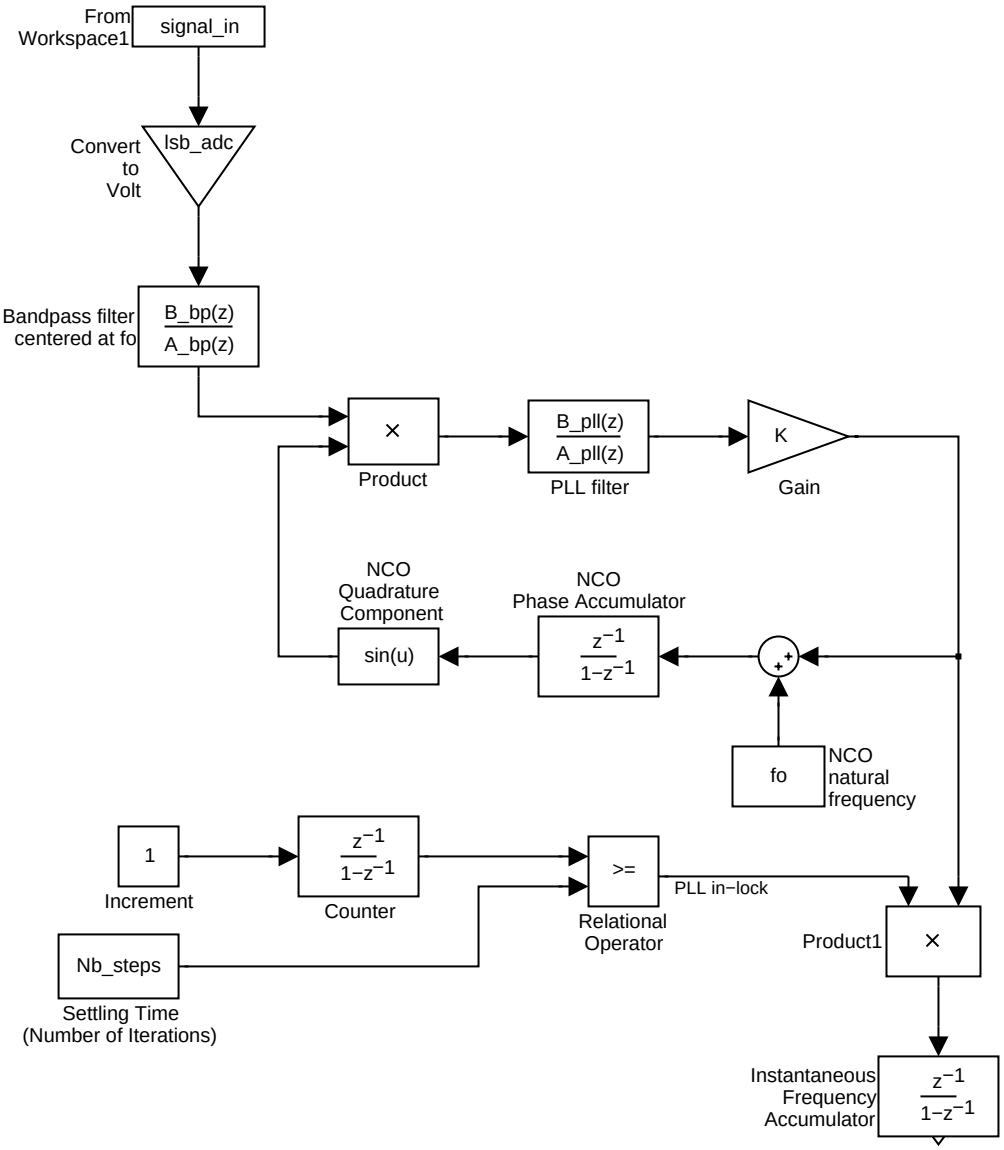

Figure C.1: Simulink Source File: “S1.mdl”

```
%ENTER INPUT FILE HERE
fid_input_file_S1 = fopen('300902_setup2_d4.bin','r');
% simulation parameters
DS = 1000;
sim_time = DS * 20e2;
nb_iterations = 50;
PLL_settling_time = 2e4;
den = 128;
cf_num = 53;
% filter design IIR Bandpass filter
f_dig_poles = ([-5/1000, 0, 5/1000] + (cf_num/den)) * pi;
r_poles = [0.99, 0.99, 0.99];
fpoles = [r_poles .* exp(j*f_dig_poles),
r_poles .* exp(-j*f_dig_poles)];
K = 1 / 7308;
B_bp = K;
A_bp = poly(fpoles);
% DPLL design
a = 0.999;
B_pll = (1 - a) * [1 -2*cos(0.8*pi) 1] / ((1-cos(0.8*pi))^2
+ (sin(0.8*pi))^2);
A_pll = [1 -a];
% ADC lsb
resol_dac = 2^12;
lsb_adc = 2 / resol_dac;
% PLL loop gain
K = 5e-3;
% NCO natural frequency
fo = cf_num * pi / den;
[N,wp] = ellipord(5e-5,5e-4,0.01,70); clear wp;
[B_lp,A_lp] = ellip(N,0.01,70,5e-5); clear N;
% open files for input signal
fid_10khz_file = fopen('S1_out.bin','w');
% load input signal
data_raw = fread(fid_input_file_S1,sim_time + 1,
'int16=>double');
signal_in.time = [];
signal_in.signals.dimensions = 1;
signal_in.signals.values = data_raw;
clear data_raw;
% run the simulation
xInitial = [];
Nb_steps = PLL_settling_time;
sim('freq_shift02');
% save output_signal
```

```
fwrite(fid_10khz_file, data_10khz(2:(sim_time / DS) + 1), ...
'double');
clear data_10khz;
% loop to run the successive runs
for I = 2:nb_iterations
Nb_steps = 0; I
xInitial = xFinal;
% load signal
data_raw(1) = signal_in.signals.values(sim_time + 1);
clear signal_in
data_raw(2:sim_time + 1) = fread(fid_input_file_S1,sim_time
,'int16=>double');
signal_in.time = [];
signal_in.signals.dimensions = 1;
signal_in.signals.values = data_raw.';
clear data_raw;
% run the simulation
sim('freq_shift02');
% save output_signal
fwrite(fid_10khz_file, data_10khz(2:(sim_time/DS) + 1), ...
'double');
clear data_10khz;
end %loop for
% close files
fclose(fid_input_file_S1);
fclose(fid_10khz_file);
% save content of offset phase accumulator
dfo = xFinal.signals(8).values / (sim_time  * nb_iterations
- PLL_settling_time);
save S1_out_dfo dfo;
```

C.2 Simulink And Matlab Source Files For Pass 2

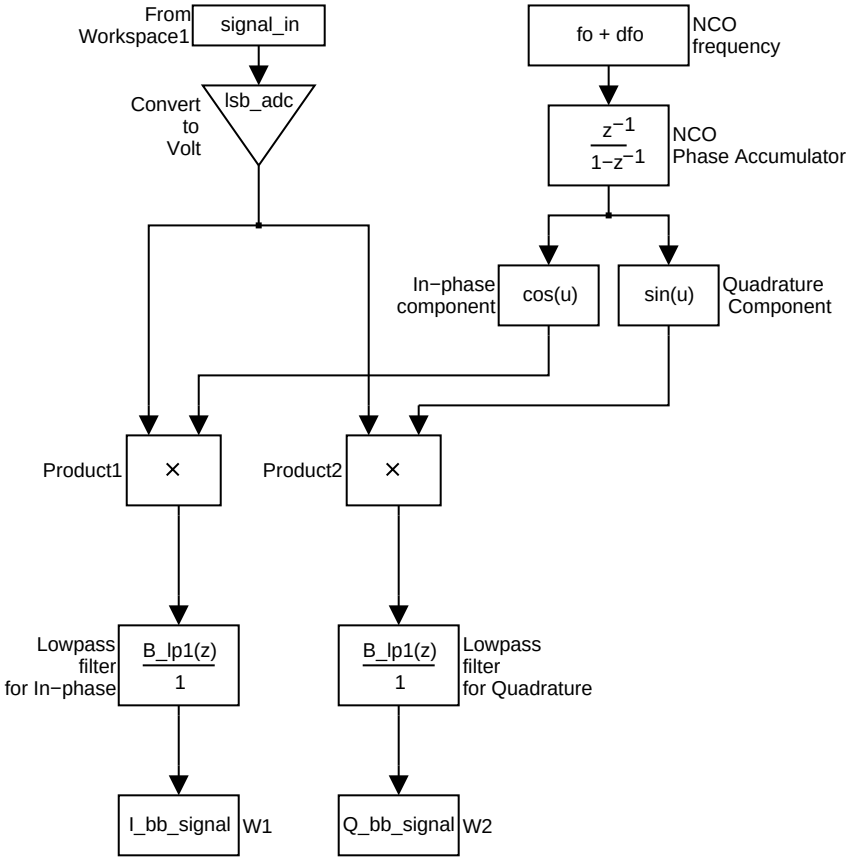

Figure C.2: Simulink Source File: “S2.mdl” (Process 1)

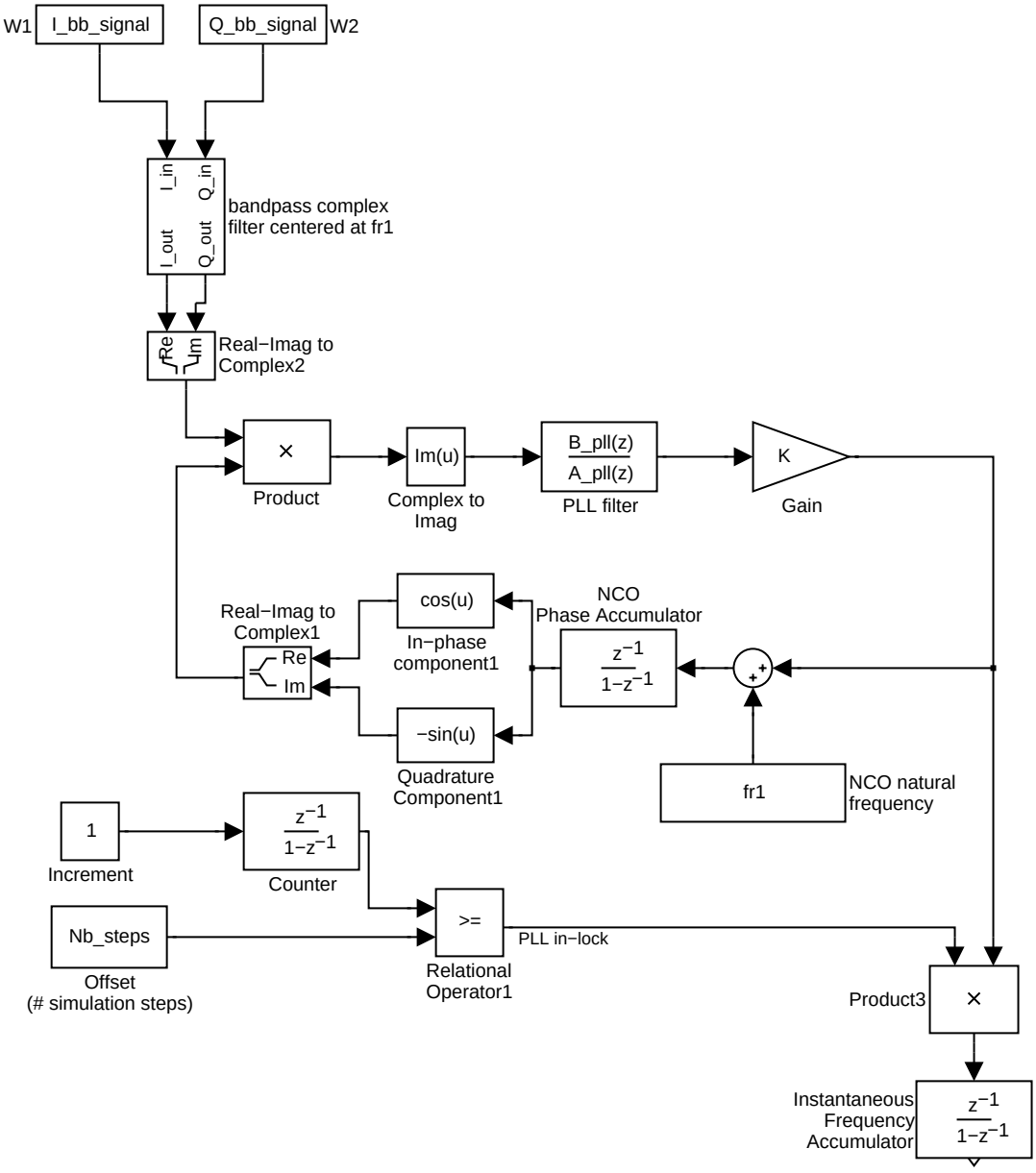

Figure C.3: Simulink Source File: “S2.mdl” (Process 2)

```
% S2_run.m
clear;
%ENTER INPUT FILE HERE
fid_input_file_S2a = fopen('300902_setup2_d4.bin','r');
% NCO natural frequency for frequency shift to baseband
den = 128;
cf_num = 53;
fo = cf_num * pi / den;
nb_iterations = 50;
load S1_out_dfo;
% simulation parameters
sim_time = 1000 * 20e2;
PLL_settling_time = 1e5;
% filter design FIR Lowpass filter
[Nf, Ff, Af, Wf] = remezord([30/256+2.5e-3 0.125],
[1 , 0], [0.001 0.001], 1);
B_lp1 = remez(Nf, Ff, Af, Wf);
clear Nf; clear Ff; clear Af; clear Wf;
% complex filter to extract the 9th tone
f_dig_poles = ([-5/1000, 0, 5/1000] + (24 / den)) * pi;
r_poles = [0.99, 0.99, 0.99];
fpoles = [r_poles .* exp(j*f_dig_poles),
r_poles .* exp(-j*f_dig_poles)];
K = 10^(-88/20);  % requires 21dB gain at DC
fzeros = [r_poles .* exp(-j*f_dig_poles)];
B_bp1 = K * poly(fzeros);
A_bp1 = poly(fpoles);
B_bp1_real = real(B_bp1);
B_bp1_im = imag(B_bp1);
A_bp1_real = A_bp1;
A_bp1_im = A_bp1_real;
% DPLL design
a = 0.999;
B_pll = (1 - a);
A_pll = [1 -a];
% ADC lsb
resol_dac = 2^12;
lsb_adc = 2 / resol_dac;
% NCO natural frequency
fr1 = 24 / den * pi;
% PLL loop gain
K = 5e-3;
% open files for input and output signals
fid_I_output_file = fopen('S2a_I.bin','w');
fid_Q_output_file = fopen('S2a_Q.bin','w');
```

```
% load input_signal
data_raw = fread(fid_input_file_S2a,sim_time + 1,
'int16=>double');
signal_in.time = [];
signal_in.signals.dimensions = 1;
signal_in.signals.values = data_raw;
clear data_raw;
% run the simulation
xInitial = [];
Nb_steps = PLL_settling_time;
sim('freq_shift04');
% save output_signals
fwrite(fid_I_output_file, I_bb_signal(1:sim_time),'double');
fwrite(fid_Q_output_file, Q_bb_signal(1:sim_time),'double');
clear I_bb_signal; clear Q_bb_signal;
% loop to run the successive runs
for I = 2:nb_iterations
Nb_steps = 0;I
xInitial = xFinal;
% load signal
data_raw(1) = signal_in.signals.values(sim_time + 1);
clear signal_in
data_raw(2:sim_time + 1) = fread(fid_input_file_S2a,sim_time
,'int16=>double');
signal_in.time = [];
signal_in.signals.dimensions = 1;
signal_in.signals.values = data_raw.';
clear data_raw;
% run the simulation
sim('freq_shift04');
% save output_signals
fwrite(fid_I_output_file, I_bb_signal(1:sim_time),'double');
fwrite(fid_Q_output_file, Q_bb_signal(1:sim_time),'double');
clear I_bb_signal; clear Q_bb_signal;
end %loop for
% close files
fclose(fid_I_output_file);
fclose(fid_Q_output_file);
fclose(fid_input_file_S2a);
% save content of offset phase accumulator
dfr1 = xFinal.signals(11).values / (sim_time  * nb_iterations
- PLL_settling_time);
save S2a_out_dfr1 dfr1;
```

C.3 Matlab Source File For Pass 3

```
% Compute_interpol.m
clear;
% Initialization
fr1 = 24 / 128 * pi;
load S2a_out_dfr1;
b = 1 / (1 + (dfr1 / fr1));
Nb_read = 1e6;
Nb_iterations = 100e6 / Nb_read;
% Process the I component:
start_smpl = 1;
stop_smpl = Nb_read;
start_smpl_interpol = start_smpl;
stop_smpl_interpol = stop_smpl - 1;
% Open file to read and write the data
fid_I_input_file = fopen('S2a_I.bin','r');
fid_I_output_file = fopen('S2a_I_interpol.bin','w');
% Process input file and save result in output file
% Process first block
x = start_smpl : stop_smpl;
y = (fread(fid_I_input_file,Nb_read,'*double')).';
xx = start_smpl_interpol : b : stop_smpl_interpol;
yy = spline(x, y, xx);
fwrite(fid_I_output_file,yy,'double'); clear yy;
% Process successive blocks of data and save result
for I = 2:Nb_iterations - 1,
y_last_values(1:3) = y(length(y)-2:length(y)); clear y;
y = y_last_values; clear y_last_values;
start_smpl = stop_smpl - 2;
stop_smpl = I * Nb_read; clear x;
start_smpl_interpol = xx(length(xx)) + b; clear xx;
stop_smpl_interpol = stop_smpl - 1;
x = start_smpl : stop_smpl;
y = [y (fread(fid_I_input_file, Nb_read, '*double')).'];
xx = start_smpl_interpol : b : stop_smpl_interpol;
yy = spline(x , y, xx);
fwrite(fid_I_output_file,yy,'double'); clear yy;
end
% Process last block
y_last_values(1:3) = y(length(y)-2:length(y)); clear y;
y = y_last_values; clear y_last_values;
start_smpl = stop_smpl - 2;
stop_smpl = Nb_iterations * Nb_read; clear x;
start_smpl_interpol = xx(length(xx)) + b; clear xx;
```

```
stop_smpl_interpol = stop_smpl;
x = start_smpl : stop_smpl;
y = [y (fread(fid_I_input_file, Nb_read, '*double')).'];
xx = start_smpl_interpol : b : stop_smpl_interpol;
yy = spline(x , y, xx);
fwrite(fid_I_output_file,yy,'double'); clear yy;
fclose(fid_I_output_file);
fclose(fid_I_input_file);
clear fid_I_output_file; clear fid_I_input_file;

% Process the Q component
start_smpl = 1;
stop_smpl = Nb_read;
start_smpl_interpol = start_smpl;
stop_smpl_interpol = stop_smpl - 1;
% Open file to read and write the data
fid_Q_input_file = fopen('S2a_Q.bin','r');
fid_Q_output_file = fopen('S2a_Q_interpol.bin','w');
% Process input file and save result in output file
% Process first block
x = start_smpl : stop_smpl;
y = (fread(fid_Q_input_file,Nb_read,'*double')).';
xx = start_smpl_interpol : b : stop_smpl_interpol;
yy = spline(x, y, xx);
fwrite(fid_Q_output_file,yy,'double'); clear yy;
% Process successive blocks of data and save result
for I = 2:Nb_iterations - 1,
y_last_values(1:3) = y(length(y)-2:length(y)); clear y;
y = y_last_values; clear y_last_values;
start_smpl = stop_smpl - 2;
stop_smpl = I * Nb_read; clear x;
start_smpl_interpol = xx(length(xx)) + b; clear xx;
stop_smpl_interpol = stop_smpl - 1;
x = start_smpl : stop_smpl;
y = [y (fread(fid_Q_input_file, Nb_read, '*double')).'];
xx = start_smpl_interpol : b : stop_smpl_interpol;
yy = spline(x , y, xx);
fwrite(fid_Q_output_file,yy,'double'); clear yy;
end
% Process the last block
y_last_values(1:3) = y(length(y)-2:length(y)); clear y;
y = y_last_values; clear y_last_values;
start_smpl = stop_smpl - 2;
stop_smpl = Nb_iterations * Nb_read; clear x;
start_smpl_interpol = xx(length(xx)) + b; clear xx;
```

```
stop_smpl_interpol = stop_smpl;
x = start_smpl : stop_smpl;
y = [y (fread(fid_Q_input_file, Nb_read, '*double')).'];
xx = start_smpl_interpol : b : stop_smpl_interpol;
yy = spline(x , y, xx);
fwrite(fid_Q_output_file,yy,'double'); clear yy;
fclose(fid_Q_output_file);
fclose(fid_Q_input_file);
```

C.4 Matlab Source Files For Pass 4

```
% Compute_fft.m
%ENTER OUTPUT FILE HERE
fid_output_file_mag = ...
fopen('300902_setup2_d4_mag_interpol.bin','w');
fid_output_file_phase = ...
fopen('300902_setup2_d4_phase_interpol.bin','w');
% compute succesive N-point FFTs of I & Q signal
% Parameters
Nb_read = 8e5;
N = 256; % Specify the number of points for the FFT
Nb_ffts = 3125;
Nb_iterations = 125;
%open input and output files
fid_input_file_I = fopen('S2a_I_interpol.bin','r');
fid_input_file_Q = fopen('S2a_Q_interpol.bin','r');
for loop = 1:Nb_iterations,
% read I & Q signals from input files
if (loop < Nb_iterations)
I_signal = (fread(fid_input_file_I, Nb_read, '*double')).';
Q_signal = (fread(fid_input_file_Q, Nb_read, '*double')).';
else
I_signal = (fread(fid_input_file_I, '*double')).';
Q_signal = (fread(fid_input_file_Q, '*double')).';
if (Nb_read - length(I_signal)) > 0
I_signal = [I_signal zeros(1, Nb_read - length(I_signal))];
Q_signal = [Q_signal zeros(1, Nb_read - length(Q_signal))];
end
end
% Initialization
signal_start = 1;
signal_stop = N;
freq_abs_array = [];
freq_phase_array = [];
```

```
% Compute successive N-point FFTs
for I = 1:Nb_ffts,
sig_bb_fft = fft(I_signal(signal_start:signal_stop) -
j * Q_signal(signal_start:signal_stop),N);
index_fft = N - (5*(6*N/256)) + 1;
step_fft = 6 * N / 256;
freq_abs_row = [];
freq_phase_row = [];
% extract amplitude and phase values for all 11 tones
for J = 1:11,
if (J == 5)
index_fft_old = index_fft;
index_fft = index_fft - 2*N/256;
freq_abs_row = [freq_abs_row abs(sig_bb_fft(index_fft))];
freq_phase_row = [freq_phase_row angle(sig_bb_fft(index_fft))];
index_fft = index_fft_old;
elseif (J == 7)
index_fft_old = index_fft;
index_fft = index_fft + 2*N/256;
freq_abs_row = [freq_abs_row abs(sig_bb_fft(index_fft))];
freq_phase_row = [freq_phase_row angle(sig_bb_fft(index_fft))];
index_fft = index_fft_old;
else
freq_abs_row = [freq_abs_row abs(sig_bb_fft(index_fft))];
freq_phase_row = [freq_phase_row angle(sig_bb_fft(index_fft))];
end
index_fft = index_fft + step_fft;
if (index_fft == (N + 1))
index_fft = 1;
end
end
% Update amplitude and phase arrays with the new values for
% all 11 tones
freq_abs_array = [freq_abs_array; freq_abs_row];
freq_phase_array = [freq_phase_array; freq_phase_row];
signal_start = signal_stop + 1;
signal_stop = signal_start + N - 1;
clear freq_abs_row;
clear freq_phase_row;
clear sig_bb_fft;
end
% save magnitude and phase to file
% WARNING!!!: In order to recover properly the data
% when reading the file, read by blocks of Nb_ffts * 11
% in matrices of Nb_ffts rows by 11 columns
```

```
fwrite(fid_output_file_mag,freq_abs_array,'double');
fwrite(fid_output_file_phase,freq_phase_array,'double');
clear freq_abs_array; clear freq_phase_array;
clear I_signal;clear Q_signal;
end
% close the files
fclose(fid_input_file_I);fclose(fid_input_file_Q);
fclose(fid_output_file_mag);fclose(fid_output_file_phase);
```